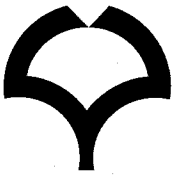

Osaka University

# Photo-orientation Processes of Spectrally Distinguishable Photo-isomers

Hidekazu Ishitobi

*December, 2001*

Department of Applied Physics,
Osaka University

# Photo-orientation Processes of Spectrally Distinguishable Photo-isomers

**Hidekazu Ishitobi**

Department of Applied Physics,
Osaka University

*December, 2001*

## Contents

## Introduction

The growing interest that has arisen in photosensitive chromophores containing polymeric films in the past few years has been driven by requirements in the areas of optoelectronics, photonics, and optical signal processing. Such materials have been used for polarization holography, optical data storage, integrated optics, molecular switching, all-optical modulation, second harmonic generation (SHG), and optical switching. Photo-orientation of photo-excited chromophores alleviates centrosymmetry and isotropy, thereby inducing anisotropy and quadratic and cubic optical nonlinearities. Optical poling techniques, e.g. induced molecular polar orientation, which result in second order nonlinear optical (NLO) effects have been reported only recently, and optically induced nonpolar orientation which results in optical anisotropy has been known for a long time. At the beginning of past century, photo-induced anisotropy in certain materials on irradiation with polarized light has been discovered by Weigert and since then it has been called the Weigert effect [1]. In the 1960's, this effect was widely studied in viscous solutions containing azo-dye molecules and the role of photo-orientation by photoisomerization was pointed out and studied by Neoport and co-workers [2]. In 1980's Todorov and co-workers introduced azo-dye chromophores into polymer films and used photo-orientation for polarization holography studies [3,4], and in 1990's a tremendous interest in the photo-orientation of azo dyes in polymer films has been witnessed because of the possibility of the coupling of photo-orientation and photoisomerization with nonlinear optics [5 -18].

For fundamental understanding of the photo-orientation process itself and its correlation with the micro-cogent environment of the chromophore, much of the optically induced photo-orientation studies have focused on azo dye containing materials. However, despite this activity, studies of light-induced orientation of chromophores other than azobenzene derivatives and azobenzene-type molecules have rarely been reported. In my research, the separation of optical orientation processes of both photoisomers of each of the spiropyran (SP) and diarylethene (DE) chromophores studied is discussed, by using polarized UV-visible spectroscopy, and by taking advantage of the natural spectral differences exhibited by the photoisomers in UV-vis region. In particular, it will be shown that the apparent optically induced orientation of SP and DE depends on the UV and visible photochemical transition bands.

Analytical and theoretical tools are required for quantified studies of photo-orientation by photoisomerization, and for understanding photo-orientation processes. Zimmerman et al. [19], Fisher [20], and Rau et al. [21] developed an

optical pumping population change based theoretical background for photoisomerization within a pure photochemical framework; e.g. that framework in which photo-orientation effects can be disregarded. This feature can be true in low viscosity solutions where photo-induced molecular orientation can be overcome by molecular rotational diffusion. In polymeric environments, especially in thin solid film configurations, spontaneous molecular mobility can, however, be strongly hindered and photo-orientation effects are appreciable. Michl et al. [22] performed intensive research on infrared vibrations and UV-vis electronic transitions of molecules which are already oriented either by introduction into stretched polymer films or after photo-orientation. The first theory that coupled photoisomerization, and photo-orientation processes was developed by Sekkat and Dumont in 1992 [7], and its mathematical foundation is based on the formalism of Legendre polynomials. However, further theoretical developments are needed to quantify coupled photoisomerization and photo-orientation processes, and the most important concept that needs to be clearly addressed, within the framework of photo-orientation, is the polarization nature of the optical transition itself. I will present the analytical theory that allows for the quantification of coupled photoisomerization and photo-orientation in A $\leftrightarrow$ B photoisomerizable systems. I will use it to study quantitatively both the photoisomerization and photo-orientation of a series of photoisomerizable chromophores in films of polymer, including photochromic spectrally distinguishable SP and DE-type chromophore. The way these chromophores move upon isomerization and the isomers transitions symmetry will also be discussed.

Chapter 1

# Brief Review of Linear and Nonlinear Optical Properties Induced by Photo-orientation of Azobenzene Derivatives and its Applications

## 1-1 Introduction

During the last 10 years, a lot of new optical phenomena are discovered, and the linear absorbance and refractive index changes in solid systems have exploited ordering effects in azo polymers. More recently, stable relief gratings have been drawn in the same kind of azo polymers. The large number of potential applications in reversible optical data storage, diffraction, and holography has stimulated a great deal of experimental and theoretical work, a research on which is now extending to different photochromic systems. The extraordinary growth and development of nonlinear optical (NLO) materials during the past 15 years has rendered photonic technologies an essential part of many components used in our daily life, in computer networks and telecommunication systems. Among all the inorganic and organic materials which have been developed recently to reach the best figures of merit, photochromic molecules play a prominent role. First some of them have large molecular hyperpolarizabilities (first and second). Second, the coupling between photochromism and NLO properties leads to very specific features that can be used in processing materials for second-order NLO: for example, creation of noncentrosymmetry, which is a prerequisite for second-order NLO, can be induced by photoassisted poling and all-optical poling. In some cases, photoswitching of NLO properties of photochromic materials can lead to the conception of new devices for data storage or opto-optical switching.

## 1-2 Photoinduced Birefringence and Dichroism

### 1-2-1 Basic Mechanism and Experimental Results

The Weigert effects [1], which is the property of some materials to become dichroic and birefringent when irradiated by polarized light, has been known since the beginning of the century in photographic silver emulsions. This photoinduced anisotropy (PIA) was observed in the 1960s in viscous liquids and polymers containing azo derivatives by Neoport and Stolbova [2], and was applied some years later as a potential means of polarization holography by T. Todorov et al. [3,4]. Since then, there have been many works dealing with PIA in amorphous and liquid crystalline polymers and mono- multilayers doped or functionalized with azo

derivatives. More recently, a few groups have investigated PIA phenomena in polymers doped with spiropyrans [23-25].

The generally agreed upon mechanism is the following : when irradiated by linear polarized light, photochromic molecules, considered as anisotropic (or cigar-like-shaped), undergo photoisomerization cycles, for example, trans→cis→trans isomerization for azo derivatives and change their orientation, tending to line up in a direction perpendicular with the direction of polarization of the excitation (**Figure 1-1**). When probed with a polarized light beam, such a medium shows increased absorption and refractive index in a perpendicular polarization direction. Irradiation of the sample with unpolarized or circularly polarized light at normal incidence restores isotropic absorption.

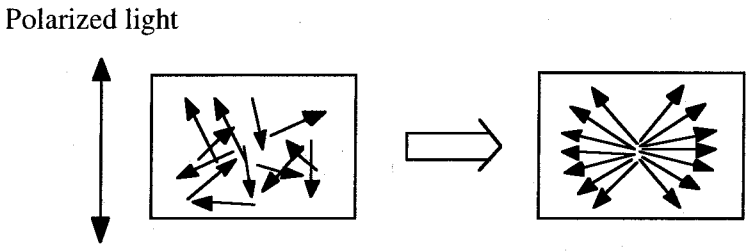


**Figure 1-1.** Optical generation of anisotropy. The molecules excited with polarized light tend to align in a direction perpendicular to the polarization.

In liquids, this anisotropy would relax quickly, but can persist for a long time in rigid matrixes. PIA can be quantitatively defined by two quantities : the macroscopic order parameter S

$$S = \frac{A_{//} - A_{\perp}}{A_{//} + 2A_{\perp}}$$

where $A_{//}$ and $A_{\perp}$ represent the absorbance with a polarization parallel and perpendicular to the polarization of the excitation, respectively, and the birefringence

$$\Delta n = n_{//} - n_{\perp}$$

$n_{//}$ and $n_{\perp}$ being the refractive indices for polarizations parallel and perpendicular to the polarization for the excitation, respectively.

Pump-probe method has been used to study photoinduced dichroism in thin films and monolayers. For dichroism measurements, polymer films deposited on a glass slide are pumped by a linearly polarized beam (**Figure 1-2**) [26]. A probe light beam coming from a white light source and almost parallel with pumping beam is

focused on the sample, and the absorbance is measured for parallel and perpendicular polarizations.

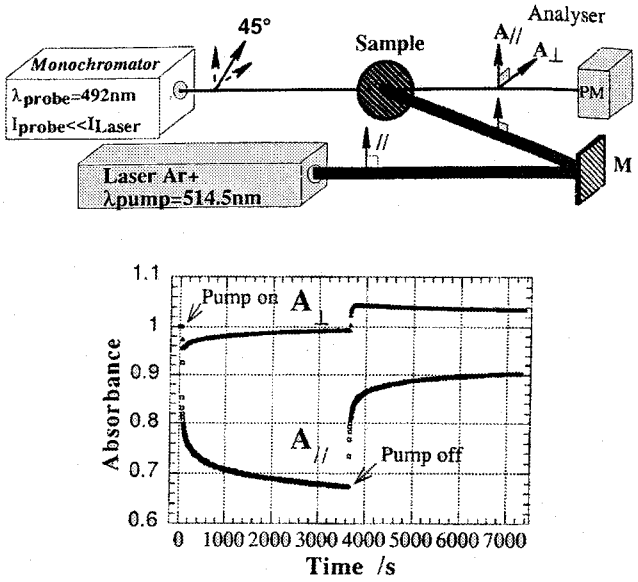


**Figure 1-2.** Photoinduced dichroism in polymer films. Upper part : experimental setup for the pump-probe visible measurements and the successive analyses of the $A_{//}$ and $A_{\perp}$ time-dependent absorbance variations. (PM, photomultiplier ; M, mirror). Lower part : time evaluations of parallel and perpendicular absorbances during a 3600-s exposure ("Pump on" ; I = 10 mW/cm$^2$) to a linearly polarized pump beam, followed by a 3600-s relaxation period ("Pump off") for a 5% DR1/PMMA sample (1 μm thickness). DR1 stands for disperse red one. PMMA stands poly-(methyl methacrylate). Ref. [26].

Different setups have been used for birefringence measurements. In the simplest arrangement, the sample is placed between two crossed polarizers in the pass of a laser (reading) beam chosen at a wavelength out of the absorption spectrum of the photochrome. Another (writing) beam, almost collinear with the preceding one, pumps the photochrome in its absorption band. Photoinduced birefringence creates a change in transmission of the probe beam, this change being maximum when the polarization vector of the pump beam is set to 45° with respect to the polarization vector of the probe beam. A powerful method uses attenuated total reflection (ATR). This method is a generalization of the Kretschmann method using surface plasmons which are transverse magnetic waves propagating along a metal-dielectric interface, their field amplitudes decaying exponentially perpendicular to the interface. These free waves can be coupled with guided waves in the thin organic layer (amorphous polymer or Langmuir-Blodgett-Kuhn layer).

Resonance conditions allow very accurate determination of the refractive index (accuracy < $10^{-3}$) and thickness, and are very sensitive to any changes occurring inside or at the surface of the film. **Figure 1-3** [6] shows the experimental setup. The sample is a glass slide coated with a silver layer on which the organic layer is deposited. The glass face of the slide is put in optical contact with a half-sphere. The reflectivity of a near-infrared diode laser beam is measured through the half-sphere, as a function of the incidence angle. The angular positions of the dips in reflectivity (Fabry-Perot dips), with polarization perpendicular (transverse electric, or TE) or parallel (transverse magnetic, or TM) to the incidence plane, give the three components of the refractive index and the thickness of the films. Photoinduced birefringence induces a shift the angular position of the dips, from which changes in the refractive indexes (and thickness) can be determined.

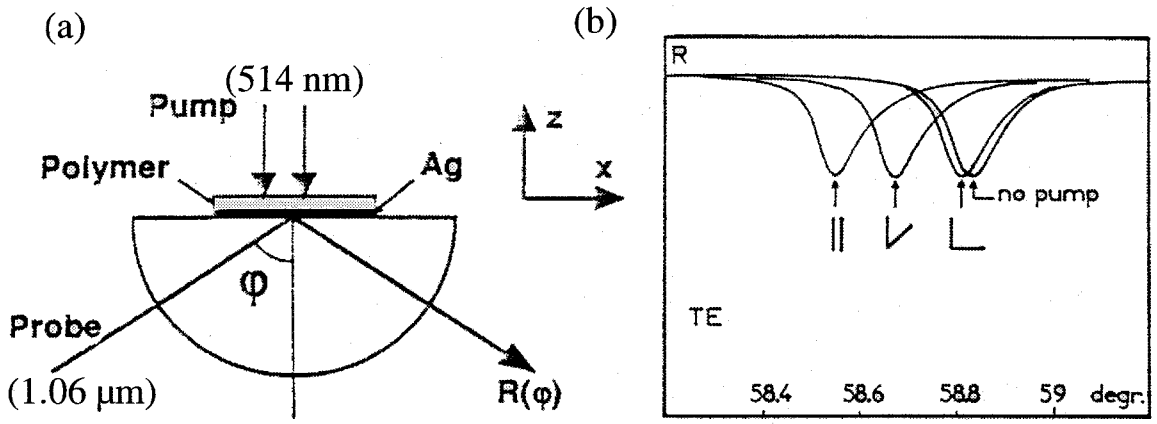


**Figure 1-3.** ATR experiment. (a)ATR Experimental arrangement. The probe is a 1.06 μm CW laser beam. Reflectivity is recorded as a function of the incidence angle for different pump polarizations. (b)Photoinduced shifts of a TE mode by a 514 nm pump beam polarization. The pump beam intensity was ≈140 mW/cm$^2$ but, for practical reasons, the pumping was operated through the halfsphere and the silver layer : a large part of the energy (~75%) was reflected back. The concentration of disperse red 1 (DR1) in PMMA is 5% (w/w). With parallel pumping the shift corresponds to $\Delta n_y = -3.6 \times 10^{-3}$. Ref. [6].

### 1-2-2 Azobenzene Derivatives in Polymer Matrix

The first photochromic polymer used as an optical recording medium containing an azo dye (methyl red or methyl orange) dispersed in a matrix of poly (vinylalcohol). In this system, optical dichroism and birefringence have been observed; however, the PIA birefringence only lasts a few tens of seconds.

It has been shown that polymers doped with azo derivatives such as DR1(disperse red one) did not yield stable PIA (only 35% of the orientation is conserved 1 h after the end of irradiation); on the contrary, the same polymer with covalently linked azo groups gives stable PIA (80% of the orientation is conserved) [8]. The higher the Tg, the larger the stability of the written materials. The written information can be erased either by heating the materials above Tg or by irradiating it with circularly polarized light.

The influences of different structural and external parameters have been examined in azo polymers to achieve the highest and most stable birefringence and/or dichroism. For example, Natansohn et al. [27] studied the effect of the size of the photochromic groups; they compared two polymers: poly (DR1M) and a similar polymer with a nitronaphthyl group instead of the nitrophenyl group (poly (NDR1M)), and they found that the poly (NDR1M) exhibited a slower writing rate, but there was no significant difference in the maximum birefringence achieved and in the relaxation rate. The same authors [28] synthesized a copolymer of methyl methacrylate containing a rigid group with two azo bonds, and measured a photoinduced birefringence higher by a factor of 5 than the birefringence inducible in a typical azo homopolymer containing a chromophore with only one azo group.

As the relaxation of the orientation is related to the free volume in the polymer, it is interesting to increase the Tg to freeze almost all molecular movement of polymer segments at room temperature. The problem is that photoisomerization can be hindered and become so slow that any PIA is prevented. Sekkat et al. [15-17] have found that photoisomerization of azobenzene derivatives still occurs in high-Tg polyimides whose structure is given in **Figure 1-4**. These polyimides differ in the method of incorporation of azo chromophore into the polyimide (PI) backbone. In PI-1 and PI-2 (Tg = 350° and 252°C, respectively), the chromophore (an azo group with donor and acceptor substituents) is incorporated rigidly into the backbone without any flexible connector, or tether. PI-3a and PI-3b (Tg = 228° and 210°C, respectively), on the other hand are side-chain polyimides where the azo dye is tethered to the main chain vis a flexible tether. The authors have shown that, in all these copolymer, trans → cis photoisomerization occurs, even at 325°C below Tg in PI-1. PIA is also observed in the four systems after irradiation with the polarized green light of a frequency-doubled $Nd^{+3}$ : YAG laser, but in contrast to PI-3b films, which do show some relaxation of the nonpolar orientation, a quasi-permanent orientation was induced in PI-1 and PI-2.

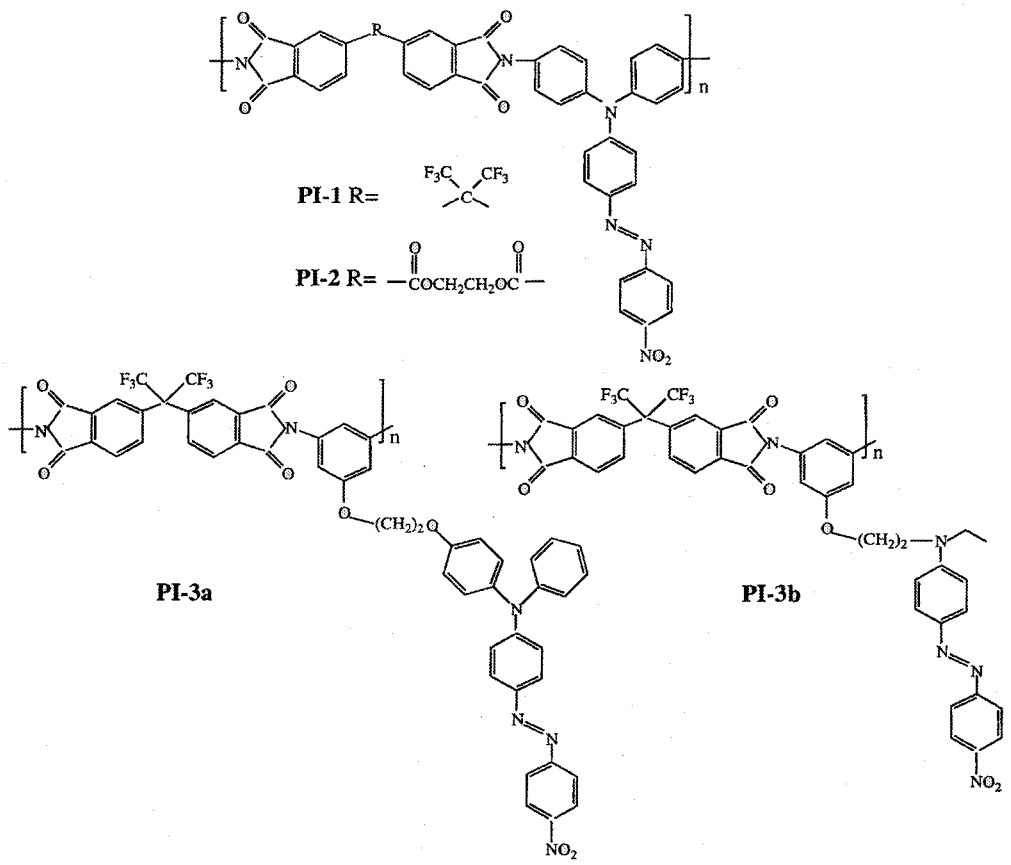


**Figure 1-4.** Structure of azo polyimides studied in PIA. Ref. [15-17].

The effects of temperature, irradiance, film thickness, and pressure on PIA dynamics and efficiency have also been studied recently. It has been shown that the growth and decay of birefringence signals can be fitted by a biexponential. Song et al. [29] found no change in rate constants for different pump irradiations; their data also show that the amplitude of the exponential describing the fast process increases linearly with pump irradiance. On the contrary, Natansohn et al. [30] found that both rate constants of the biexponential growth increase with increasing irradiance, as predicted by the three-level model of Sekkat and Dumont. Natansohn et al. also pointed out that three irradiance values used by Song et al. were in a domain which may appear linear in their results as well. Lagugné Labarthet et al. [26] have shown that the rate constants for birefringence are not connected with the rate constants for the trans → cis photochemical reaction, which can also be described by a biexponetial kinetics; they concluded that the values of the rate constants for birefringence growth were modulated by the rotational diffusion constants. As concerns temperature influence, Natansohn et al. [31,32] found that the absolute value of the photostationary order parameter decreases monotonically as a function of temperature, approaching zero as the systems restore their isotropic distribution

of chromophores around Tg. The rate constant for the fast process increases with increasing temperature for one of the polymers studied (poly(MEA)), and decreases for another one (poly(DR1M)). These opposite variations were interpreted as the result of two competing processes: on one hand, there is alignment due to the polarization of the laser; on the other hand, there is a tendency toward disorder and restoration of the equilibrium isotropy. Dipolar interactions present in poly(DR1M) seem to be the origin of the decrease of the rate constant for increasing temperatures. The same authors found no clear variation of the rate constant of the slow growth with temperature. On the contrary, Song et al. [29] found that both fast and slow rate constants had positive and almost equal activation energies (29 ± 2kJ·mol$^{-1}$). Film thickness also influences the maximum birefringence obtainable and growth rate. Natansohn et al. [31,33] argued that, due to large laser intensity absorption by the azobenzene moiety, the intensity of the writing beam decreases rapidly as it propagates through the specimen, thus leading to a decrease in rate constants. However, Song et al. did not find any variation of rate constants with film thickness. They only found a variation of preexponetial factors [29]. Pressure reduces the free volume and suppresses the photo-orientation of the chromophores in films of this polymer. G. Kleideiter et al. [18] showed that PIA by photoisomerization of a push-pull azobenzene chromophore flexibly tethered to a poly(methyl-methacrylate) polymer is hindered by hydrostatic pressure. They showed that the efficiency decreases with increasing pressure.

### 1-2-3 Self-Assembled and Langmuir-Blodgett Monolayers

Since the first studies of Blair et al. [34] dealing with the photoresponse of mixed monolayers of some polymers with photochromic spiropyrans and azo polymers, a lot of work on monolayers containing different photochromes has been done, stimulated by the research on command surfaces for liquid crystal alignment. Self-assembled monolayers (SAMs) are molecular films prepared by immersing a suitable substrate into a solution containing surface active molecules (azo-silane). The molecules then self-assemble at the solid-solution interface to a well-organized monomolecular layer with a structural order comparable to that of Langmuir films. Many examples are based on the O-Si bond formation between the silyl headgroup of amphiphile molecules and the polar silanol groups on glass or quartz substrates. One example of such a structure is given in **Figure 1-5** [13], with the hydrophobic tail bearing the azobenzene derivative. In these monlayers, the photoisomerization of the azobenzene group still occurs with a cis state thermally stable over several hours. UV dichroism and optical anisotropy are observed. Furthermore, it was

possible to follow the change of optical thickness during irradiation of the sample with UV light, which gives information about the reaction rates.

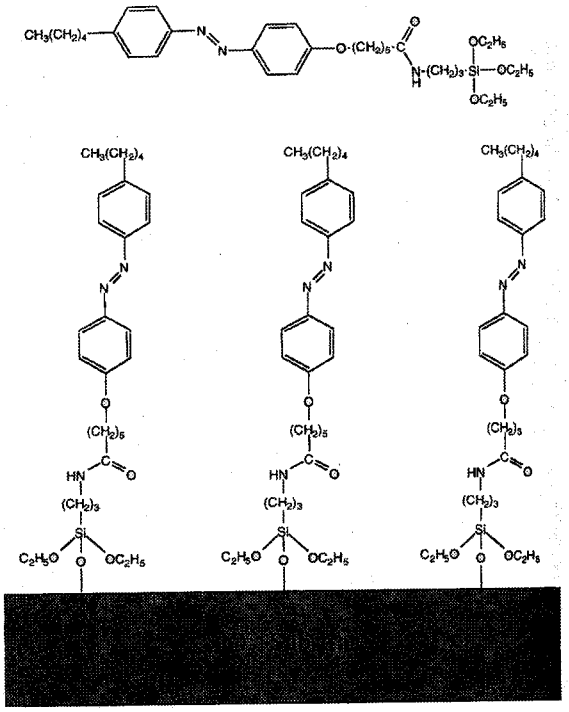

**Figure 1-5.** Top: structural formula of 4-[6-carboxy-(3-amidopropyl)triethoxysilane]-4'-pentylazobenzene, referred to in the text as azo-silane, which leads to a self-assembled monolayer. Bottom: idealized schematic drawing of a SAM on a $SiO_2$ substrate. Ref. [13].

Amphiphilic molecules can be deposited as monolayers at the air-water interface. These layers can be transferred to a solid support by dipping and withdrawing a suitable substrate through this well organized film. These so called Langmuir-Blodgett-Kuhn (LBK) layers have been studied during the last 20 years for potential applications in optical storage [35], nonlinear optical properties, and command surface of liquid crystal cells. Various techniques have been developed for the optical characterization of such ultrathin coatings. In LBK layers, reversible photoinduced birefringence was observed by the ATR (Attenuated Total Reflection) technique. The initial anisotropy induced by the depositing technique (out-of-plane refractive index being larger than the in-plane ones) was turned off by UV irradiation, and was restored under blue irradiation. However, in these LBK layers, no photoselection was observed, contrarily to the same systems deposited as amorphous films by the spin-cast technique. In other words, the changes of anisotropy observed in the LBK films were insensitive to the polarization of the

exciting light; this was interpreted as a consequence of the subtle manner of reorientation of the azo units imposed by the LBK deposition technique.

### 1-2-4 Dynamics of Photoinduced Anisotropy

On the basis of mechanisms found for azo dyes in polymers, Sekkat and Dumont developed in 1992 [7] a phenomenological theory for photo-orientation. The theory is based on a four-energy level diagram (**Figure 1-6**), which takes into account both the trans and cis populations and their respective orientation change upon photoisomerization. This model can also be applied to other photochromic systems such as spiropyran/photomerocyanine. Three different processes have been considered in this model (**Figure 1-7**): angular hole burning (AHB), angular redistribution (AR), and rotational diffusion (RD). Angular hole burning is due to the strongly anisotropic polarizability of the trans azo dye, whose transition dipole moment is oriented along the long axis of the molecule. A linearly polarized light beam selectively pumps molecules whose transition dipole moment axis is parallel to its polarization (probability $\propto \cos^2\theta$). As part of the excited trans molecules may relax to the ground state of the cis isomer, which has a relatively long lifetime (from a few seconds to infinity, depending on the photochrome), optical pumping produces an anisotropic depletion of the angular distribution of the trans isomer: this is AHB. As cis molecules generally absorb at the same wavelength, they can also be excited, but for the cis isomer of cyanomethoxyazobenzene, it has been shown that the polarizability tensor is almost isotropic, which will imply no AHB for the cis form. If AHB is the only mechanism, anisotropy disappears with the lifetime of the cis state. Experimentally, anisotropy has a longer lifetime than the cis state in doped polymers and can be permanent in copolymers. This can be explained by a rotation of the molecules during the trans $\rightarrow$ cis $\rightarrow$ trans photoisomerization cycle. This rotation (AR) may be spontaneous spherical, but a more realistic explanation is now that reorientation occurs during the isomerization reactions. In the absence of external field (which not be the case in photoassisted poling), the rotation is isotropic with respect to the initial direction of the trans molecule, but after several trans $\rightarrow$ cis $\rightarrow$ trans cycles, the result is an accumulation of molecules in the direction of the smallest probability of pumping, i.e., the direction perpendicular to the pump polarization direction, so AR amplifies and perpetuates the anisotropy created by AHB. On the reverse, rotational diffusion (RD), which is the rotational Brownian motion of molecules resulting from thermal agitation, tends to randomize the orientation and then to fill the distribution holes.

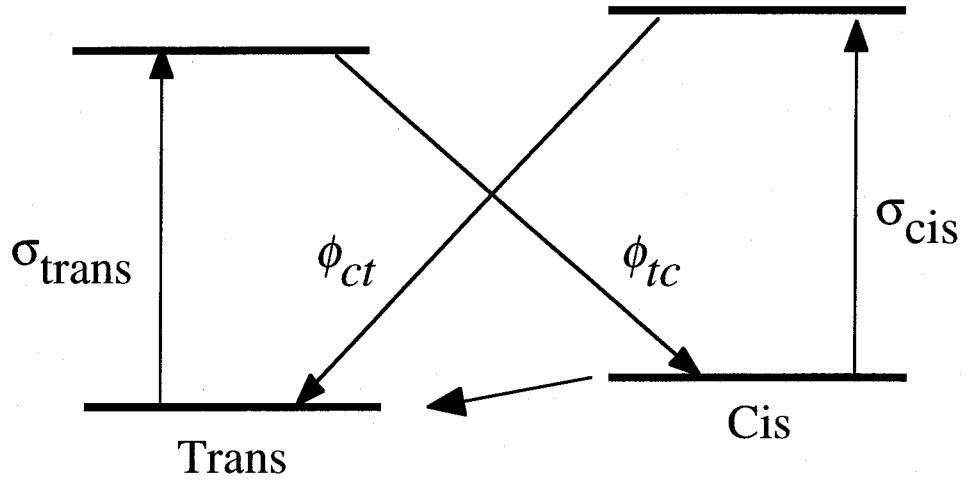


**Figure 1-6.** Four-level model for the photoisomerization process of azobenzene. $\phi_{tc}$ and $\phi_{ct}$ are the quantum yields for trans → cis and cis → trans conversions, respectively, and $\sigma_{trans}$ and $\sigma_{cis}$ are the extinction coefficients for trans and cis states.

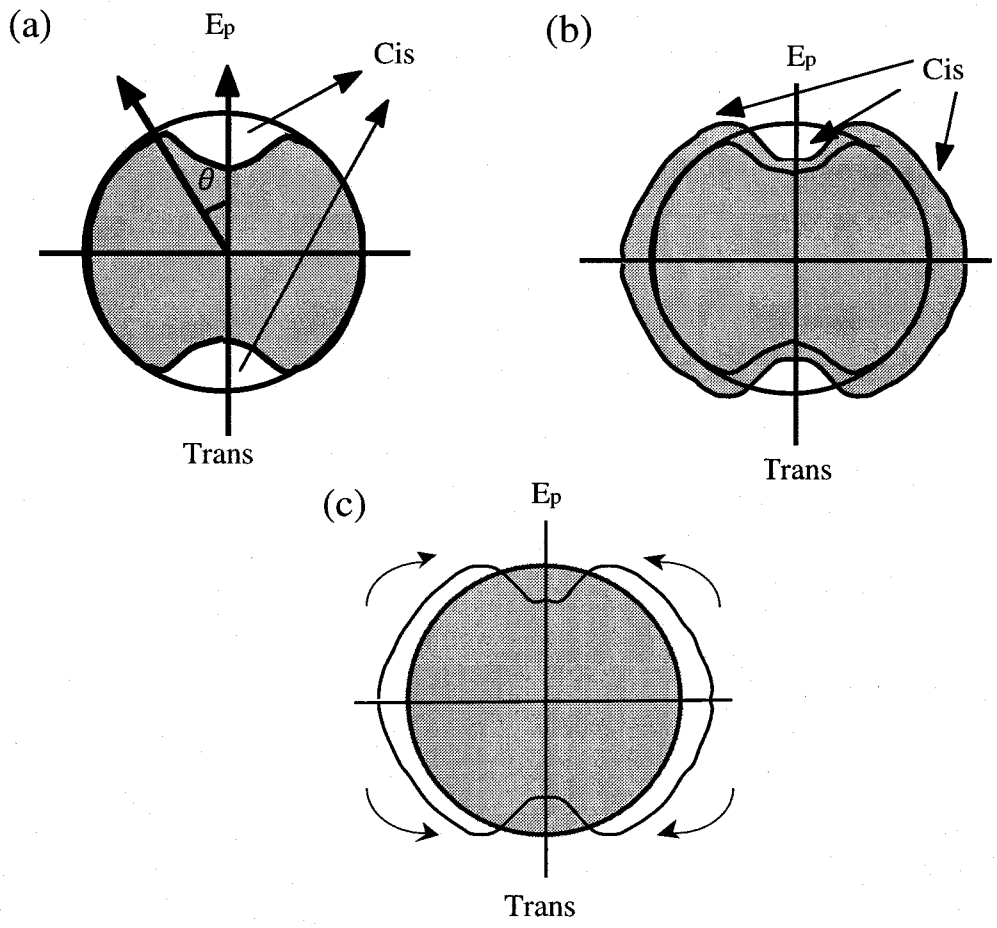


**Figure 1-7.** Three different photoinduced processes. (a)angular hole burning (AHB), (b)angular redistribution (AR), (c)rotational diffusion (RD)

### 1-2-5 Applications

The first application was developed by Todorov et al. [3,4] who used azo polymers to register polarization holograms. Such holograms are recorded with two interfering light beams whose linear or circular polarizations are perpendicular, contrary to ordinary holographic gratings (intensity gratings) where both beams have parallel polarizations. In the last case, the light intensity is sinusoidally modulated; in contrast, in the first case, the intensity of resulting light field is constant, and only its polarization is periodically and spatially modulated in accordance with the change of phase shift between the two beams. In azo polymers, this modulation created a spatially modulated refractive index anisotropy. Polarization holography was thought to give higher efficiencies (up to 50%) than ordinary holography, because of the strong absorption of photochromes which limits the penetration of light in the depth of the films. However, ordinary holography has also been developed in liquid crystal polymers [36], and because of cooperative effects described above, efficiencies as high as 80% have been obtained [37].

Photoinduced birefringence in copolymers with azo derivatives has also been proposed for reversible optical data storage as PIA can be created and erased many times, as long as photodegradation processes are avoided.

Photoinduced birefringence can also be used to pattern optical waveguides, which are necessary for the development of passive and active devices in integrated optics for telecommunications. Besides photoinduced birefringence, photobleaching or a photoinduced homogeneous refractive index change of materials doped with different photochromes has also led to the fabrication of efficient waveguides and optical elements. The relative contribution of the isotropic and anisotropic parts of photoinduced changes in the refractive index of azo dye/polymer systems has been determined, and it has been concluded that the induced anisotropy is related to the dye molecules which are involved in reversible photoisomerization, whereas the isotropic changes, which are stronger, are related to the polymer matrix as well.

## 1-3 Second-Order Nonlinear Optical Properties

### 1-3-1 Principle

Although in this thesis there is no studies related to photoisomerization induced NLO effects, it is informative to know the full potential of photo-orientation by photoisomerization, especially that of photo-induced quadratic and cubic optical nonlinearities. A brief recall of nonlinear optics is important at this point.

Comprehensive treatments of the physics of NLO originating from interaction of atoms and molecules with light can be found elsewhere. Electric field ($E_a$), such as an applied dc field or a propagating electromagnetic wave, always induces displacements of the electrons cloud. In an applied oscillatory field, the electrons will oscillate at the applied frequency. At low field strengths, the magnitude of such an induced polarization will be proportional to the applied field. At high field strengths, the polarization is no longer linear. To account for this nonlinearity, it is common to develop the dipole moment $\mu$ of the molecule as a power series expansion in the local electric field $E_L$:

$$\mu = \mu_0 + \alpha E_L + \beta E_L E_L + \gamma E_L E_L E_L + \ldots \qquad (1\text{-}1)$$

In this equation, $\mu_0$ is the permanent dipole moment of the molecule, $\alpha$ is the linear polarizability, $\beta$ is the first hyperpolarizability, and $\gamma$ is the second hyperpolarizability. $\alpha$, $\beta$, and $\gamma$ are tensors of rank 2, 3, and 4, respectively. Symmetry requires that all terms of even order in the electric field of the above equation vanish when the molecule possesses an inversion center. This means that only noncentrosymmetric photochromic molecules will have second-order NLO properties. In a dielectric medium consisting of polarizable molecules, the local electric field at a given molecule differs from the externally applied field due to the sum of the dipole fields of the other molecules.

Molecules possessing the largest $\beta$ coefficients contain donor and acceptor substituents linked through an intervening π-backbone. Paranitroaniline is a classical model for these push-pull nonsymmetric molecules. Molecular engineering of this kind of structure has been developed during the 20 years to increase the $\beta$ values. This has been done by using more potent donating or accepting moieties or increasing the conjugation length between the substituents. Photochromic compounds, which are generally π-conjugated systems, have potential NLO properties. As the colored form is more π-conjugated, we may expect a higher $\beta$ value. The possibility to switch between two different NLO responses by irradiation of a material having both NLO and photochromic properties is attractive for application in optical signal processing.

In second-order NLO, molecules with high quadratic hyperpolarizability ($\beta$) and, on a macroscopic scale, materials with high nonlinear susceptibility ($\chi^{(2)}$) are targeted. $\beta$ and $\chi^{(2)}$ are responsible for NLO efficiency. Both are third-order tensors, and noncentrosymmetry (respectively on molecular levels and macroscopic scales) is necessary to get nonzero values. Since $\chi^{(2)}$ is a geometry-sensitive average of $\beta$ over all the molecules contained in a volume unit (**eq. (1-2)**), molecules have to be gathered in a noncentrosymmetric fashion (**Figure 1-8**).

$$\chi^{(2)} = \frac{\sum \beta}{V} \qquad (1\text{-}2)$$

(a) Centrosymmetric medium : $\chi^{(2)} = 0$

(b) Noncentrosymmetric medium : $\chi^{(2)} \neq 0$

**Figure 1-8.** Centrosymmetric (a; $\chi^{(2)} = 0$) and noncentrosymmetric (b; $\chi^{(2)} \neq 0$) media. Arrows represent the dipole moments of molecules.

### 1-3-2 Photoassisted Poling (PAP)

The most widely employed method (**Figure 1-9**) [38] to obtain a poled structure in a polymer is to heat a thin film up to its glass transition temperature (Tg), to apply a high dc voltage, and finally to cool the sample to room temperature with the voltage still on. A static field ($E_0$) of a few MV·cm$^{-1}$ is applied across the sample, either by putting the sample between two electrodes or by corona discharge. This process is called thermally assisted poling (TAP)

When the material is photochromic, a process based on photoisomerization can be employed. However, compared to PIA, the application of a dc electric field (poling field) in addition to the pumping beam which induces photoisomerization is necessary, since the symmetry of the latter does not allow the creation of a noncentrosymmetric order. The PAP technique was first reported by Sekkat and Dumont in 1992 [7]. The experimental setup commonly used is shown in **Figure 1-9**. This configuration allows the application of optical pumping and a subsequent and/or simultaneous dc electric field. In appropriate materials, the so-called PAP process allows to create a noncentrosymmetric order even below the Tg to be created. Compared to TAP, heat is replaced by optical pumping, which enables the molecules to get into motion.

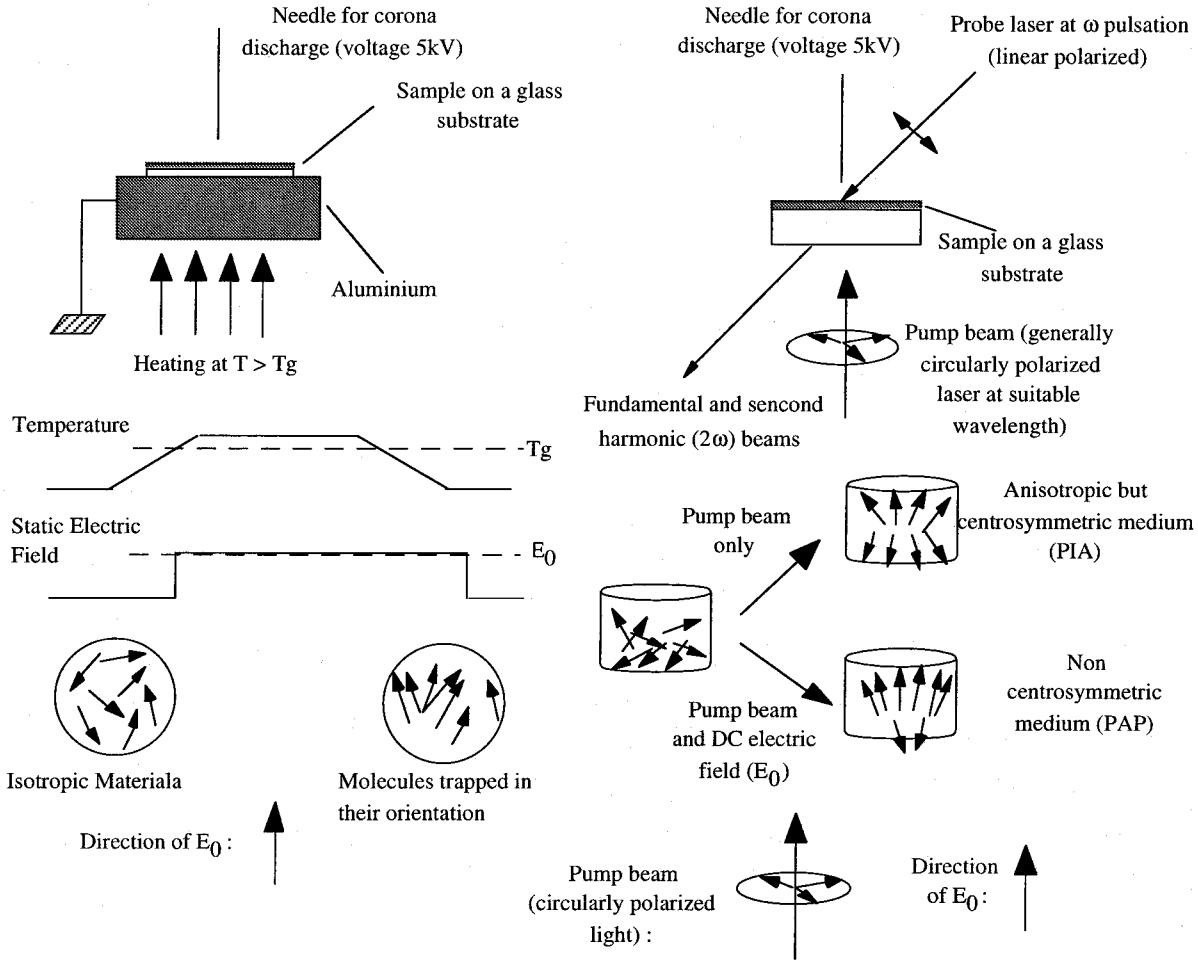


**Figure 1-9.** Poling methods for amorphous polymers. Upper left: setup for TAP, which allows heating to the glass transition temperature (Tg) and application of a poling electric field ($E_0$) by corona discharge. Lower left: time sequence for TPA, showing the application of $E_0$ when the sample is cooled from Tg to room temperature. Upper right: setup for PAP by the application of $E_0$ and a pump beam at a suitable wavelength for photochromic reaction. A prove beam (e.g., a $Nd^{+3}$ : YAG nanosecond pulse laser, 1064 nm) allows second harmonic generation (SHG) measurements. Lower right: schematic view of the PAP mechanism compared to that of PIA. In both cases, molecular dipoles line up perpendicular to the pump beam's polarization. $E_0$ breaks the symmetry between "upward" and "downward" orientations. Ref. [38].

SHG, ATR, and stark (electroabsorption) spectroscopy were employed to evidence PAP. The first examples arise from PMMA doped with DR1, and poly(DR1M-co-MMA) (**Figure 1-10**) [7]. The initial appearance of the electrooptic signal at the onset of E is due (partly in the case of the doped polymer and totally in the case of the side-chain polymer) to the Kerr effect, which does not require poling.

The subsequent increase of the electrooptic signal is the poling process itself that occurs during the trans → cis isomerization cycles. It is due to the noncentrosymmetric order created by photoexcitation under a dc electric field. After the dc electric field is switched off, the electrooptic signal is maintained. This evidences the achievement of a poled structure. In the case of the doped polymer, it is worthwhile to note that some chromophores can orient even when optical pumping is not applied; however, there is no remnant poling when the poling field is removed. In terms of the NLO response as well as orientational stability after poling, the side-chain copolymer turned out to be a better material (**Figure 1-10**). An electrooptic coefficient $\gamma_{33}$ of 5.7 pm·V$^{-1}$ 40 h after the poling process and a $d_{33}$ of 7-10 pm·V$^{-1}$ measured by SHG 1 h after the poling process [8] are reported for the side-chain copolymer. In this polymer, photoisomerization during PAP pulls on the polymer main chain, leading to a stabilizing rearrangement. PAP with a pulsed pump beam was also reported [39].

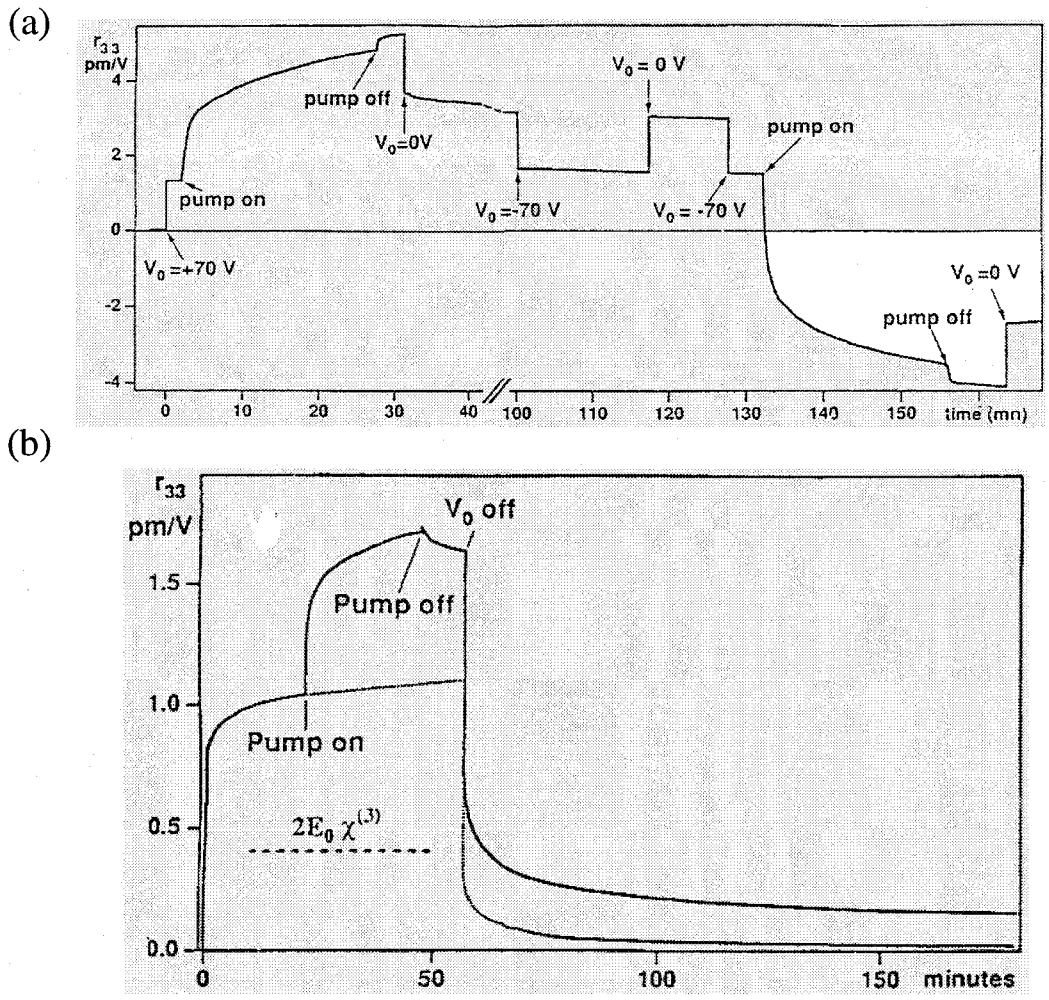


**Figure 1-10.** PAP of DR1 polymer films (thickness around 1 μm) monitored by the ATR technique. $V_0$ is the voltage corresponding to the poling electric field. The

pump beam is an argon ion laser (circularly polarized, 488 nm). (a) Poly (DR1M-co-MMA) copolymer (pump intensity ca. 30 $mW \cdot m^{-2}$), after the poling sequence (0 - 40 min); the effect of a reverse electric field with and without optical pumping is shown (100 - 170 min). (b) DR1-doped PMMA (pump intensity ca. 8 $W \cdot m^{-2}$). The dotted line shows the effect of $V_0$ alone. Both curves show that, though the electric field alone yields an electrooptic signal ( $\gamma_{33}$) due to $\chi^{(3)}$, there is no remnant $\gamma_{33}$. Ref. [7].

PAP was applied in other polymer materials of spiropyran/photomerocyanine (nitro-BIPS, **Figure 1-11** [40]) in PMMA. Compared to DR1, the unstable photoisomer (photomerocyanine) is more stable, and the gap between the dipolar and polarizability properties between the isomers is larger. This provides particular interest, since separate contributions of the photoassisted process and spontaneous thermal diffusion process could be evidenced and compared. By analogy to what is observed with mechanical stress, the angular mobility was proved to be dependent on the time sequence of the application of optical pumping and of a dc electric field. The shorter delay between both, the higher the efficiency. In addition, a simultaneous application of both perturbations yields a more efficient orientation than a consecutive one (**Figure 1-12** [41]), which evidences a synergistic effect of the dc field and optical pumping. According to these results, the volume created around the photochromic species during photoreaction allows easier rotation, and thus poling of the chromophores.

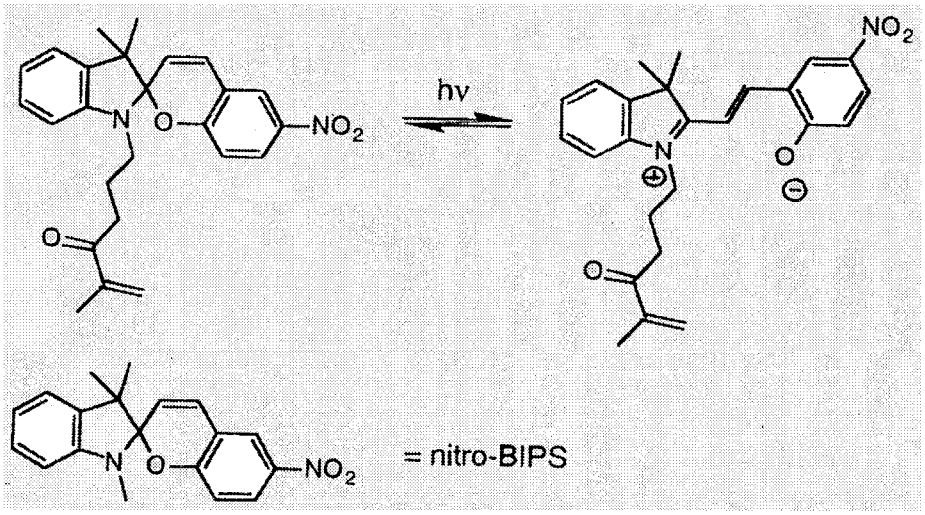


**Figure 1-11.** Light-induced activation of second-order NLO properties base on aggregation of photomerocyanine (right). This product is obtained from photochromic nitro-BIPS-type spiropyran (left). Ref. [40].

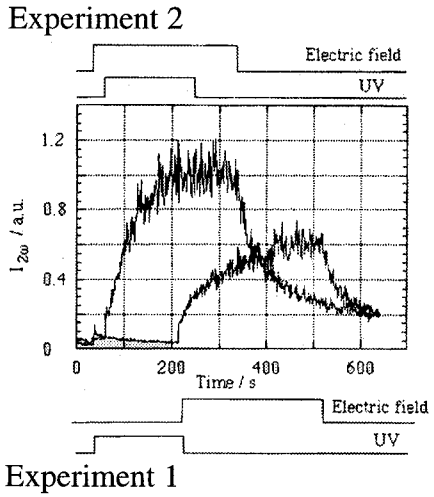


**Figure 1-12.** PAP on a spiropyran (nitro-BIPS, **Figure 1-11**) doped PMMA film (25% w/w) probed by SHG ($I_{2\omega}$) at 1064 nm, pumping at 355 nm, 10 $mW \cdot cm^{-2}$. Experiment 2 (simultaneous poling and pumping) yields a higher SHG signal than experiment 1 (poling after pumping). Ref. [41].

### 1-3-3 All-Optical Poling (AOP)

A monochromatic wave is centrosymmetric and thus cannot induce noncentrosymmetry by itself. Hence, In PAP based on the excitation of photochromes in their absorption band, superimposition of a dc electric field is needed.

Another way to induce noncentrosymmetry is all-optical poling(AOP). A coherent superposition with the appropriate phase difference of two optical waves, one at the frequency ω and another at 2ω, yields a noncentrosymmetric resultant field, E, by combination of the respective electric fields $E_\omega$ and $E_{2\omega}$ (**Figure 1-13** [42]). In other words, E makes the difference between "upward" and "downward" molecules, and can be differently selected. For a given location, the quadratic susceptibility ($\chi^{(2)}$) is proportional to $<E^3>$, the time average of $E^3$. A nonzero value of $<E^3>$ breaks centrosymmetry, and thus induces polarity. An induced susceptibility ($\chi^{(2)}_{ind}(z)$ at abscissa z) is created, as expressed in **eq. (1-3)**. ΔΦ and Δk are, respectively, the phase and the wave vector differences between the two beams, and α is the absorption loss coefficient at 2ω (absorption loss at ω is neglected).

$$\chi^{(2)}_{ind}(z) \propto \left|E^2_\omega E^*_{2\omega}\right| \cos(\Delta\Phi + \Delta k z) \exp(-\frac{\alpha}{2} z) \qquad (1\text{-}3)$$

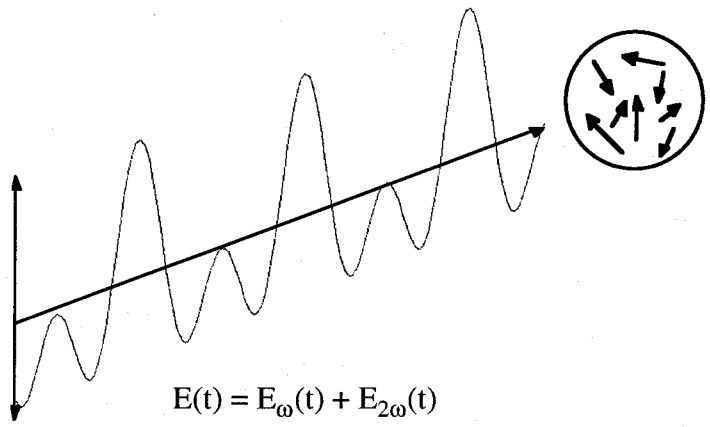


**Figure 1-13.** Noncentrosymmetric field E resulting from the combination of $E_\omega$ and $E_{2\omega}$. Excitation of a centrosymmetric arrangement of molecules yields a noncentrosymmetric order. Ref. [42].

The first examples of AOP were reported on tetrahydrofuran solution of 4-diethylamino-4'-nitrostilbene [43], and poly(DR1M-co-MMA) [44]. The experimental configuration to achieve this is shown in **Figure 1-14** [43]. During the first step of the process, linearly polarized ω and 2ω beams (respectively beam 1 and beam 3) are applied. This is called the seeding process. Then, beam 3 is stopped, and the achievement of a polar order is evidenced by the generation of beam 4 at 2ω. Forward (beam 1) or backward (beam 2) configuration are possible for the ω beam. The former is reported to lead to more efficient seeding than the latter.

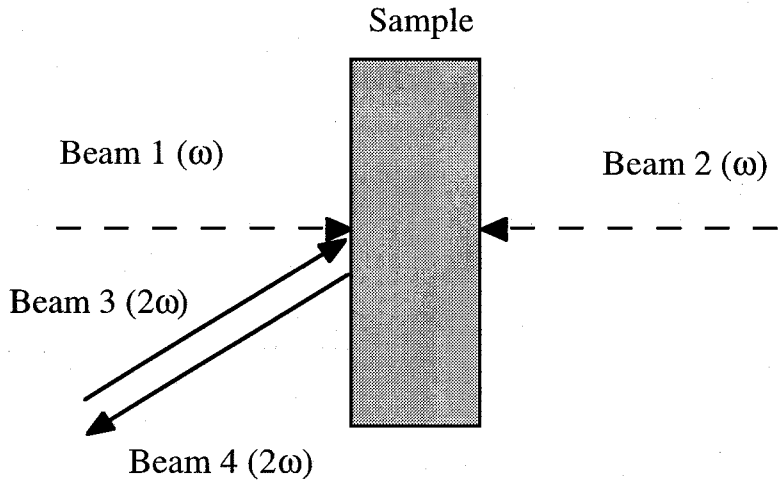


**Figure 1-14.** Beam configuration for AOP. During seeding, beam 3 (2ω) is combined with beam 1 (ω, forward configuration) or beam 2 (ω, backward configuration). After seeding, beam 3 is stopped, and SHG (beam 4) is generated due to the polar order created in the sample. Ref. [43].

The mechanism is interpreted as a light-induced excitation of chromophores, leading to orientational hole burning and angular redistribution. However, compared to the case of PAP where excitation at only one wavelength is considered, each process involved in AOP is composed of three terms, respectively originating from ω-excitation, 2ω-excitation, and the interference between both. The orientation dynamics depends on the value of $|E_{\omega}^{2}E_{2\omega}|$, whereas the seeding ratio ($|E_{2\omega}E_{\omega}^{2}|$) has to be optimized if one seeks high $d_{33}$ values. The highest values in poly (DR1M-co-MMA) were estimated at around 70 pm·V$^{-1}$ [45].

It has also been demonstrated that, in dispersive materials such as polymers, the periodicity of the field pattern written in the sample corresponds to the coherence length, and phase matching can be achieved by AOP [46,47]. SHG is thus proportional to the square of the optical path length. Other studies concern the use of circularly polarized seeding beams [48].

Up to now, only DR1-type photochromes were used in AOP. The comparison between DR1-doped PMMA and the side-chain equivalent, poly (DR1M-co-MMA), showed the influence of the rotational diffusion constant on the poling growth rate and on the maximum SHG activity. There is a trade-off between matrix rigidity and photoinduced reorientation efficiency. The higher diffusion in the guest-host polymer compared to the side-chain analogue results in faster growing (3 times), but in a lower value of SHG(2.5 times) [47].

AOP was also reported in rigid polyimides. The influence of the seeding temperature on the maximum $d_{33}$ value as well as on the orientational stability was studied. The $d_{33}$ value ranged from 2.6 pm·V$^{-1}$ (seeding at room temperature) [49] to 6.9 pm·V$^{-1}$ (seeding at 150°C). Stable patterns (seeding at 150°C) [50] of optical recording readable by an IR probe were thus written. Seeding rates as well as relaxation rates after seeding are compared between PMMA and polyimide matrixes. As expected, both seeding and relaxation occur faster in PMMA [51].

PMMA with low absorbing chromophores (DR1 analogue bearing a phosphine oxide instead of a nitro group) [52] exhibits a NLO activity ($d_{33}$ = 8 pm·V$^{-1}$). Trade-off between NLO efficiency and transparency is in an important problem, and such a chromophore is particularly interesting.

This poling method is not limited to photochromes, and can also be applied to molecules which absorb neither ω nor 2ω. Examples are N, N-diethylnitroaniline side-chain PMMA [53], and ethyl violet in propanediol [54] and in a hybrid(sol-gel) matrix [55]. Ethylviolet is an octupolar molecule (noncentrosymmetric and non dipolar) with significant quadratic hyperpolarizability.

AOP leads naturally to a phase-matched pattern [53], which is advantageous for applications. Adding the fact that a wide range of systems such as nonphotochromic,

nondipolar molecules as well as rigid polymers can be poled by AOP, it can be considered as a powerful method.

### 1-4 Surface Relief Gratings

In 1994, Rochon et al. [56,57] found large surface relief gratings could be directly recorded at room temperature on azobenzene-containing polymer films using two interfering polarized Ar ion laser beams. Tripathy et al. [58-60] have also produced high efficiency surface gratings from azo side-chain high Tg polymers. The experimental setup used by these authors and an example of a surface relief grating registered by this method and observed by atomic force microscopy (AFM) are given in **Figure 1-15** [61].

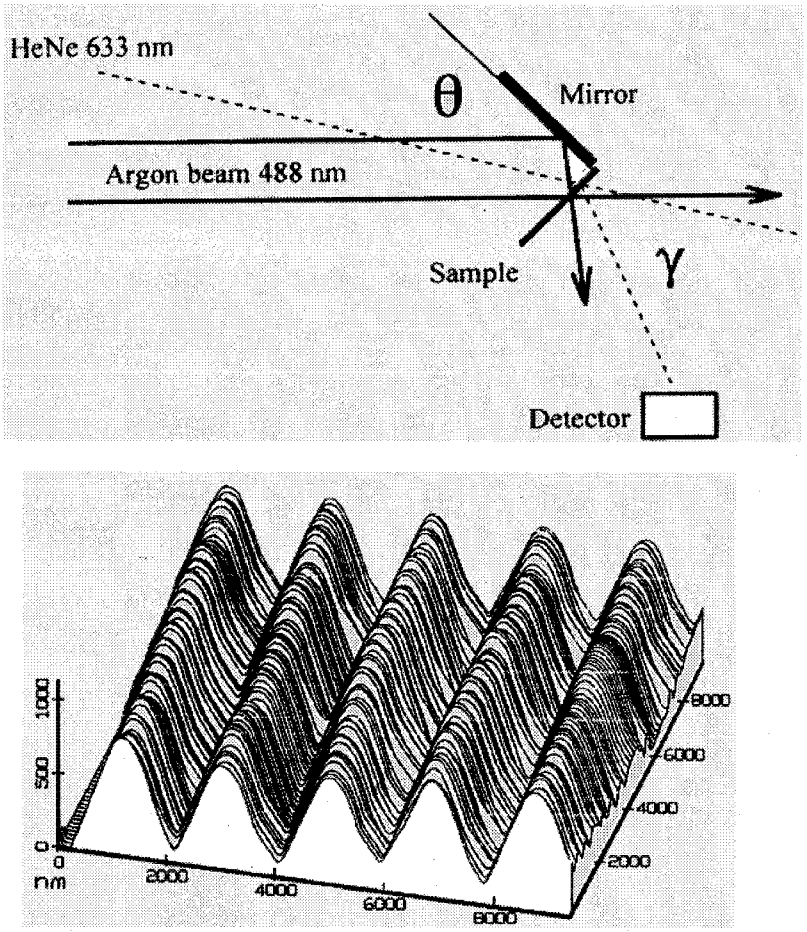


**Figure 1-15.** Optically inscribed diffraction gratings in azo polymer films. Upper part: experimental setup for grating inscription. Lower part: atomic force microscope surface profile of an optically inscribed grating in a poly(DR13A) copolymer. Ref. [61].

The gratings were optically inscribed onto the films with a single beam of an argon ion laser (488 nm, irradiation power : 1 ~ 100 mW) split by a mirror and reflected coincident onto the film surface which is fixed perpendicular to the mirror. Quarter wave plates are used to change the beam polarization from linear to circular, and the diffraction efficiency is monitored by measuring the first-order diffracted beam of a 1 mW, 633 nm beam from a He-Ne laser. Changing the incidence angle of the writing beam allows the intensity profile spacing on the sample, and then the grating spacing, to be changed. In such conditions, irradiation of the polymer films during a few seconds with intensities of 5-200 $mW \cdot cm^{-2}$ produces reversible volume birefringence gratings, with low diffraction efficiency (less than 1%). If the film is exposed to the writing beam for longer than a few seconds, an irreversible process begins, creating an overlapping and highly efficient surface grating written on the time scale of minutes, so there is an initial and rapid growth (on the order of seconds) corresponding to the production of the reversible volume birefringence grating, and then a slower and irreversible process (of the order of minutes) which creates surface gratings observed by AFM, with efficiencies up to 50%. It has been established that the phase relationship between the surface and volume gratings is such that the light intensity maxima of the fringes coincide with the surface profile minima [57]. Also, from dynamical experimental studies and polarization analyses of the transmitted ±1 order diffraction beams during recordings, the contributions of the two distinct processes (i.e., the formation of a birefringence grating and of a surface relief grating) have been clearly characterized, and quite interesting different results on DR1 dye-doped and -functionalized polymer films have been put into evidence [62]. Once written till saturation of the diffraction efficiency, the grating profile is not photoerasable either by linearly or circularly polarized light or by long-term exposure to moderate power probe beams. However, if the gratings are inscribed at modest intensities, Tripatht et al. [63] demonstrated that it was possible to erase the gratings under specific polarization conditions for both the writing beam and the erasing beam. In any case, the gratings can be erased thermally by heating the polymer film to Tg. Once a grating is written, another gratings can be inscribed, superposed on the first one. Up to 10 coincident gratings have been stored with good resolution [61]. Tripatht et al. [59] and Barrett et al. [61] agree that, when exposed to the same fluence and intensity of light, the samples with grating spacing near 0.8 μm present the largest surface modulation depth.

The influence of the polarization of both writing beams on the diffraction efficiency is an important observation which is not completely understood. Tripathy et al. [59] have shown that when both writing beams are p-polarized (polarization parallel with the incidence plane), diffraction efficiency is larger than when both

beams are s-polarized (polarization perpendicular to the incidence plane) [59]. More precisely, the maximum efficiency (27%) and the maximum surface modulation (360 nm, for an initial thickness of 800 nm) are observed when both beams are polarized at 45° with respect to s-polarization [64]. **Figure 1-16** shows the dynamics of the increase of diffraction efficiency in these polarization conditions, for a laser intensity of 55 $mW \cdot cm^{-2}$. This figure puts into evidence the two distinct processes discussed above: a fast increase during the first 60 s, which is due to birefringence, and a slow and large increase during almost 1 h, due to the surface relief.

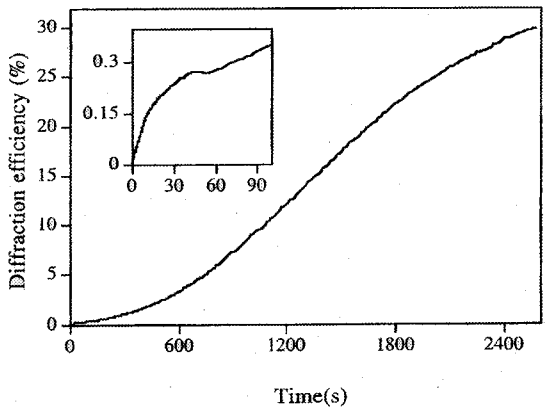


**Figure 1-16.** Diffraction efficiency as a function of time under a mixed recording condition (both beams are polarized at 45° with respect to s-polarization). The inset shows the initial stages of the grating formation. Ref. [64].

It has been observed by several authors [57,60] that illuminated regions of the grating correspond to pits and dark regions to peaks of the surface, except in the case of a side-chain liquid crystalline polyester of low Tg where the opposite result was obtained [65]. More surprising is the fact that irradiation of the film with a polarization grating resulting from the interference of two orthogonal circularly polarized beams also creates the largest surface modulation (> 350 nm) although the total intensity across the film is constant in this case [64]. Such a result has been confirmed by three other groups [65-69]. Very recently, Ramanujam et al. have demonstrated that it is possible to obtain surface gratings in an azobenzene side-chain polyester(Tg = 63°C) after irradiation by the single pulse of a Q-switch frequency-doubled $Nd^{3+}$:YAG laser (532 nm, 5-7 ns duration, energy of 10 mJ) [70]. After exposure, AFM investigations reveal the presence of a surface relief grating with a surface modulation greater than 400 nm for a spatial frequency of 160 lines $mm^{-1}$. In this case, the depth modulation was concomitant with a refractive index modulation, both reaching a steady-state value less than 10 s after the end of the

pulse, so it appears that, at least in this low-Tg polymer, one pumping cycle alone per azo derivative is enough to induce birefringence and surface relief.

Since the first observations, it was recognized by different authors that the mechanism at the origin of surface relief gratings was neither a swelling due to light absorption nor an ablation process in the regions of high intensity [56-59]. The process is also connected with the photoisomerization process of azobenzene derivatives. All the models proposed so far agree with the need of a mass transport well below Tg, but they cannot explain all the phenomena induced.

Approaches to the unique application possibilities of surface relief gratings have only been recently explored [71-73]. Such gratings could be considered for applications such as holographic storage, optical filters, and resonant couplers. For example, subwavelength gratings could be made by this approach, which could be used in the making of wave plates and antireflection surfaces for the visible. Rochon et al. have made selective wavelength light couplers for slab waveguides by this process [71,73]. The major advantages of this process are (1) the easy one-step processing, without any development, (2) large surface modulation, and (3) precisely controlled modulation depth [74]. The new demonstration of recording holograms after 5 ns exposure opens the door to instant holography, with possible applications in holographic cinematography [70].

### 1-5 Spectrally Distinguishable Photo-isomers of Spiropyran and Diarylethene

As presented above, the main research on photo-orientation is so far focused on azobenzene derivatives. Absorption bands of a trans and cis isomer of azobenzene derivatives are overlapped(see **Figure 1-17**), so it is difficult to distinguish the photo-orientation processes induced by trans $\rightarrow$ cis and cis $\rightarrow$ trans isomerization. Since the thermal decay time of the cis isomer of azobenzene derivatives is very short such as a few seconds, it is also difficult to measure the processes. Compared to the azobenzene derivatives, both isomers of spiropyran and diarylethene are spectrally distinguishable as shown in **Figure 1-18** [6]. The stable and thermally unstable isomers are henceforth referred to in the text as the A and B isomers, respectively. In the visible region, only B isomer of both spiropyran and diarylethene has an absorption band. We can individually evaluate the photo-orientation processes of each A $\rightarrow$ B and B $\rightarrow$ A isomerization. While B isomers of spiropyran are thermally unstable, ones of diarylethene are stable. We can also distinguish the both photo- and thermal- isomerization processes. Spiropyran and diarylethene have been extensively studied, because they have potential for data storage. Especially, diarylethene can be used for rewritable high density data recording by two-photon absorption. Studying spiropyran and diarylethene

improve the understanding of the photo-orientation in photoisomerizable chromophores.

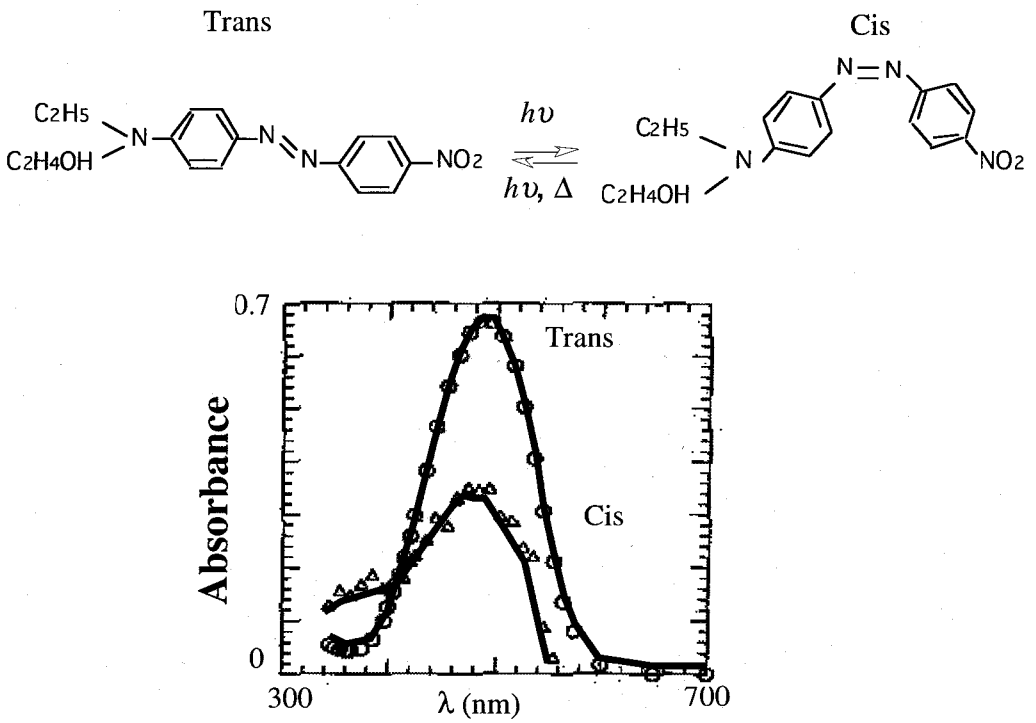


**Figure 1-17.** Upper : chemical structure and isomerization of DR1. Lower : absorption spectra of DR1-trans and cis. Ref. [6].

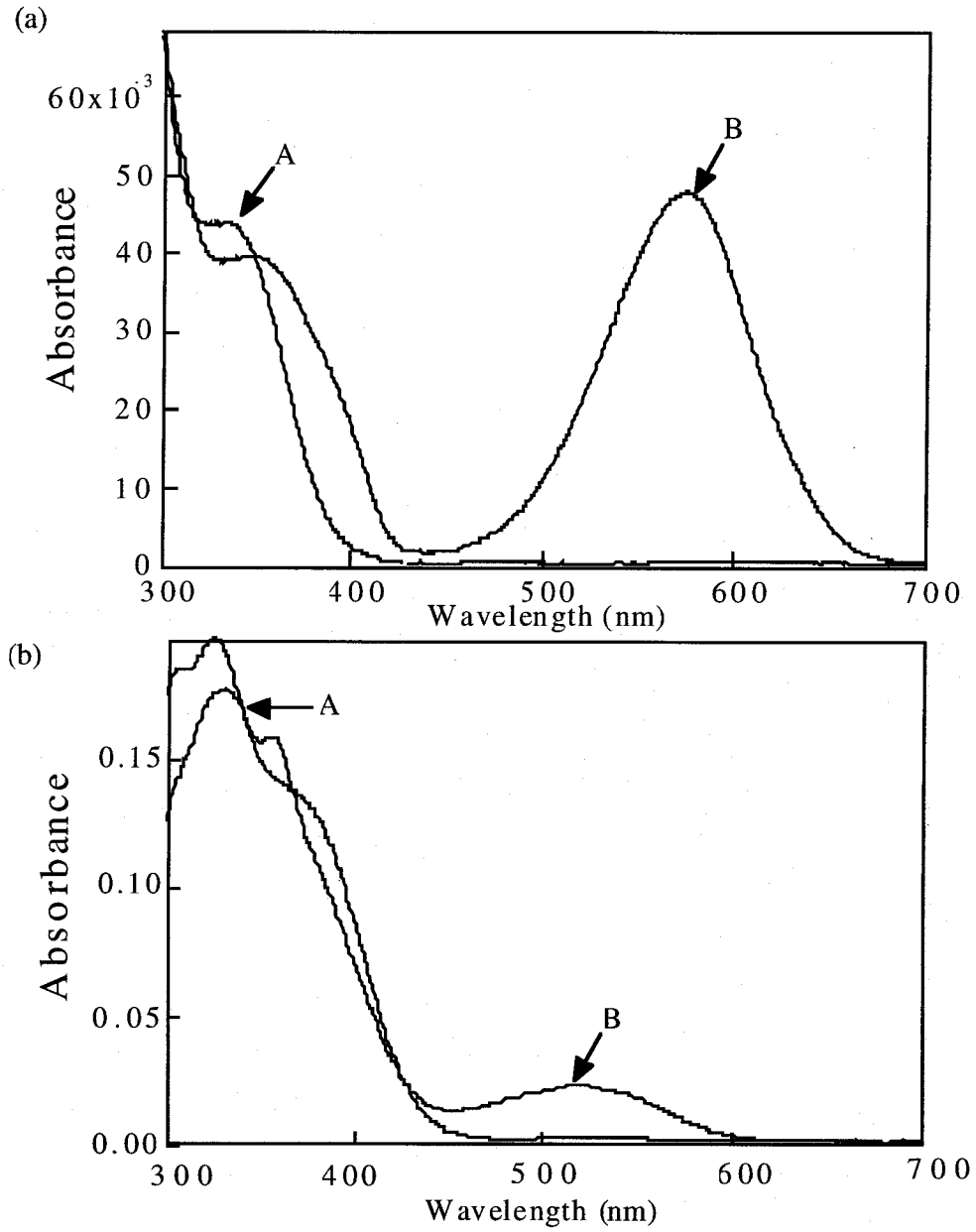


**Figure 1-18.** (a) Absorption spectra of spiropyran (a) and diarylethene (b) before and after UV irradiation to the photostationary state.

Chapter 2

# Basic Photochemical Properties of Spiropyrans and Diarylethenes in Polymer Matrix

Before studying the photo-orientation processes of SP and DE, I investigated basic photochemical properties of them. Sample film preparation is based on spin-coating technique. Thermal decay constants were measured from absorbance changes in real-time. Spectral changes induced by UV and visible light, in which isosbestic points were clearly observed, demonstrate the photoisomerization reactions of chromophores in PMMA matrix. Photodegradation results from side reactions or molecular destruction are discussed.

## 2-1 Sample Preparation

The structure formula of 1,2-dicyano-1,2-bis-(2,4,5-trimethyl-3thienyl)ethene, and 6-nitro-1',3',3'-trimethylspiro[2H-1-benzopyrane-2,2'-indoline], referred to in the text as DE and SP, respectively, and their photochemical isomers are shown in **Figure 2-1**. The DE and SP chromophores have two photochemical isomers, a stable isomer and a thermally unstable isomer, namely the open-ring and close-ring forms for DE, and the spiropyran and photomerocyanine for SP. Light irradiation produces photoreaction in both the A $\rightarrow$ B and A $\leftarrow$ B directions, and the thermal reaction proceeds in the A $\leftarrow$ B direction. In contrast to the colored photomerocyanine (PM) form which usually fades after several minutes at room temperature , the colored close-ring form of DE is stable for more than 3 months at 80°C [75]. Both of the A and B isomers of DE and SP can absorb UV light and simultaneously induce the A $\rightarrow$ B and A $\leftarrow$ B photoisomerizations. When either of DE or SP is irradiated with visible light, only the B isomer can appreciably absorb light and induce the A $\leftarrow$ B photoisomerization. In other word, the A and B forms of the chromophores studied and the related photochemical and photophysical processes can be individualized inasmuch as the spectral features of the photochemical isomers can be distinguished.

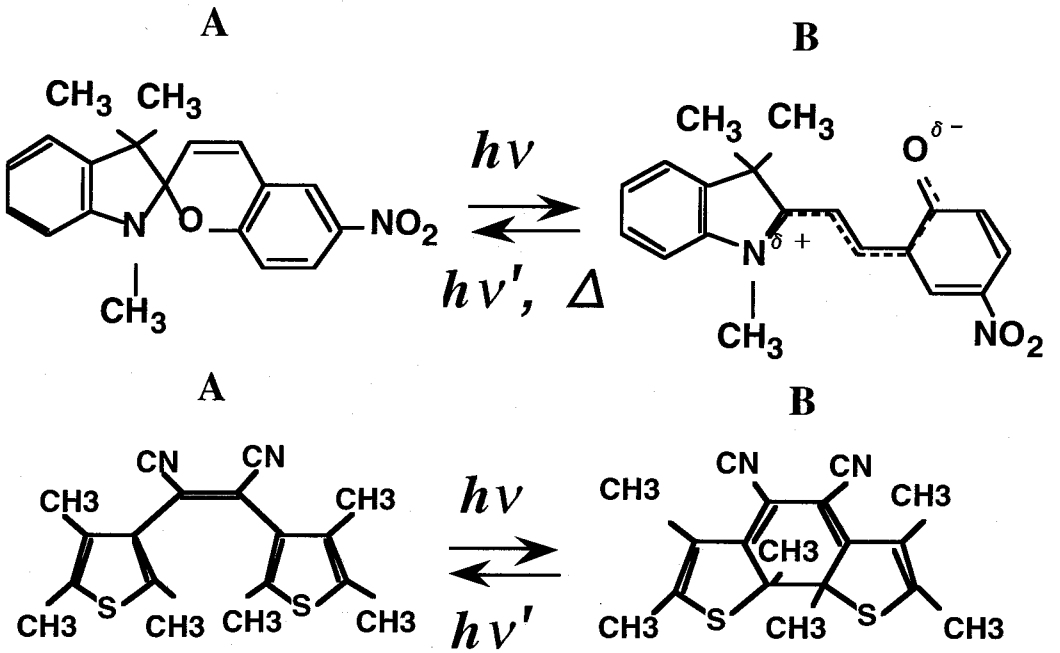


**Figure 2-1.** Chemical structures and isomerization of (top) SP and (bottom) DE isomers.

Guest-host films of PMMA (glass transition temperature, Tg = 110°C, and molecular weight, $M_\omega$ = 40000) doped with DE or SP were prepared by spin-casting from a 2-Butanone solution on cleaned glass substrates. The weight ratio of the chromophore relative to the polymer was 1.7% for SP and 10% for DE to ensure an absorbance that is large enough in the visible region of the spectrum. At the weight ratio (10%) of the DE chromophore relative to the polymer, a loading ratio at which chromophores aggregation do not occur for DE in PMMA. Differential scanning calorimetry (DSC) measurements (**Figure 2-2**) that we have performed on both PMMA and the 10% DE/PMMA, demonstrate that the Tg of PMMA decreases appreciably from 110 to 72°C with the added DE solute. The DE dopants swell significantly the polymer chains for a larger volume, and consequently, are not closely packed by the PMMA matrix. Furthermore, if aggregation is present, it strongly distorts molecular absorption spectra due to inter-molecular interaction, and the spectrum of a $1\times10^{-4}$ M of a $CCl_4$ solution of DE is identical to that in the PMMA films both prior to and after irradiation even though the chromophores concentration is much smaller in this solution than in the DE/PMMA samples. Residual solvent was removed from the films by heating for 1h larger than 110°C near the polymer Tg; a temperature at which polymer segmental motion is large enough to free possibly trapped solvent molecules. The films were removed from the oven and allowed to slowly cool to room temperature. The film thickness was

measured by atomic force microscope and was typically ~0.77 μm for DE and ~0.65 μm for SP.

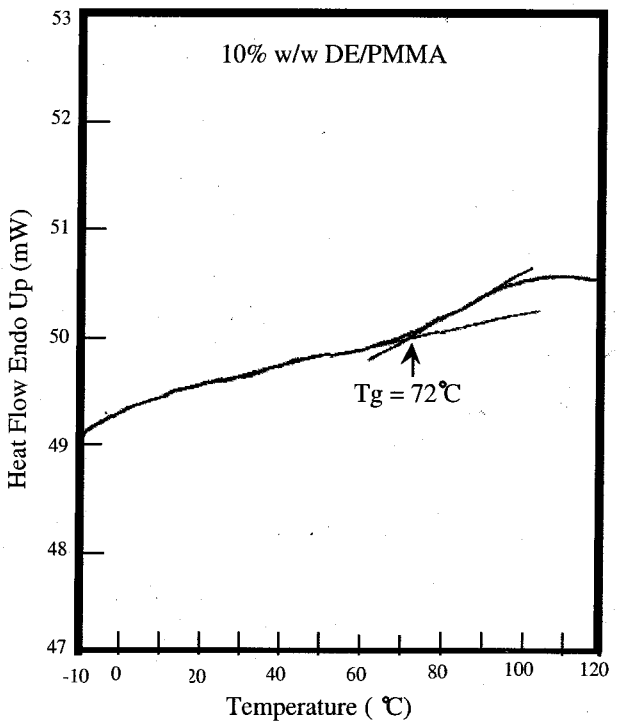


**Figure 2-2.** Tg measurement of 10% DE/PMMA by Perkin-Elmer thermal analysis. The sample was heated from -20.00 °C to 120.00 °C at 10.00 °C/min.

## 2-2 Thermal Recovery

The decreasing of the concentration of B isomers of DE and SP by a thermal back reaction is shown in **Figure. 2-3**. No absorbance change was observed during the B→A thermal back reaction of the DE chromophore over 24 hours, e.g. the closed-ring form (the B isomer) of the DE chromophore is stable at room temperature for this time period. Compared with DE, the colored photomerocyanine isomer (B isomer) of the SP chromophore persists for several minutes at room temperature. A biexponential fading (B→A thermal recovery) of this form at room temperature was observed with rate constants (k) of $k_1$= 0.00125 $s^{-1}$ and $k_2$= 0.0001 $s^{-1}$ and weighting factors (amplitudes) 0.5157 for $k_1$ and 0.4017 for $k_2$ in reasonable agreement with previous results in papers ($k_1$= 0.0012 $s^{-1}$ and $k_2$= 0.00009 $s^{-1}$) [76]. Although the polymer free volume, the free volume distribution, or both, could influence the fading rate constants, in the absence of aggregation, the biexponential behavior is, however, usually attributed to the dual form of the photomerocyanine, e.g. the quinonic and zwitterionic forms.

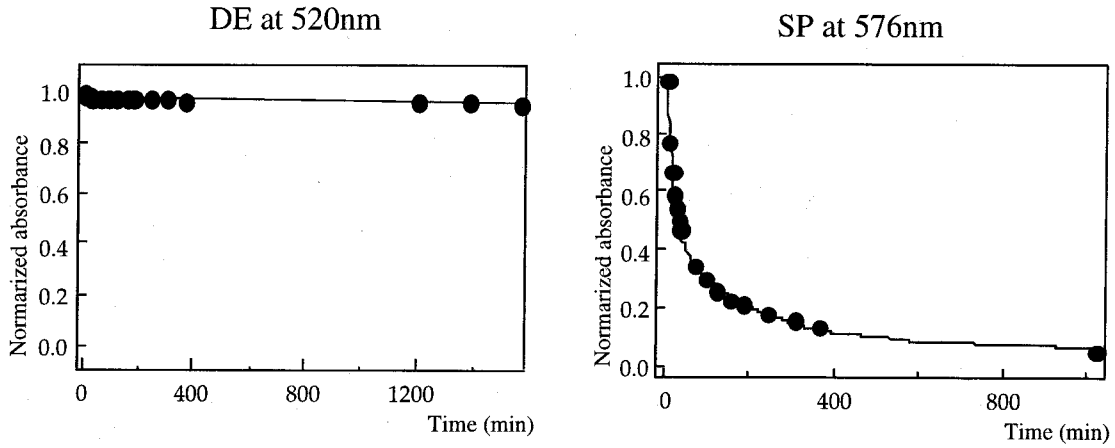


**Figure 2-3.** Thermal back reaction of (left) DE and (right) SP in PMMA in real-time. Wavelengths used for measurements of absorption changes are 520nm for DE and 576nm for SP.

### 2-3 Photoisomerization

Irradiation was performed by UV (365 nm : FWHM = 30 nm; glass filter, UV-D33S from Irie Co.) and green (546 nm : FWHM = 5 nm; interference filter, VPF-25C-10-50-54610 from Sigma) lights from a high pressure mercury lamp (Nikon Co.) to induce the A↔B and A←B photoreactions, respectively. A UV-vis spectrometer (Model UV-1600 from Shimadzu Co.) was used to record the spectra of the film samples.

Photoisomerization of both DE and SP clearly occur in films of PMMA. Spectra taken before, and after several amounts of UV and green irradiation exhibit shape changes and isosbestic points at about 329, 377 and 429 nm for DE and 317, 339 and, less pronounced, 440 nm for SP, clearly demonstrate the forth A→B and back B→A photoisomerization reactions(see **Figure. 2-4** for DE and **Figure. 2-5** for SP; the insets are expanded views of the visible region of the spectra, and the irradiation dose is indicated). The isosbestic points shifted slightly when film samples are irradiated with green versus UV lights.

B isomer of SP i.e. PM has two forms (trans-PM, cis-PM). Specroscopically we cannot distinguish these two forms, so discussions on transitions of the B isomer of SP is an average of the transitions of these two forms. B isomer of DE also has two forms (parallel-type, anti-parallel-type) [77]. Since the parallel-type does not absorb the light, transitions of B isomer of DE originate from only one form (anti-parallel-type).

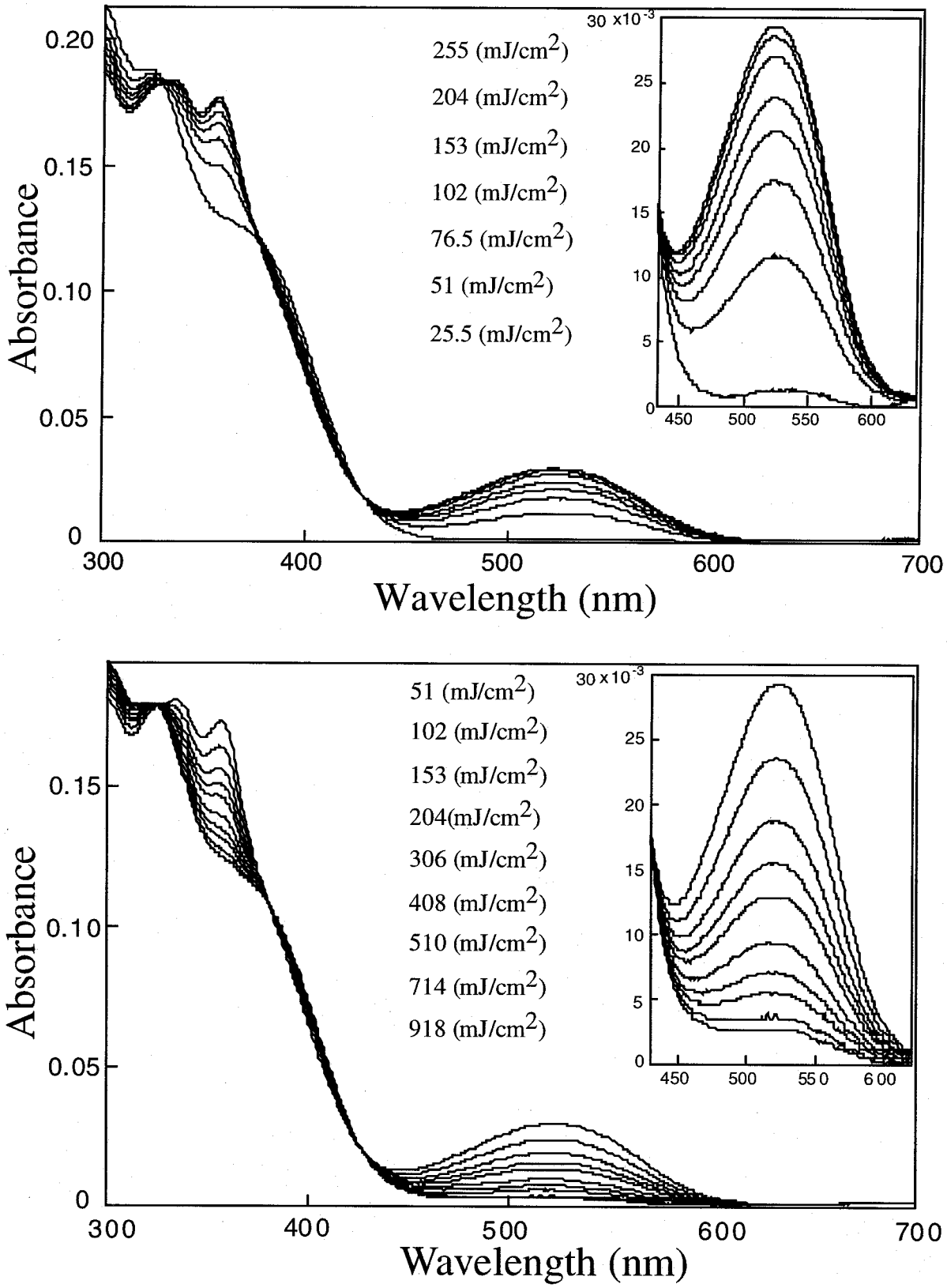


**Figure 2-4.** UV-vis absorption spectra of DE/PMMA before and after various amount of (Upper) UV and (Lower) green irradiations. The irradiation dose is indicated.

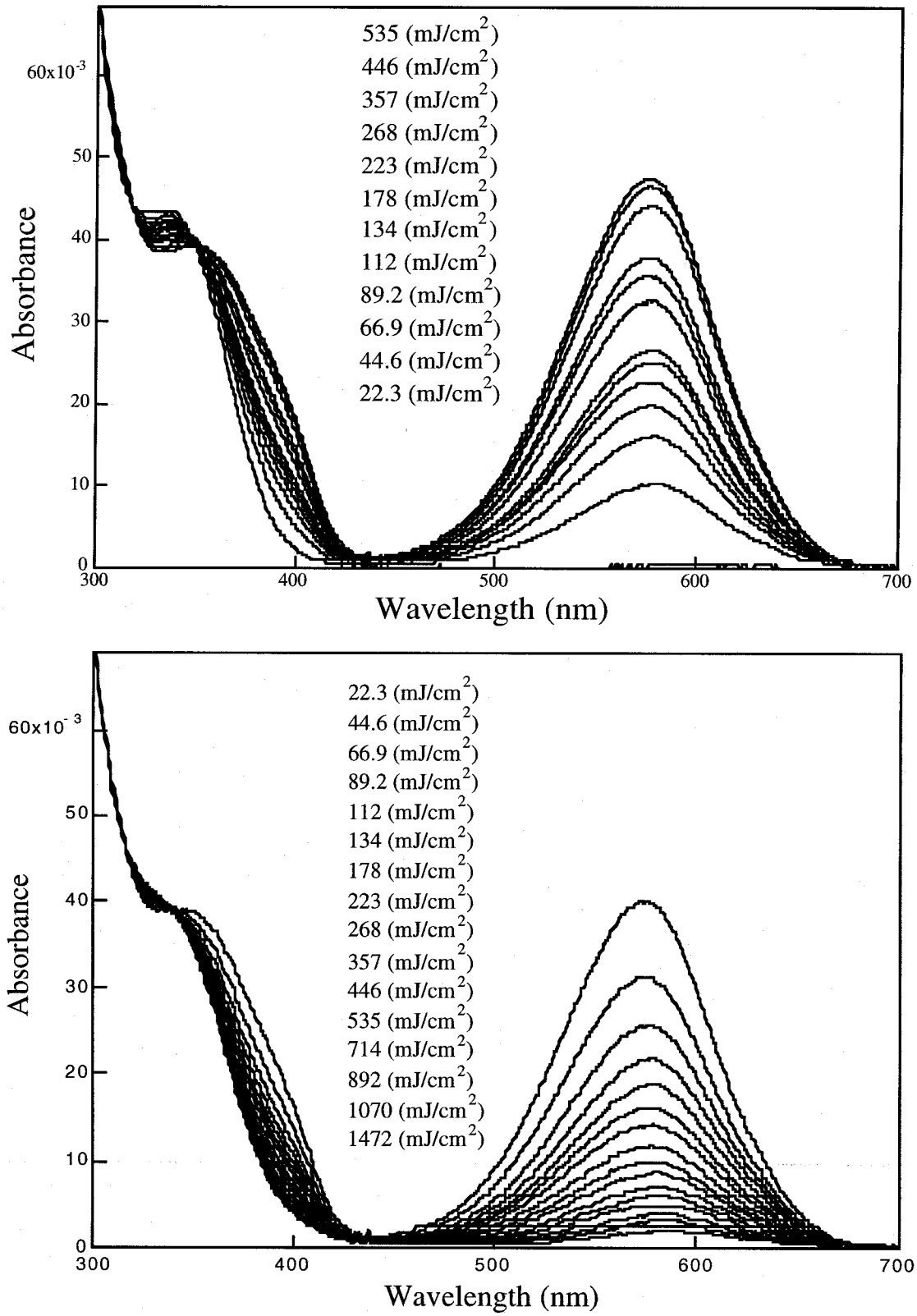


**Figure 2-5.** UV-vis absorption spectra of SP/PMMA before and after various amount of (Upper) UV and (Lower) green irradiations. The irradiation dose is indicated.

## 2-4 Photodegradation

Photodegradaion occurs in cycles of A→B and A←B photoisomerization due to destruction of isomers by fatigue. Even though DEs are robust chromophores, the irreversal photodegradation occurs. Absorption changes at the visible region i. e. population change of B isomer, by cycles of irradiation by UV and visible light are shown in **Figure 2-6** for DE and **Figure 2-7** for SP. Irradiation dose of both UV and green light are strong enough to induce photoisomerization to the steady state. The colored intensity of DE and SP decreases to 80% and 20% respectively, after 10 and 11 UV-visible irradiation cycles. Last points in the **Figures 2-6** and **2-7** are absorbances after 10 cycles irradiation followed by heating the samples for 10min at 130°C above $T_g$ of samples. As the molecules having their transition moments oriented in the perpendicular plane to the irradiation pass are no more excited, it is possible that the decrease of absorption results from such non-photoactive molecules. But the absorbance after heating is not much different from that after 10 cycles irradiation for both DE and SP cases. So the decreases of absorbance are due to the photodegradation. The extent of photodegradation of DE is smaller than that of SP as expected.

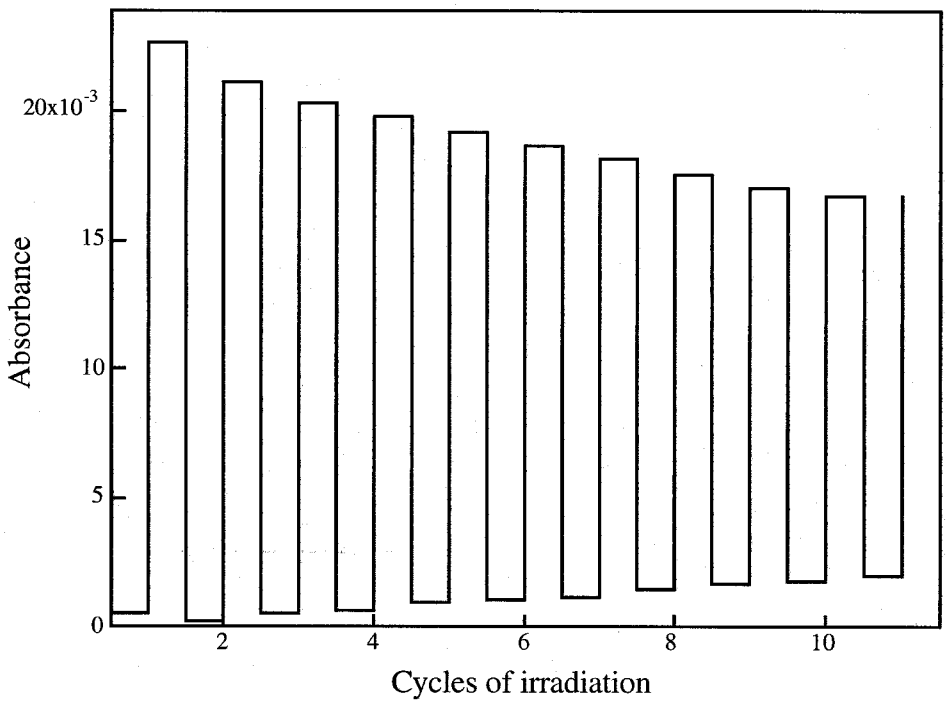


**Figure 2-6.** Photodegradation of DE by 10 cycles of irradiation by UV (365 nm) and green (546 nm) light. Absorption was measured at the wavelength of 520 nm. UV and green irradiation dose are 4050 mJ/cm$^2$ and 4776 mJ/cm$^2$ respectively.

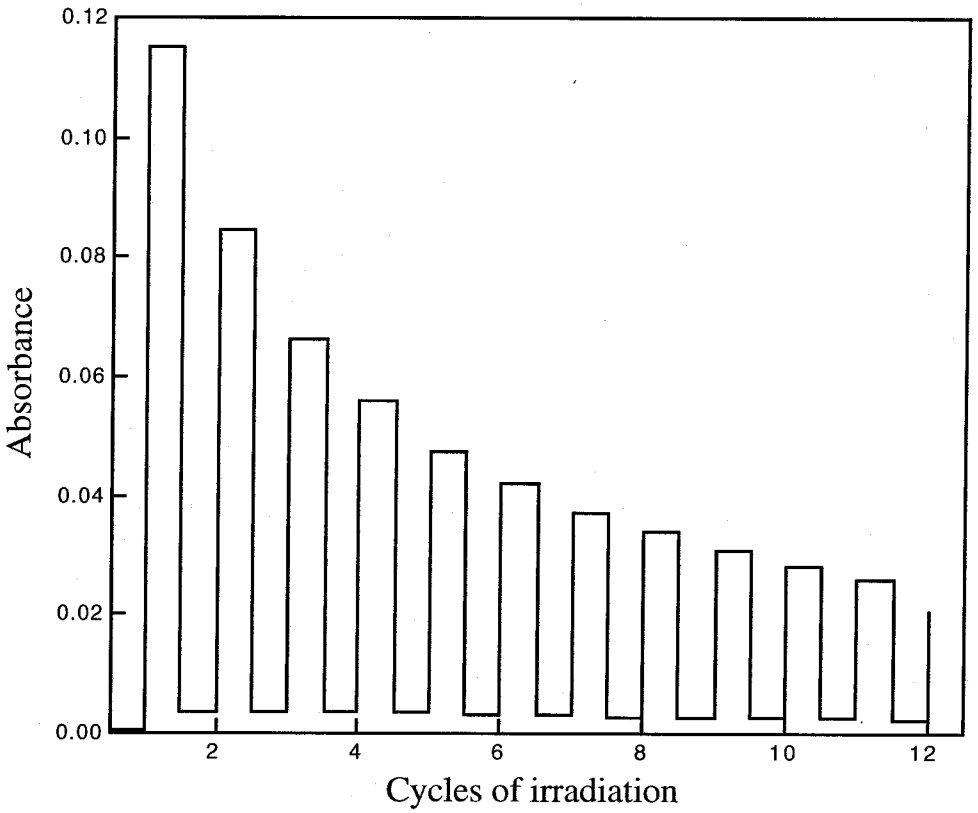


**Figure 2-7.** Photodegradation of SP by 11 cycles of irradiation by UV (365 nm) and green (546 nm) light. Absorption was measured at the wavelength of 576 nm. UV and green irradiation dose are 3974 mJ/cm$^2$ and 4968 mJ/cm$^2$ respectively.

Chapter 3.

# Spectral Features of Photo-orientation of Spiropyrans and Diarylethenes

In this chapter, I present evidence of individualized optically induced orientation in photoisomers of SP and DE. The light-induced orientation studied on the entire UV-vis spectrum of the chromophores shows spectral dependencies which inform about the relative orientation of the directions of the ultra-violet (UV) and visible photochemical transitions of the chromophores.

## 3-1 Photo-orientation by Linearly Polarized UV Light

Irradiation was performed by linearly polarized UV (365 nm : FWHM = 30 nm) and green (546 nm : FWHM = 5 nm) lights from a high pressure mercury lamp to induce the A ↔ B and A ← B photoreactions, respectively. A UV-vis spectrometer was used to record linearly polarized spectra, e.g. $Abs_{//}$ and $Abs_{\perp}$, of the film samples. The polarized spectra were recorded for probe light linearly polarized either parallel ($Abs_{//}$) or perpendicular ($Abs_{\perp}$) to the polarization of the irradiation light. The spectra were recorded after the end of the irradiation. Dark conditions were employed to avoid the influence of the room light on the isomerization reaction.

**Figure 3-1** shows the dichroic spectra observed in films of DE/PMMA and SP/PMMA. The insets in **Figure 3-1(a)** are expanded views of both the UV and visible absorptions of the DE chromophore. These spectra were obtained 30 s after polarized UV irradiation (irradiation dose: 78 $mJ/cm^2$). It is clear that $Abs_{//}$ and $Abs_{\perp}$ are different, in other words the irradiated samples show anisotropic absorbance upon polarized UV irradiation. Identical spectra were recorded for $Abs_{//}$ and $Abs_{\perp}$ prior to UV irradiation, demonstrating that the samples were in-plane isotropic at that time. The order parameter S, $(Abs_{//} - Abs_{\perp})/(Abs_{//} + 2Abs_{\perp})$, and the dichroic ratio R, $Abs_{//}/Abs_{\perp}$, achieved under polarized irradiation are summarized in **Table 3-1** for all the experiments described in this thesis. It is particularly remarkable from **Figure 3-1** that $Abs_{//}$ is higher than $Abs_{\perp}$ in the visible band where the absorption of the A form is negligibly small and only the B form exhibits an appreciable absorption. This result is confirmed by real-time dichroism experiments we performed(*vide infra*). This clearly shows that when the DE and SP chromophores undergo the A ↔ B photoreaction under polarized UV light, the B isomer is formed with its *visible* transition dipole moment parallel to the UV polarization. $Abs_{\perp}$ is higher than $Abs_{//}$ in the UV band; a feature which shows that the UV transition dipole moment of the DE and SP chromophores is perpendicular to the UV

polarization after several cycles of the A↔B photoisomerization. This shows that the direction of the UV transition of the mixture of the A and B isomers and the visible transition of the B isomer of the oriented chromophores are perpendicular to each other. Further evidence of this phenomenon will be given later.

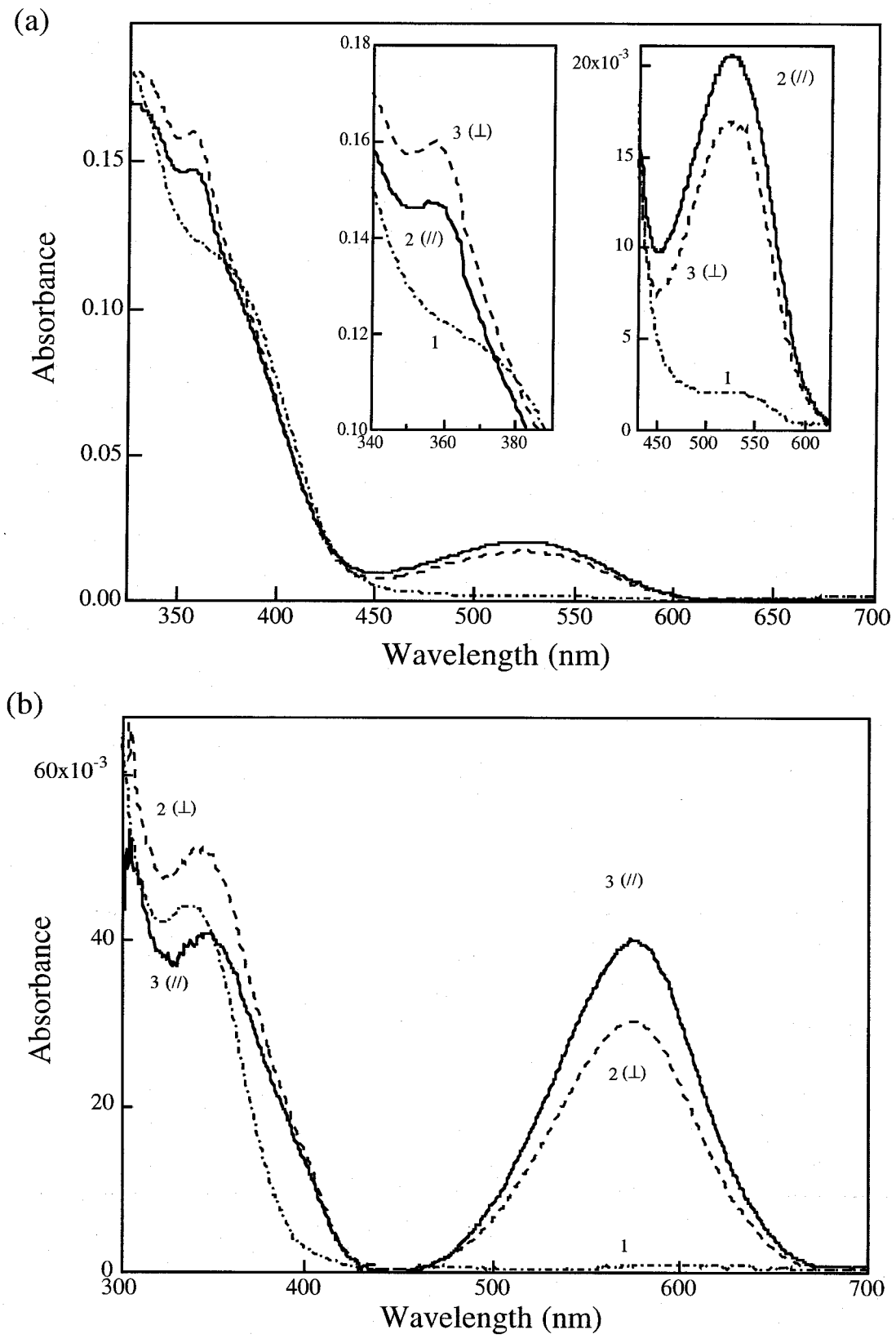


**Figure 3-1.** UV-vis absorption spectra of PMMA films containing (a) diarylethene and (b) spiropyran before (1) and after (2, 3) linearly polarized UV irradiation. The probe light was also linearly polarized, and spectra were obtained for both parallel,

$Abs_{//}$, and perpendicular, $Abs_{\perp}$, orientations. The insets in (a) are expanded views of both the UV and visible absorption of the diarylethene chromophore. Identical spectra were obtained for both $Abs_{//}$ and $Abs_{\perp}$ prior to UV irradiation. For both of the diarylethene and spiropyran chromophores, inasmuch as the orientational hole burning and orientational redistribution processes occur with $Abs_{\perp} > Abs_{//}$ within the irradiation wavelength band, note the inversion of the sign of the dichroism between the UV and visible bands of the spectra.

**Table 3-1.** Order Parameter, S, and Dichroic Ratio, R, of diarylethene and spiropyran containing PMMA films achieved under polarized UV and Green light irradiation. S and R are defined in the text.

| Irradiation wavelength (nm) and dose ($mJ/cm^2$) | Order parameter, *S*<br>Dichroic ration, *R* | | | |
|---|---|---|---|---|
| Chromophore | Diarylethene | | Spiropyran | |
| Analysis wavelength (nm) | 360 | 520 | 345 | 570 |
| 375 and 78 | -0.03 | +0.07 | -0.07 | +0.10 |
| | 0.93 | 1.22 | 0.81 | 1.32 |
| 365 and 401 | -0.04 | +0.05 | | +0.07 |
| | 0.90 | 0.16 | | 1.22 |
| 546 and 117[a], and 72[b] | +0.01[a] | -0.06[a] | | -0.04[b] |
| | 1.03[a] | 0.83[a] | | 0.89[b] |

S and R are defined in the text.

**Figure 3-2** shows the absorbance of linearly polarized probe light (at 360 and 520 nm for DE, and 570 nm for SP) at various angles, $\Psi$, between the polarizations of the probe and UV lights. The UV irradiation dose was 401 $mJ/cm^2$. Sinusoidal behavior is clearly shown, and demonstrates the nonpolar orientational distribution of the isomers transitions in both the UV and visible bands. For DE, perpendicularly oriented transitions are clearly shown for the UV and visible bands. The small drift (smearing-out of the modulation) in the absorption data is due to rotational diffusion of the chromophores. Perpendicularly oriented transitions are clearly shown for the UV and visible bands *(vide infra)*. In the UV region, the A and B isomers have comparable extinction coefficients, and the apparent orientation can be

due to both isomers. In the visible region, the orientation observed is only due to the B isomer since the visible-band observed absorption is due to the B isomer only. While the B isomer of the DE chromophore is practically stable at room temperature during the amount of time required to perform this experiment, e.g. 1 h 56 min, the B isomer of the SP chromophore is unstable during the time of the experiment performed on the SP chromophore, e.g. 1 h 37 min *(vide infra)*. The data shown in **Figure 3-2** (right) have been obtained after normalization by the double exponential recovery of the A form during the A←B thermal back reaction with the rate constants and weighting factors given above. The value of the rate constant which corresponds to the long time relaxation processes, e.g. $k_2$, had to be increased to 0.00014 $s^{-1}$ due to rotational diffusion which tends to randomize the chromophores orientation. The small drift (smearing-out of the modulation) in the absorption data of DE is also due to the rotational diffusion of the chromophores.

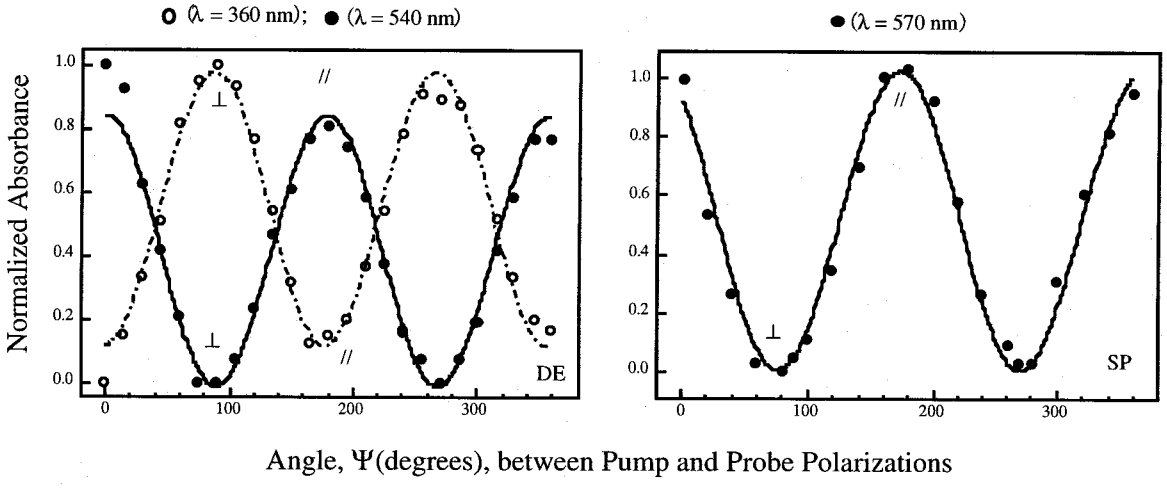


**Figure 3-2.** Dependence of the absorbance of PMMA films containing (left) diarylethene and (right) spiropyran on the angle, Ψ, between UV irradiation and probe beam polarizations. The normalized absorbance is defined as (Abs - $Abs_{min}$)/(Abs - $Abs_{max}$); where $Abs_{min}$ and $Abs_{max}$ are the maximum and minimum absorbences, respectively. The // and ⊥ signs stand for the directions parallel and perpendicular to the UV polarization, respectively. The markers are experimental data points, and the full and dashed lines are $\cos^2\Psi$ theoretical fits. The analysis wavelengths are indicated. Note the apparent π/2 angle-shift between the UV and visible orientational distributions of the diarylethene chromophore.

The light polarization sensitivity of the photoisomerization of DE and SP derivatives originates from the anisometric shape of these chromophores. Rigorously, the tensor of the chromophore's linear polarisability is anisometric, and light absorption is proportional to the cosine square of the angle between the

transition dipole moment and the polarization of the exciting light. Within a photochemical transition band, a long molecular axis (LMA) can be assigned along the direction of the transition dipole moment, and the chromophores that are most likely to be excited are the ones of which the LMAs are oriented along the polarization of the exciting light. This selective depletion creates anisotropy by burning a hole into the initial isotropic orientational distribution of the chromophores (orientational hole burning, OHB). In principle, isotropy can be restored by rotational diffusion. Reorientation of the molecular axis of the chromophore during the photoisomerization reaction (orientational redistribution, OR) will also contribute to the observed anisotropy, since the chromophores that are oriented along the polarization of the exciting light present the highest probability of being excited and reoriented. DE and SP chromophores exhibit orientational features that are not observed for previously studied photochemical chromophores. So, the term reorienation includes both the physical processes of the reorientation of the chromophore as a block, or block reorientation, and the reorientation due to the isomeric shape change without any block rotation, or isomeric reorientation. The block and isomeric reorientation processes are due to the reorientation of the chromophore's LMA after a full A $\rightarrow$ B $\rightarrow$ A or B $\rightarrow$ A$\rightarrow$ B cycle and a A $\rightarrow$ B or B $\rightarrow$ A isomerization, respectively.

When only one isomer, say the more stable isomer A, can absorb the excitation light the apparent anisotropy which results from pure OHB is measured at the irradiation wavelength, or at a wavelength where only A absorbs. The anisotropy observed for the less stable photoisomer B which is inherent to the excitation light, measured at a wavelength where only B absorbs, informs about the reorientation of the chromophore's axis within the A $\rightarrow$ B photoisomerization. This behavior has been observed for azobenzene molecules introduced into a polyglutamate polymer. For the DE and SP chromophores studied in this paper, both of the A and B photoisomers absorb UV light, and the UV-band anisotropy results from both of the OHB and OR processes which lead to a net orientation of the chromophore axis perpendicular to the polarization of the excitation light (see the anisotropic absorbance of the UV-band in **Figure 3-1**). The contribution of the isomeric reorientation of the chromophore's axis within the thermal A $\leftarrow$ B recovery to the UV-band anisotropy is negligible for the anisotropy observed at early decay times, a feature which holds true for the dichroic spectra presented in this thesis.

### 3-2 Photo-orientation by Linearly Polarized Green Light

Reorientation of the chromophore's axis can also be observed within the A$\leftarrow$B photoisomerization. Such an observation was made for both DE and SP

chromophores, and is depicted in **Figure 3-3**. This figure shows the sample spectra at a photostationary state attained after unpolarized UV light irradiation (irradiation dose: 1.026 J/cm$^2$ and 864 mJ/cm$^2$ for DE and SP, respectively), and the dichroic spectra obtained after a subsequent linearly polarized green irradiation (irradiation dose: 117 mJ/cm$^2$ and 72 mJ/cm$^2$ for DE and SP, respectively). Identical spectra were recorded for both parallel, $Abs_{//}$, and perpendicular, $Abs_{\perp}$, absorbances prior to green irradiation at the photostationary state. Since the photomerocyanine form of the SP chromophore is thermally unstable, the data of **Figure 3-3 (b)** have been normalized by the double exponential fading of the photomerocyanine with the rate constant $k_2 = 0.00014\ s^{-1}$ that also accounts for rotational diffusion. Therefore, only the data of the visible region of the spectra are shown in **Figure 3-3 (b)**, since in this region, the observed absorbance is directly proportional to the concentration of the photomerocyanine. For both of the DE and SP chromophores, $Abs_{\perp}$ is higher than $Abs_{//}$ in the absorption band of the B isomer; a finding which proves that the chromophores visible transition dipole moment is oriented perpendicular to the green polarization. This observed anisotropy is due to OHB in the orientational distribution of the B isomer. Here also, the apparent anisotropy observed in the UV region of the DE chromophore (**Figure 3-3 (a)**) is opposite in sign to that observed in the visible region in agreement with the results of **Figures 3-1 and 3-2**. The observed anisotropy in the UV region can be due to both the OHB of the B isomer and anisotropic orientation of the A isomer processes; each as a result of the 546 nm green irradiation induced B $\rightarrow$ A photoreaction and isomeric reorientation. The optically induced reorientation of the chromophore's axis on going from one isomer to the other, within a single isomerization reaction, is attributed to the differing structures of the A and B isomers (isomeric reorientation) *(vide infra)*. In contrast to azobenzene derivatives, it seems that the photo-induced ring-closing (photocyclization) and opening in the chromophores studied leads to an opposite UV and visible electronic polarization (molecular polarizability) of the A and B forms of the chromophores.

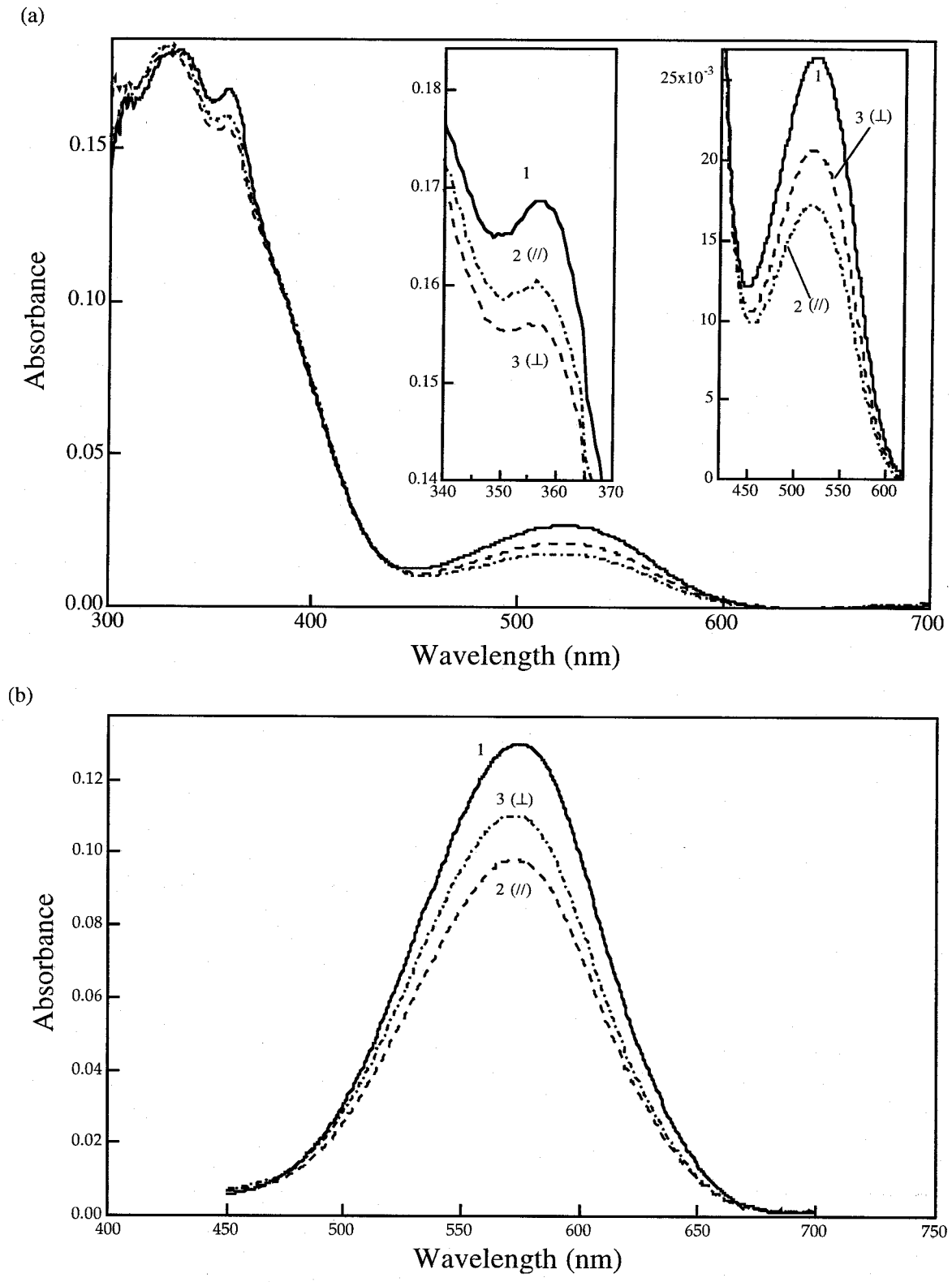


**Figure 3-3.** UV-vis absorption spectra of PMMA films containing **(a)** diarylethene and **(b)** spiropyran before (1) and after (2, 3) linearly polarized green irradiation. The probe light was also linearly polarized, and spectra were obtained for both parallel, $Abs_{//}$, and perpendicular, $Abs_{\perp}$, orientations. The insets in (a) are expanded views of

both the UV and visible absorption of the diarylethene chromophore. The green irradiation followed unpolarized UV irradiation after which identical spectra were obtained for both $Abs_{//}$ and $Abs_{\perp}$. For both of the diarylethene and spiropyran chromophores, the OHB process occurs with $Abs_{\perp} > Abs_{//}$ within the irradiation wavelength band. Note the inversion of the sign of the dichroism between the UV and visible regions of the spectra for the diarylethene chromophore.

Qualitative discussions on the experimental results give that UV and visible transitions of SP and DE are oriented perpendicularly. For quantitative evaluation of photo-orientation processes, theory of photo-orientation is required to compare the experimental results. In the next chapter, I will describe a new model to analyze photo-orientation processes quantitatively. This theory enables to extract the photochromic and photo-orientation parameters such as quantum yields and the angle between UV and visible transitions.

Chapter 4

# Theory of Photo-orientation

In this chapter, I will present a model which is based on purely polarized optical transitions, and the related rigorous solutions of the equations of the theory of molecular optical orientation coupled with isomerization of spectrally distinguishable isomers. This enables the full quantification of the photo-orientation processes.

## 4-1 Purely Polarized Transitions Symmetry

We consider that all the chromophores are initially in the form A, e.g. the isomer A, and that they are randomly oriented into a viscous medium (polymer film). Both of the A and B isomers can absorb UV light, and only the isomer B can absorb visible light. A $\leftrightarrow$ B photo-conversion, e.g. photoisomerization, is assumed to occur upon excitation of purely polarized transition with light linearly polarized along the laboratory axis Z, and the A $\leftarrow$ B spontaneous interconversion by thermal activation, e.g. thermal back isomerization, is assumed to occur on the time scale of the experiment. The effect of the polymeric environment on the spectra of the isomers A and B is assumed to be identical. Analysis is performed at a wavelength which is absorbed by isomer B. The observed absorbance and anisotropy are directly proportional to the concentration and orientation of only B isomer, because only B isomer absorbs the light at analysis wavelength. For all the equations, the sub- and super-scripts A and B, if any, refer to the isomers A and B, respectively.

We define a site-fixed right-handed orthogonal system of axes for each of the isomers A and B in which the molecule can exist, such that the angle between the z and z' axes is $\chi$. In isomers A and B, the electric dipole moments $M_A^{UV}$ and $M_B^{UV}$ responsible for excitation of a UV photochemical transition at a given irradiation wavelength are along the $z_A$ and $z_B$ axes, respectively. In form B, the electric dipole moment $M_B^{Vis}$ responsible for excitation of a visible photochemical transition at a given irradiation wavelength is at an angle labeled $\omega$ with respect to the $z_B$ axis, and lies in the plane which contains the latter and bisects the angle between x' and y' (see **Figure 4-1**). For each of the isomers A and B, any polarized transition can be represented in the fixed molecular coordinates of the isomer in question by an inclination angle, say $\omega$ also for simplicity, with respect to a reference oriented transition that is rigidly fixed to the molecular coordinates, say that transition which corresponds to the irradiation wavelength, in the same manner as we represented the UV and vis transitions of the B isomer in **Figure 4-1**. This model which is based on the choice of the molecular coordinates facilitates strongly the use of the theory

of the light induced orientation of highly symmetric photoisomers. It alleviates the concept of the somewhat ambiguous molecular anisometry that is based on an arbitrary choice of fixed molecular axes.

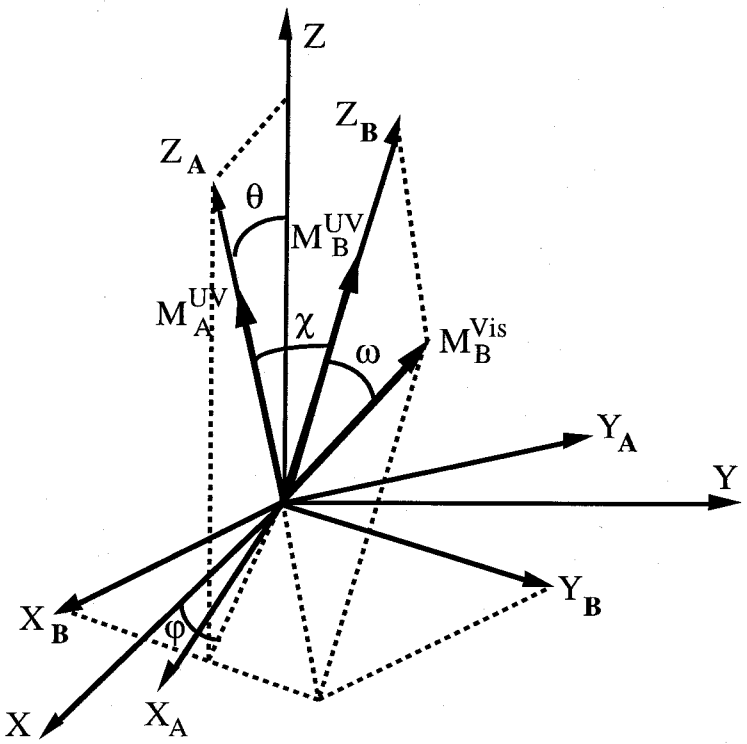


**Figure 4-1.** (X, Y, Z) indicate the laboratory coordinates axes, and ($X_{A,B}$, $Y_{A,B}$, $Z_{A,B}$) indicate the isomers fixed molecular coordinates axes. The angles θ, φ, χ, and ω, and the transition electric dipole moments $M_A^{UV}$, $M_B^{UV}$, and $M_B^{Vis}$ are as defined in the text.

Let me first derive the theoretical expressions of measurable quantities by linear dichroism experiments including the isotropic absorbance, anisotropy and order parameter for an arbitrary orientational distribution function of photo-oriented molecules within the framework of the model above. The squares of the projections of $M_A^{UV}$, $M_B^{UV}$ and $M_B^{Vis}$ into Z are

$$\begin{aligned} \left|M_A^{UV} \bullet Z\right|^2 &= \left|M_A^{UV}\right|^2 \cos^2\theta; \\ \left|M_B^{UV} \bullet Z\right|^2 &= \left|M_B^{UV}\right|^2 \cos^2\theta; \\ \left|M_B^{Vis} \bullet Z\right|^2 &= \left|M_B^{Vis}\right|^2 (\cos\omega\cos\theta + \sin\omega\sin\theta\sin\varphi)^2. \end{aligned}$$

With bulk azimuthal symmetry, the statistical molecular orientation for each of the photo-oriented A and B isomers is described by an orientational distribution

function $G_{A,B}(\theta)$ that depends only on the polar angle, and it can be expressed in the standard basis of Legendre polynomials. $C_{A,B}(\Omega)$ is given by:

$$C_{A,B}(\Omega) = \frac{C_{A,B}}{2\pi} G_{A,B}(\theta),$$

with

$$G_{A,B}(\theta) = \sum_{n=0}^{\infty} \frac{2n+1}{2} A_n^{A,B} P_n(\cos\theta). \qquad (4\text{-}1)$$

where $P_n(\cos\theta)$ is the Legendre polynomial of the nth order and where $A_n^{A,B}$ is the corresponding isomer's geometrical order parameter given by:

$$A_n^{A,B} = \int_0^{\pi} G_{A,B}(\theta)\ P_n(\cos\theta)\ \sin\theta\ d\theta$$

with

$$A_0^{A,B} = 1. \qquad (4\text{-}2)$$

For all the equations of this thesis, the sub- and super-scripts A and B, if any, stand for the isomers A and B, respectively. The macroscopic optical properties, in particular the anisotropic absorbance, are obtained by averaging over the orientational distribution function $G_{A,B}(\theta)$, by projecting the optical fields on the polarized transition axis. The obtained dipole is projected on the laboratory axes and orientational averaging is performed. For an arbitrary analysis wavelength $\lambda$ (visible), the non vanishing components of the absorbance tensor are given by:

$$Abs_{//}^{B} = \varepsilon_B^{\lambda} C_B l\left\{1 + 2P_2(\cos\omega)A_2^B\right\},$$
$$Abs_{\perp}^{B} = \varepsilon_B^{\lambda} C_B l\left\{1 - P_2(\cos\omega)A_2^B\right\},$$

where $P_2(\cos\omega)$ is the second order Legendre polynomial of $\cos\omega$ given by:

$$P_2(\cos\omega) = \frac{1}{2}(3\cos^2\omega - 1),$$

with $\omega$ the angle that defines the orientation of a transition that corresponds to the analysis wavelength versus the irradiation wavelength transition. In other words, if analysis is done at the irradiation wavelength, $\omega = 0$ and $P_2(\cos\omega_{A,B}) = 1$. $Abs_{//}^{B}$ and $Abs_{\perp}^{B}$ stand for absorption of light polarized parallel and perpendicular to the polarization of the irradiation light, respectively. We represent by $C_B$, and $\varepsilon_B^{\lambda}$ the concentrations and the isotropic extinction coefficients, e.g. those coefficients that can be measured from the isotropic absorbance spectra, of the isomers B, respectively.

$\varepsilon_B^\lambda$ is proportional to $\left|M_B^\lambda\right|^2$. $l$ is the sample thickness. So, for each of the A and B isomers, the isotropic absorbance $\overline{A_B} = (Abs_{//}^B + 2Abs_\perp^B)/3$, the anisotropy $\Delta A_B = Abs_{//}^B - Abs_\perp^B$, and the optical order parameter $S_B = \Delta A_B / 3\overline{A_B}$ are given by:

$$\begin{aligned} \overline{A_B} &= \varepsilon_B C_B l; \\ \Delta A_B &= 3\varepsilon_B P_2(\cos\omega) C_B A_2^B l; \text{ and} \\ S_B &= P_2(\cos\omega) A_2^B. \end{aligned} \tag{4-3}$$

## 4-2 Phenomenological Theory and General Equations

The time dependent expression of photo-orientation is derived by considering the elementary contribution per unit time to the orientation by the fraction of the molecules $dC_{A,B}(\Omega)$ whose representative moment of transition is present in the elementary solid angle $d\Omega$ near the direction $\Omega(\theta,\varphi)$ relative to the fixed laboratory axes (**Figure 4-1**). This elementary contribution results from orientational hole burning, and orientational redistribution, and rotational diffusion. The transitions are assumed to be purely polarized, and the irradiation light polarization is along the Z axis. The elementary contribution to photo-orientation is given by:

$$\begin{aligned} \frac{dC_A(\Omega)}{dt} &= -3F\phi_{AB}'\varepsilon_A' \cos^2\theta\ C_A(\Omega) + 3F\phi_{BA}'\varepsilon_B' \int_{\Omega'} C_B(\Omega')\cos^2\theta' P^{BA}(\Omega' \to \Omega) d\Omega' \\ &\quad + \frac{1}{\tau_B}\int_{\Omega'} C_B(\Omega')\, Q^{BA}(\Omega' \to \Omega) d\Omega' + D_A \Re \cdot \left[\Re C_A(\Omega) + C_A(\Omega)\Re\frac{U_A}{kT}\right], \\ \frac{dC_B(\Omega)}{dt} &= -3F\phi_{BA}'\varepsilon_B' \cos^2\theta\ C_B(\Omega) + 3F\phi_{AB}'\varepsilon_A' \int_{\Omega'} C_A(\Omega')\cos^2\theta' P^{AB}(\Omega' \to \Omega) d\Omega' \\ &\quad - \frac{1}{\tau_B} C_B(\Omega) + D_B \Re \cdot \left[\Re C_B(\Omega) + C_B(\Omega)\Re\frac{U_B}{kT}\right]. \end{aligned} \tag{4-4}$$

$P^{AB}(\Omega' \to \Omega)$, $P^{BA}(\Omega' \to \Omega)$, and $Q(\Omega' \to \Omega)$ are the probabilities that the electric transition dipole moment of the chromophore will rotate in the A $\to$ B and B $\to$ A photoisomerizations, and B $\to$ A thermal isomerization, respectively. The orientational hole burning is represented by a probability proportional to $\cos^2\theta$, and the last term in each of the equations above describes the rotational diffusion that is due to Brownian motion. The latter is a Smoluchowski equation for the rotational diffusion characterized by a constant of diffusion $D_A$ and $D_B$ for the A and B isomers, respectively, where $\Re$ is the rotational operator. $k$ is the Boltzmann constant, and $T$ is the absolute temperature, and $U_{A,B}$ is an interaction energy to which the isomers can be subjected. Depending on the type of interaction, $U_{A,B}$ can

be polar or nonpolar. It is polar when the chromophores are isomerized in the presence of an electric field, and nonpolar when intermolecular interactions, such as liquid crystalline-type interactions, are present. I will not discuss these two cases, and I will consider the case of $U_{A,B} = 0$ where friction is the only constraint additional to isomerization. F' is a factor which takes into account that only some part of the totally absorbed amount of light induces photoreaction, and it is defined in the **Appendix** [78]. The notations and units which are used in photochemistry are adopted since the final theoretical expressions need to be compared to linear dichroism, e.g. polarized absorbance, measurements. In **eqs. (4-4)**, as well as in all the equations used in the rest of the chapter, the primed quantities, except for $\theta'$ and $\Omega'$, refer to an analysis at the irradiation wavelength, and the unprimed ones refer to an arbitrary analysis wavelength. The normalizations are:

$$\int_{\Omega} C_A(\Omega)\, d\Omega = C_A; \qquad \int_{\Omega} C_B(\Omega)\, d\Omega = C_B,$$

$$C_A + C_B = C,$$

$$\int_{\Omega'} P^{AB,BA}(\Omega' \rightarrow \Omega) d\Omega' = 1, \qquad \int_{\Omega'} Q^{BA}(\Omega' \rightarrow \Omega) d\Omega' = 1, \qquad (4\text{-}5)$$

The redistribution processes $P^{AB}(\Omega' \rightarrow \Omega)$, and $P^{BA}(\Omega' \rightarrow \Omega)$, and $Q^{BA}(\Omega' \rightarrow \Omega)$ depend only on the rotation angle $\chi$ between $\Omega$ and $\Omega'$, and they can also be expressed in terms of Legendre polynomials with $P_n^{A\rightarrow B}$ and $P_n^{B\rightarrow A}$ and $Q_n^{B\rightarrow A}$ as expansion parameters, respectively. These parameters characterize the molecules orientational memory after the A→B and B→A photoisomerization reactions, and B→A thermal isomerization.

$$P^{AB}(\chi) = \frac{1}{2\pi} \sum_{q=0}^{\infty} \frac{2q+1}{2} P_q^{A\rightarrow B} P_q(\cos\chi),$$

$$P^{BA}(\chi) = \frac{1}{2\pi} \sum_{q=0}^{\infty} \frac{2q+1}{2} P_q^{B\rightarrow A} P_q(\cos\chi),$$

$$Q(\chi) = \frac{1}{2\pi} \sum_{m=0}^{\infty} \frac{2m+1}{2} Q_m^{B\rightarrow A} P_m(\cos\chi),$$

with $$P_0^{A\rightarrow B} = P_0^{B\rightarrow A} = Q_0^{B\rightarrow A} = 1. \qquad (4\text{-}6)$$

When Legendre formalism is used, the variations of the A and B orientational distributions are given by the variations of their expansion parameters, e.g. $C_n^{A,B} = C_{A,B} A_n^{A,B}$. Indeed, by substituting **eqs. (4-1)**, **(4-2)**, **(4-5)**, and **(4-6)** into **eqs. (4-4)** and using the orthogonality of Legendre polynomials, and the following recurrence

equations, e.g. **eq. (4-7)**, and the important relation (**eqs. (4-8)**), the general rate equations, e.g. **eqs. (4-4)**, resume to the system of equations given by **eqs. (4-9)**.

$$\frac{d}{dx}\left[(x^2-1)\frac{dP_n(x)}{dx}\right] = n(n+1)P_n(x), \qquad (4\text{-}7)$$

$$x^2(2n+1)P_n(x) = \frac{(n+1)(n+2)}{2n+3}P_{n+2}(x) + \left[\frac{(n+1)^2}{2n+3} + \frac{n^2}{2n-1}\right]P_n(x) + \frac{n(n-1)}{2n-1}P_{n-2}(x),$$

$$\int_0^{2\pi} P_n(\cos\chi)d\Phi = 2\pi P_n(\cos\theta)P_n(\cos\theta'), \qquad (4\text{-}8)$$

where $\cos\chi = \cos\theta\cos\theta' + \sin s\theta\sin\theta'\cos\Phi$, and $\Phi = \varphi - \varphi'$ (see **Figure 4-1**). $\varphi'$ is not shown in this figure but it is the equivalent of $\varphi$ for $Z_A$.

$$\frac{dC_{A,n}}{dt} = -3F'\phi'_{AB}\varepsilon'_A\{C_A\} + 3F'\phi'_{BA}\varepsilon'_B P_n^{B\to A}\{C_B\} + kQ_n^{B\to A}C_{B,n} - n(n+1)D_A C_{A,n}$$

$$\frac{dC_{B,n}}{dt} = 3F'\phi'_{AB}\varepsilon'_A P_n^{A\to B}\{C_A\} - 3F'\phi'_{BA}\varepsilon'_B\{C_B\} - kC_{B,n} - n(n+1)D_B C_{B,n}$$

where

$$\{C_A\} = \{\kappa_{n+}C_{A,n+2} + \kappa_n C_{A,n} + \kappa_{n-}C_{A,n-2}\},$$
$$\{C_B\} = \{\kappa_{n+}C_{B,n+2} + \kappa_n C_{B,n} + \kappa_{n-}C_{B,n-2}\}, \qquad (4\text{-}9)$$

$$\kappa_{n+} = \frac{(n+1)(n+2)}{(2n+1)(2n+3)},\ \kappa_n = \frac{2n^2+2n-1}{(2n-1)(2n+3)},\ \text{and}\ \kappa_{n-} = \frac{n(n-1)}{(2n-1)(2n+1)}.$$

This system of equations shows, through even orders, that polarized light irradiation creates photo-orientation by photoisomerization. A solution to the time evolution of the A and B expansion parameters can not be found without approximations. Approximate numerical simulations are possible. I will show that for detailed and precise comparison of experimental data with the photo-orientation theory. Rigorous analytical expressions of the steady-state behavior and the early time evolution provide the necessary tool for a full characterization of photo-orientation by photoisomerization. These issues are successively discussed next.

## 4-3 Early Time Evolution of Photo-orientation

### 4-3-1 A→B Photo-orientation

At the early stage of the UV irradiation, the concentration of the B form is negligibly small with respect to that of the A form, so **eqs. (4-4)** can be simplified to

$$\frac{dC_B(\Omega)}{dt} = 3F'\Phi'_{AB}\varepsilon'_A \int_{\Omega'} C_A(\Omega')\cos^2\theta' P^{AB}(\Omega' \rightarrow \Omega)d\Omega' . \qquad (4\text{-}10)$$

After polarized irradiation, the molecular distribution is axially symmetric (the symmetry axis is defined by the direction of the irradiating light polarization), and the Legendre polynomials $P_n(\cos\theta)$ are the eigenfunctions for both the orientational distributions of the A and B forms with the order (expansion) parameters $A_n^A$ and $A_n^B$, respectively. $P^{AB}(\Omega' \rightarrow \Omega)$ depends only on $\chi$. When Legendre formalism is used, with appropriate recurrence relations, and if the extent of A→B photo-conversion $\alpha$ ($C_B = \alpha C_0$; and $C_A = (1 - \alpha) C_0$) is introduced, **eq. (4-10)** can be solved to yield the time evolution of both $\alpha$ and the order parameters $A_n^{A,B}$, so as the orientational distribution of the whole molecular system is fully known. Here, the fourth expansion parameters can be neglected, because it is a small correction to the second Legendre polynomial moment which gives the anisotropy. Therefore, the slopes, $p(\Delta)$ and $p(\Delta A)$, of $\overline{A}$ (proportional to the population change) and $\Delta A$ (proportional to the orientation) during irradiation, respectively, are rigorously given by

$$p(\Delta) = 1000 I'_0 (1 - 10^{-A'_0})\phi'_{AB}\varepsilon_B ; \qquad (4\text{-}11)$$

$$p(\Delta A) = \frac{6}{5} 1000 I'_0 (1 - 10^{-A'_0})\phi'_{AB} P_2(\cos\omega) P_2^{A\rightarrow B}\varepsilon_B . \qquad (4\text{-}12)$$

I will go on to show how **eqs. (4-11)** and **(4-12)** can be used to determine $\phi'_{AB}$ and $P_2(\cos\omega_B)P_2^{A\rightarrow B}$ from A → B photo-orientation experiments.

### 4-3-2 B→A Photo-orientation

The photo-orientation evolution, e.g. changes of $\alpha$ and the order parameters, during the A←B photoisomerization is described by a double exponential behavior (not shown), the slope of the early time evolution of the normalized isotropic absorbance, $p(\Delta_N)$, and the anisotropy, $p(\Delta A_N)$ are given by **eqs. (4-13) - (4-15)**. These equations hold for an analysis light which is absorbed only by the B isomer, and describe the orientational distribution of that isomer. **Eqs. (4-13) - (4-15)** are rigorously given by:

$$p(\Delta_N) = -k - 1000 I'_0 \frac{1 - 10^{-A'_0}}{A'_0}\varepsilon'_B\phi'_{BA} ; \qquad (4\text{-}13)$$

$$p(\Delta A_N) = -\frac{6}{5} 1000 I'_0 \frac{1 - 10^{-A'_0}}{A'_0} P_2(\cos\omega)\varepsilon'_B\phi'_{BA} ; \qquad (4\text{-}14)$$

with $\Delta_N = Abs/A_0^{'}$; and $\Delta A_N = (Abs_{//} - Abs_{\perp})/A_0^{'}$. (4-15)

**Eqs. (4-13) - (4-15)** allow for the measurement of $\phi_{BA}^{'}$ and $P_2(\cos\omega_B)$ from B→A photo-orientation experiments.

### 4-4 Steady-State of A↔B Photo-orientation

During the steady state of photo-orientation, the expansion parameters $C_{A,n}$ and $C_{B,n}$ are constants, e.g. $dC_{A,n}/dt = dC_{B,n}/dt = 0$, and if the first equation of **eqs. (4-4)** is multiplied by $P_n^{A\to B}$ and added to the second equation, the following relation, e.g. **eq. (4-16)**, is obtained after rearrangement.

$$0 = 3F^{'}\phi_{BA}^{'}\varepsilon_B^{'}\{C_B\} + \frac{k(P_n^{A\to B}Q_n^{B\to A} - 1) - D_B}{(P_n^{A\to B}P_n^{B\to A} - 1)}C_B - \frac{P_n^{A\to B}D_A}{(P_n^{A\to B}P_n^{B\to A} - 1)}C_A \qquad (4\text{-}16)$$

**Eq. (4-16)** allows for the derivation of the steady state order parameters of the isomers orientational distribution. Indeed, by making the two following assumptions, **eq. (4-16)** resumes to **eqs. (4-17)** for n=2 after rearrangement. *(i)* The diffusion rates of both the A and B isomers, $D_A$ and $D_B$, respectively, are negligibly small in comparison to the rate, k, of the B→A thermal recovery. This is a good approximation to use when the chromophores are introduced into polymers since spontaneous molecular movement in polymeric materials is most efficient near the polymer glass transition temperature, Tg, and strongly hindered far below Tg. At room temperature, $D_B/k$ is in fact small, e.g. ~ 0.03, for SP in films of PMMA. *(ii)* The process of isomeric-type reorientation is assumed, e.g. that process in which the reorientation of the transition is only due to the isomeric change in shape, and where the parameters, e.g. $P_n^{A\to B}$ and $P_n^{B\to A}$ and $Q_n^{B\to A}$, which describe the reorientation of the transition during the photo-induced and thermal isomerization reactions are equals, say equals to Q [79].

$$\frac{1}{A_2^B} = -\frac{13}{2} - \frac{k}{\varepsilon_B^{'}\phi_{BA}^{'}}\frac{1}{F^{'}}; \text{ and } \frac{1}{S_B} = \frac{1}{P_2(\cos\omega)}\left(-\frac{13}{2} - \frac{k}{\varepsilon_B^{'}\phi_{BA}^{'}}\frac{1}{F^{'}}\right) \qquad (4\text{-}17)$$

No truncation above any order has been made for the determination of $A_2^B$ and $S^B$. **Eqs. (4-17)** allows for the measurement of $\phi_{BA}^{'}$ and $P_2(\cos\omega)$ .

Chapter 5

# Experimental Quantification of Photo-orientation

In this chapter, photo-orientation coupled with photoisomerization of SP and DE are discussed. A linear relationship between slopes of the anisotropy and isotropic absorbance, and irradiation intensities, which is predicted as the theory in previous chapter (chapter 4), is clearly demonstrated experimentally. Independency of the order parameter of DE on the irradiation intensity is also shown. Quantum yields and orientation parameters are determined from a comparison between experimental results and the thoery I have developed. It is found that the UV and visible transitions of both SP and DE are perpendicular. For DE that is verified by molecular orbital calculations.

## 5-1 Experimental Setup

Real-time dichroism experiments (see **Figure 5-1**) were used to investigate the dynamics of photo-orientation of SP and DE in films of PMMA. The samples were irradiated with linearly polarized light while *in situ* transmittance measurements were performed with a probe light polarized either parallel or perpendicular to the initial irradiating light polarization. The probe beam was propagating perpendicular to the plane of the sample and linearly polarized at 45 degrees with respect to the plane of incidence of the irradiating beam. The transmitted parallel and perpendicular components were separated by a Wollaston prism and detected separately. The sample preparation is described at chapter 2. Experimental conditions for SP (i) and DE (ii) are separately described as follows.

(i) SP : The weight ratio of the chromophore relative to the polymer was 10%. The films thickness was measured by atomic force microscopy and was typically about 0.65 μm. The films were irradiated by linearly polarized UV (365 nm : FWHM = 15 nm; glass filter, UV-D33S from Irie Co.) and green (546 nm : FWHM = 5 nm; interference filter, VPF-25C-10-50-54610 from Sigma) lights from a high pressure mercury lamp (Nikon Co.) to induce the A↔B and A←B photoreactions, respectively. Consideration of the chromophores density (e.g., $1.19 \times 10^{20}$ and $0.87 \times 10^{20}$ molecules $\cdot$ $cm^{-3}$ for the A and B isomers prior to UV and green photo-orientation, respectively), the UV and green irradiation intensity range imposes about 0.14 to 1.42 and 0.26 to 1.79 incident photons per isomer per second, respectively. The probe beam was the red light ($\lambda$ = 633 nm) of He-Ne laser (power ~ 2.4 μW, and ~ 1 mm-diameter spot), so as photo-orientation processes of the isomer B are probed independently from those of the isomer A. Dark conditions

were employed to avoid the influence of the room light on the isomerization reaction.

(ii) DE : The weight ratio of the chromophore relative to the polymer was 10%. The films thickness was about 0.77 μm. The films were irradiated by linearly polarized UV light (365 nm : FWHM = 15 nm and 405 nm : FWHM = 5 nm; glass and interference, filters from Irie and Sigma Co., respectively) from a high pressure mercury lamp (Nikon Co.), and polarized green light (532 nm) from a diode pumped frequency doubled Nd:$YVO_4$ laser (Uniphase) to induce the A↔B and A←B photoreactions, respectively. Consideration of the chromophores density (e.g., $2.37 \times 10^{20}$ and $0.43 \times 10^{20}$ molecules $\cdot$ $cm^{-3}$ for the A and B isomers prior to UV and green photo-orientation, respectively), the UV and green irradiation intensity range imposes about $4 \times 10^{-3}$ to $32 \times 10^{-3}$ (for 365 nm) and $1.2 \times 10^{-2}$ to $8.5 \times 10^{-2}$ (for 405 nm) incident photons per isomer per second, and 0.55 to 8.2 incident photons per isomer per second, respectively. The probe beam was the green laser light (incident power ~ 1.2 μW, and ~ 5 mm-diameter spot).

$Abs_{//}^{B}$ and $Abs_{\perp}^{B}$ were calculated from the amount of absorbed light, and the isotropic absorbance $\overline{A_B}$, the anisotropy $\Delta A_B$, and the order parameter $S_B$ were deduced. $S_B$ was calculated at the steady-state of photo-orientation.

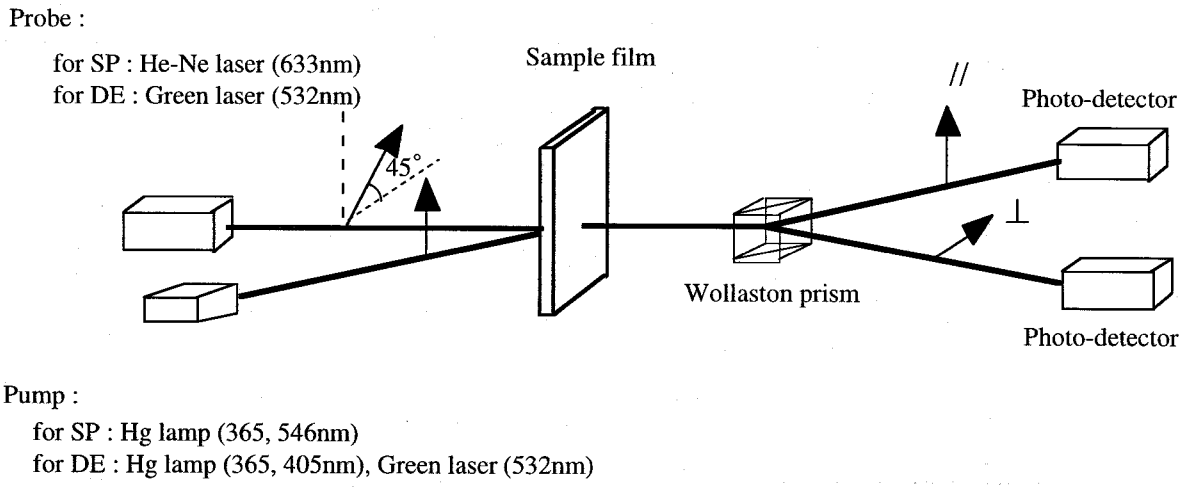


**Figure 5-1.** Experimental setup for real-time dichroism measurement.

## 5-2 Quantified Photo-orientation of Spiropyrans in Films of PMMA

**Figure 5-2** shows the time evolution of $\overline{A_B}$ and $\Delta A_B$ of SP/PMMA during and after linearly polarized UV irradiation for different irradiation power values. The occurrence of anisotropy is indicative of photo-orientation of the chromophores.

The green light induced orientation of the chromophores showed a dynamical behavior (not shown) similar to that of **Figure 5-2**. In this experiment, the SP/PMMA samples were irradiated by unpolarized UV light to the photo-stationary state, and linearly polarized green irradiation followed. The spiropyran molecules degrade after successive irradiation cycles, and each photo-orientation experiment has been done for a different previously non-irradiated sample so as to avoid degradation complications. For high irradiation doses, higher than those reported in **Figures 5-2** and **5-3**, the evolution of the isotropic absorbance exhibits a reversal at the photostationary state due to the degradation of the chromophores. The samples had similar absorbance values prior to UV irradiation, and the samples absorbances were accounted for in F'.

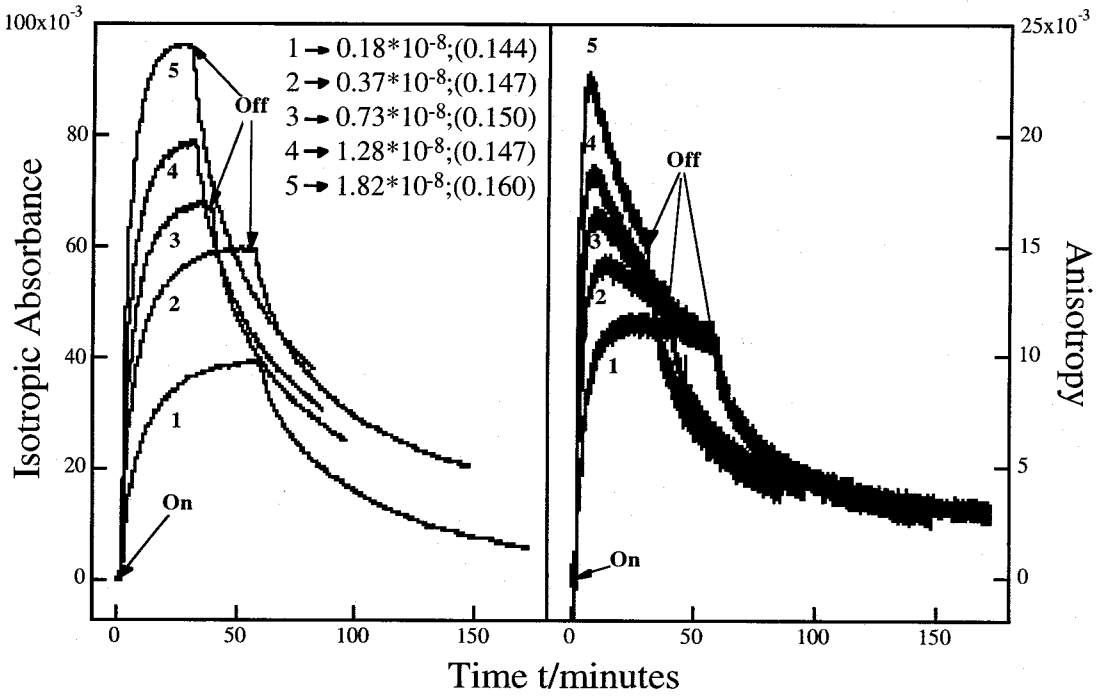


**Figure 5-2.** Real-time evolution of the isotropic absorbance (left) and the anisotropy (right) of SP in PMMA upon linearly polarized UV irradiation for several irradiation intensities. The numbers from 1 to 5 indicate the value of the irradiation intensity in units of Einstein.$s^{-1}$.$cm^{-2}$ with the corresponding sample absorbance, value between brackets, at the irradiation wavelength, e.g. 365 nm. The moments of turning the irradiation light on and off are indicated.

The fitted slopes of the early time evolution of $\overline{A_B}$ and $\Delta A_B$ showed a linear dependence on the irradiation light intensity for both UV (**Figure 5-3 (a)**) and green (**Figure 5-3 (b)**) light-induced orientation as predicted by the theory through **eqs. (4-11) - (4-12)** and **(4-13) - (4-15)**, respectively. $1/S_B$ obtained at the steady-state of the

UV light induced A↔B photo-orientation showed a linear dependence on the inverse of the irradiation light intensity also as predicted by the theory. The solid lines in **Figure 5-3** are linear fits by **eqs. (4-11) - (4-15)** and **(4-17)**, which yielded $\phi_{AB}^{365} = 0.053$, $P_2(\cos\omega_{633}^{365})P_2^{A_{365}\rightarrow B_{365}} = 0.493$, $\phi_{BA}^{365} = 0.030$, $P_2(\cos\omega_{633}^{365}) = -\ 0.345$, $\phi_{BA}^{546} = 0.003$, and $P_2(\cos\omega_{633}^{546}) = 0.642$. $\omega_{633}^{365} = 71.25$ and $\omega_{633}^{546} = 29.24$ degrees are the angles calculated, between the B isomer's transition moments at 365 and 633, and 546 and 633 nm, respectively. $\varepsilon_B^{546} = 11380$ and $\varepsilon_B^{633} = 3460$ L mol$^{-1}$cm$^{-1}$ were adapted from the literature [80], and the fastest component, e.g. k = 0.00125 s$^{-1}$, of the thermal isomerization rate was used in **eq. (4-17)** for the determination of $\phi_{BA}^{546}$.

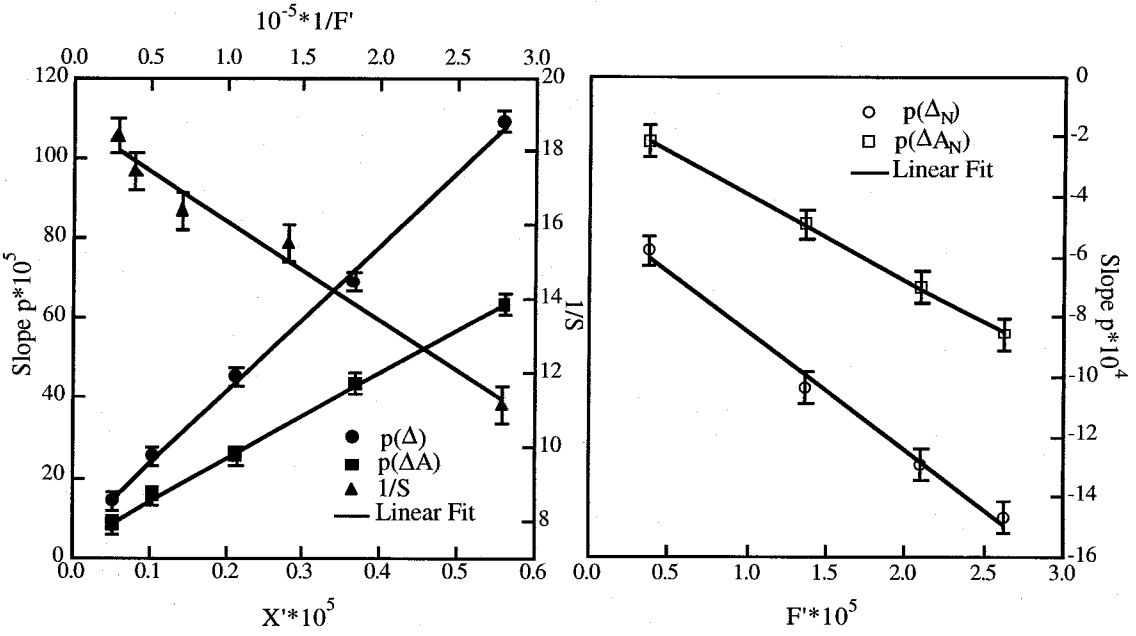


**Figure 5-3.** Experimentally observed dependence of the inverse of (a) the order parameter, 1/S, and the fitted slopes, p(Δ) and p(ΔA), and (b) p(Δ$_N$) and p(ΔA$_N$), of the observed change of the early time evolution of the isotropic absorbance and the anisotropy, respectively, on the irradiation (UV for Figure a and green for Figure b) intensity. In Figure a, the arrows indicate that 1/S, and p(Δ) and p(ΔA), are plotted versus the top and bottom axis, respectively. The full lines are linear theoretical fits by **eqs. (4-11) - (4-15)** and **(4-17)**; F' is defined in the Appendix; and $X' = F' * A_0'$.

The quantum yields are reasonably small for photoisomerization processes in polymeric environments whereby molecular movement can be hindered far below the polymer Tg, and are in agreement with those reported in the literature [80-82]. $P_2(\cos\omega_{633}^{365})P_2^{A_{365}\rightarrow B_{365}} = 0.493$ shows that the orientation of the chromophore is partially retained, e.g. not thermalized, after the UV light induced A → B photoisomerization, and $\omega_{633}^{365} = 71.25$ degree demonstrates that the direction of the

365 and 633 nm transitions of the B isomer are nearly perpendicular to each other; a feature which explains the observed inversion of the sign of the anisotropy of photo-oriented SP in PMMA for the UV versus the visible transition band. Next, the photo-orientation features of DE in PMMA are discussed.

### 5-3 Quantified Photo-orientation of Diarylethenes in Films of PMMA

Diarylethenes are contrasted to spiropyrans by the thermal stability of the B isomer, a feature that brings about interesting photo-orientation effects in spectrally distinguishable photoisomers. The order parameter is independent of the irradiation light intensity at the photostationary state. It will be shown that quantified photo-orientation of diarylethenes reveals that the closed form of such chromophores also exhibits perpendicular UV and visible transition dipole moments. **Figure 5-4** shows the time evolution of $\overline{A_B}$ and $\Delta A_B$ of DE/PMMA during and after linearly polarized UV irradiation for different irradiation power values. The green light induced orientation of the chromophores shows a dynamical behavior that reverses for long irradiation times (see **Figure 5-5**). Even though diarylethenes are robust chromophores, the reversal of the mean absorbance observed at high UV irradiation intensities is due to isomer's degradation (see **section 2-4**). To avoid possible photo-degradation complications after successive irradiation cycles, each photo-orientation experiment has been done on a different previously non irradiated sample, and for data analysis, only the slopes and the maximum absorbances at high irradiation intensities were considered.

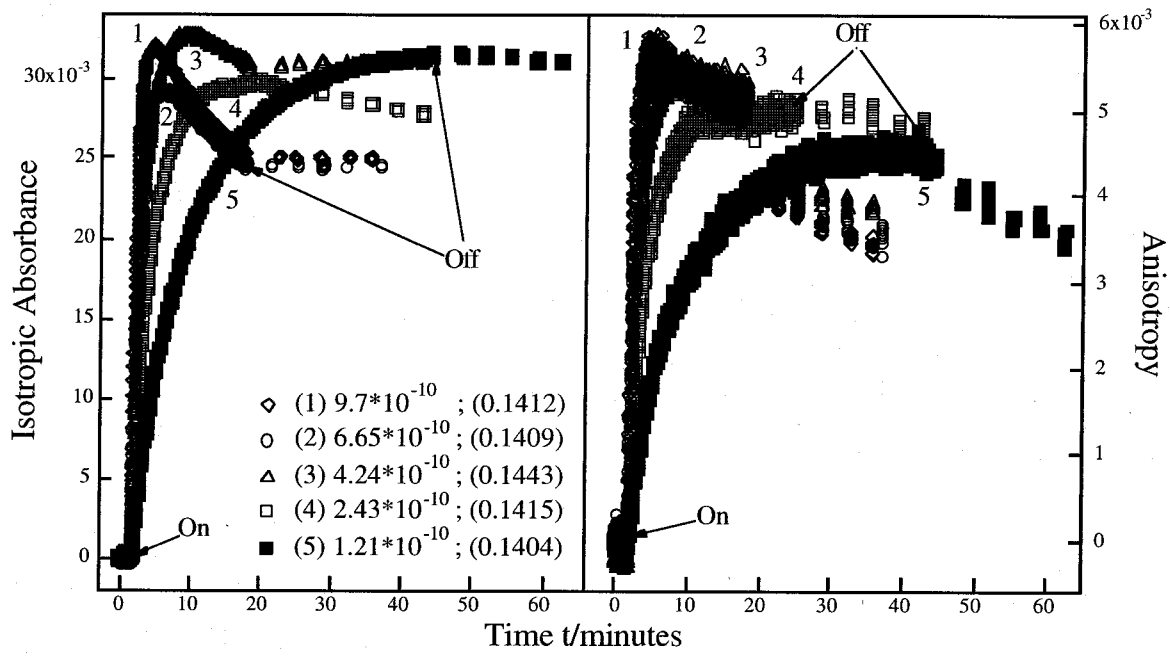


**Figure 5-4.** Real time evolution of the isotropic absorbance (left) and the anisotropy (right) of DE in PMMA upon linearly polarized UV irradiation for several irradiation intensities. Only the 365 nm UV photo-orientation is shown, 405 nm photo-orientation showed similar dynamical behavior. The numbers from 1 to 5 indicate the value of the irradiation intensity in units of Einstein $\cdot$ $s^{-1} \cdot cm^{-2}$ with the corresponding sample absorbance $A_0$, value between brackets, at the irradiation wavelength, e.g. 365 nm. The moments of turning the irradiation light on and off are indicated. Note that after irradiation, the isotropic absorbance is stable because the B isomer is thermally stable, and the anisotropy relaxes due to molecular rotational diffusion.

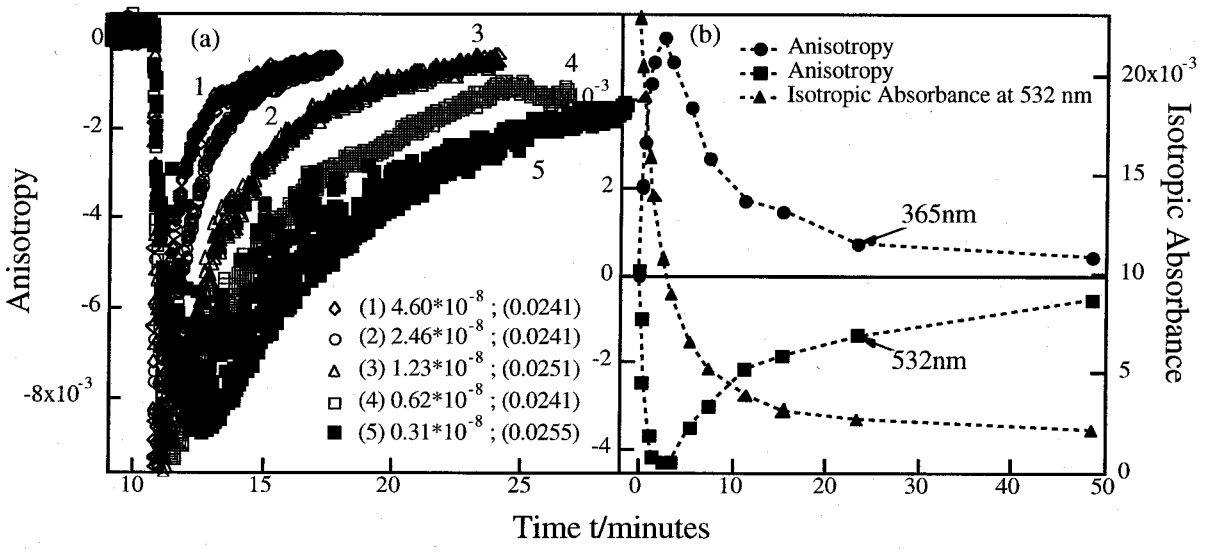


**Figure 5-5.** (a) Same as **Figure 5-4**, but for 532 nm irradiation and analysis. (b) Anisotropy observed by a UV-vis spectrophotometer after 546 nm irradiation (~1 $mW/cm^2$). In (b), the time refers to the irradiation duration.

Like for SP, the fitted slopes, $p(\Delta)$ and $p(\Delta A)$, of the early time evolution of $\overline{A_B}$ and $\Delta A_B$, respectively, showed a linear dependence on the irradiation light intensity for both UV and green light-induced orientation, and the solid lines in **Figure 5-6(a)** are linear theoretical fits by **eqs. (4-11)** and **(4-12)**.

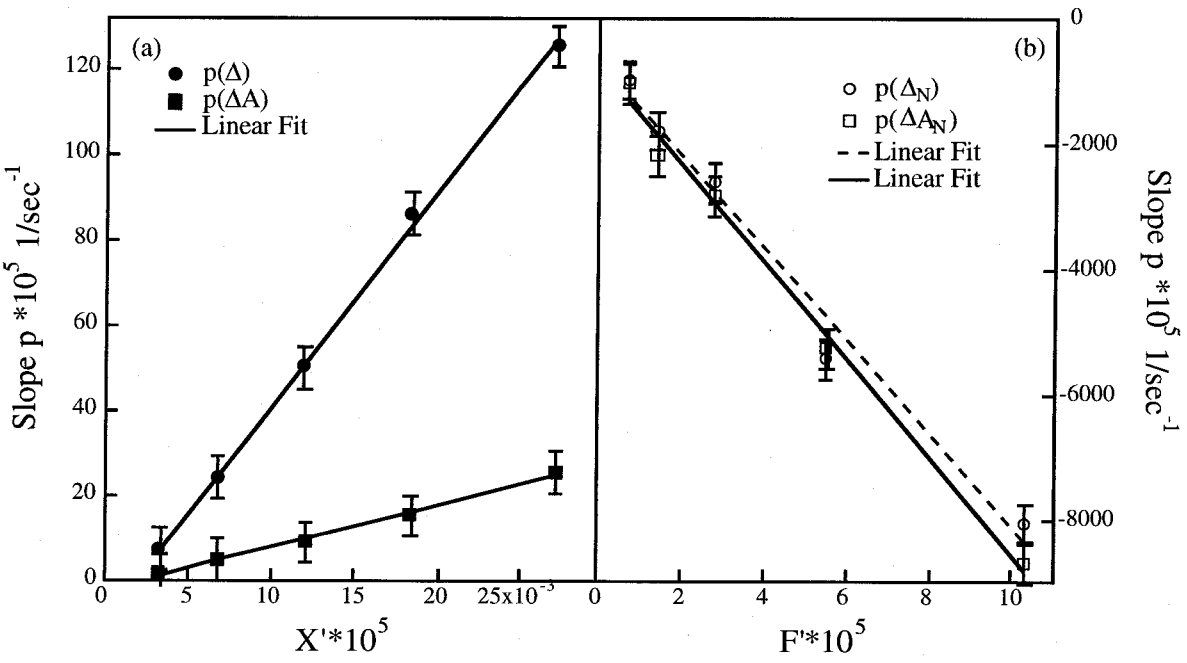


**Figure 5-6.** Slopes, (a) p(Δ) and p(ΔA), and (b) p($\Delta_N$) and p($\Delta A_N$), of the observed change of the early time evolution of the isotropic absorbance and the anisotropy, respectively, on the irradiation intensity (UV for Figure (a) and green for Figure (b)). The full lines are linear fits. $F'$ and $X'$ are as defined earlier.

The values of $S_B$ obtained at the photostationary state of UV irradiation are given in **Table 5-1**. From these values, it is noteworthy that for different irradiation intensities and wavelengths, the value of $S_B$ is fairly constant, e.g. ~ 0.060 and ~ 0.024 for 365 and 405 nm irradiation, respectively; a feature which is theoretically rationalized by **eq. (5-1)** which is obtained by **eqs. (4-17)** .

$$S_B = -\frac{2}{13} P_2(\cos\ \omega). \qquad (5\text{-}1)$$

The factor of -2/13 is the constant of photo-orientation by photoisomerization, and refers to the maximum orientation, e.g. the orientation observed at the irradiation wavelength for systems either without A ← B thermal isomerization such as diarylethenes, or where the irradiation intensity is extrapolated to infinity, such as azobenzenes and spiropyrans.

**Table 5-1.** The order parameter $S_B$ at the photostationary state of UV irradiation, and the irradiation intensity expressed in units of Einstein · $s^{-1}$ · $cm^{-2}$.

| | | | | | | |
|---|---|---|---|---|---|---|
| $I*10^{10}$ | 365 nm | 1.21 | 2.43 | 4.24 | 6.65 | 9.70 |
| | 405 nm | 3.72 | 6.76 | 13.2 | 17.3 | 26.0 |
| $S_B$ | 365 nm | 0.055 | 0.060 | 0.058 | 0.064 | 0.062 |
| | 405 nm | 0.027 | 0.026 | 0.024 | 0.021 | 0.021 |

For the evaluation of the parameters above, $\varepsilon_B$ should be known. We have determined $\varepsilon_B$ by the Fisher's method [20] (see **Appendix**) which holds not only for isotropic but also for anisotropic samples when the isotropic absorbance is considered. For this determination, two different locations which have exactly the same absorbance value in the UV region of an all cis DE/PMMA sample were irradiated by linearly polarized 365 and 405 nm UV lights to the photostationary state, respectively, and the parallel and perpendicularspectra were measured on the entire UV-vis spectrum by a spectrophotometer (Model UV-1600 from Shimadzu) with two custom built polarizers for the sample and the reference. The obtained extinction coefficients are summarized in **Table 5-2** together with the photo-chemical quantum yields and the parameters obtained from the photo-orientation experiments. The fitted slope of the isotropic absorbance of **Figure 5-6 (b)** of the green photo-orientation experiments yielded $\phi_{BA}^{532}$. It is noteworthy that for systems without A←B thermal isomerization, and if analysis is performed at the irradiation wavelength, A←B photo-orientation predictions suggest a slope ratio $p(\Delta A)/p(\Delta)$ equal to 1.2, and the slopes, calculated from **Figure 5-6 (b)**, of the green photo-orientation of DE give a ratio of $p(\Delta A)/p(\Delta)$~1.1.

**Table 5-2.** Data of coupled photoisomerization and photo-orientation of DE. The extinction coefficients are expressed in units of L · $mol^{-1}$ · $cm^{-1}$.

| λ /nm | $\varepsilon_A$ | $\varepsilon_B$ | $\phi_{AB}$ | $\phi_{BA}$ | $P_2(\cos\omega_{532}^{UV})$ | $\omega_{532}^{UV}$ | $P_2^{A_{UV}\rightarrow B_{UV}}$ |
|---|---|---|---|---|---|---|---|
| 365 | 4436 | 8332 | 1.10 | — | −0.39 | 74.3 | −0.43 |
| 405 | 2402 | 423 | 0.32 | — | −0.15 | 61.3 | −1.04 |
| 532 | 0 | 4574 | — | 0.16 | — | — | — |

To my knowledge, the quantum yields of coloring and bleaching of DE have not yet been measured, but those of other diarylethene derivatives have been determined [75]. The values which we found in PMMA by irradiation at 532 and 405 nm, e.g. $\phi_{BA}^{532} \sim 0.16$ and $\phi_{AB}^{405} \sim 0.32$, respectively, are close to those, e.g. $\phi_{BA}^{546} \sim 0.14$ and $\phi_{AB}^{334} \sim 0.27$ to 0.33, found in $CCl_4$ and benzene solutions for other diarylethene derivatives which are structurally related to DE [75]. Even though little free volume change is needed for DE ring opening and closing, the PMMA matrix does not seem to hinder the isomerization movement of the chromophore. Perhaps the large swelling of the polymer chains which is mirrored by the decrease of Tg with the added DE solutes*(vide infra)* provides enough free volume for the photo-induced movement of the chromophores. It is noteworthy that polymer thin films present a distribution of free volumes to solutes, and the films properties are averaged for chromophores in different sites. Quantum yields depend on the excitation wavelength, and when side reactions are present, they can be larger than 1. Indeed, a single photon may lead to the isomerization of more than one chromophore by side reaction isomerization. The value of 1.1 which we found for $\phi_{AB}^{365}$ at 365 nm might reflect the existence of an energy transfer between neighboring open form molecules to induce close ring isomerization, a feature that may occur in polymer films with high chromophore concentration. Other authors [83] have also found a quantum yield of 2 for the isomerization of another diarylethene derivative in films of poly(vinyl butyral), and they too have attributed it to an energy transfer from the open to the closed ring form.

$P_2^{A_{365} \rightarrow B_{365}} \sim -0.4$ and $P_2^{A_{405} \rightarrow B_{405}} \sim -1$ show that the orientation of the UV transition dipole of the chromophore is partially retained, e.g. not thermalized, upon isomerization from A to B after UV irradiation; a feature which suggests that the chromophore does not tumble indiscriminately before it cools off as it does when isomerized from B to A by green irradiation. **Figure 5-5 (b)** shows that the green light induced orientation observed at both 532 nm and 365 nm disappears after all B forms are isomerized to A forms; a feature which demonstrates that isomer A is not oriented by green light induced A←B isomerization, and the observed anisotropy at both 532 and 365 nm is due to the orientation of only isomer B. If orientation occurs in A at any time by green irradiation, some anisotropy should remain at 365 nm after all B are isomerized to A. This behavior is theoretically rationalized by $P_2^{A_{365} \leftarrow B_{532}} \sim 0$, since the orientation of A is proportional to that of B through $P_2^{A_{365} \leftarrow B_{532}}$. The lack of orientation in A may be due to the large amount of energy that needs to be dissipated during the photochemical process induced by the 532 or 546 nm photon; perhaps when the molecule is excited, it shakes strongly before it relaxes. $\omega_{532}^{365} = 74.3$ and $\omega_{532}^{405} = 61.3$ degrees demonstrate that the direction of the UV, e.g. 365 and 405 nm, and visible, e.g. 532 nm, transitions of the B isomer, e.g. the

closed form, are oriented towards perpendicular directions, and rationalize the result of **Figure 5-5 (b)**. This finding is reinforced by the result of **Figure 5-7** which shows that the calculated 365 and 532 nm transitions, with 0.96 and 0.40 respective oscillator strengths, of the closed form of DE are indeed perpendicular to each other. The UV and visible transitions of the closed form of DE have been calculated by using the CNDO/S (completely neglected differential overlap/spectroscopy) with the associated AM1 parametrization for geometry optimization which are available with the MOPAC molecular orbital software [84].

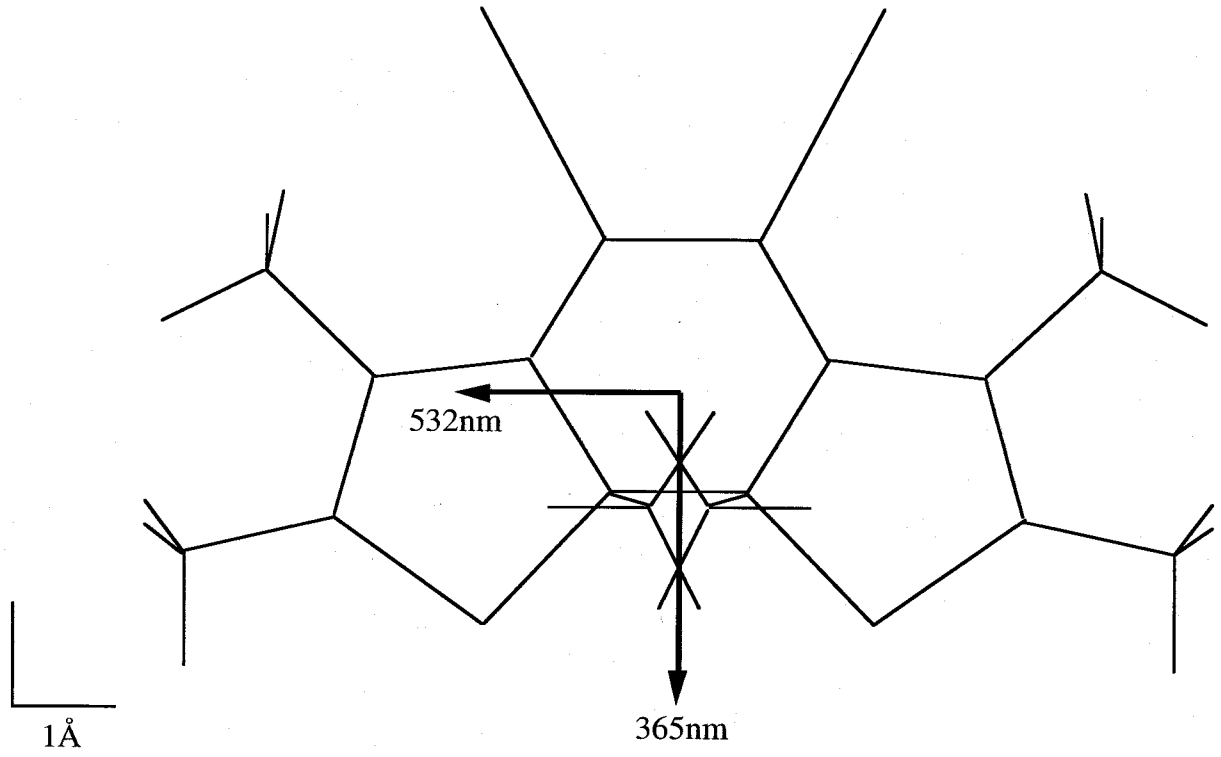


**Figure 5-7.** Drawing of the top view and transition moment vectors at 365 and 532 nm of the closed form of DE obtained by CNDO/S AM1 MOPAC molecular orbital calculations. The 532 nm is parallel to the long axis of the molecule.

## Conclusion

In this thesis, the photo-orientation of spectrally distinguishable photo-isomers, namely spiropyran and diarylethene isomers, was experimentally studied in films of polymer and an analytical theory was developed for photo-orientation quantification and verified for SP and DE in PMMA. Polarized light irradiation orients both of the photochemical isomers of spiropyran and diarylethene derivatives in polymeric thin films of PMMA. The individualized UV and Green light induced orientation that is studied on the entire UV-vis spectrum of the chromophores shows that the UV and visible transitions of the chromophores studied are perpendicular. I have presented the first theoretical treatment which allows for the quantification of optical orientation processes in individualizable photo-isomers, including the measurements of the molecules optical transitions relative orientations, and the photochemical quantum yields in ordered systems. The comparison between theory and experiments gave good insight into the photo-orientation of SP and DE in PMMA. SPs and DEs are oriented by photoisomerization via purely polarized transitions. The movement of the chromophore has been discussed for both UV and green light induced isomerization. The quantum yields and the orientation parameters are determined. The UV and visible transitions of the B isomer are perpendicular; a finding which is rationalized by molecular orbital calculations. I believe that such experimental findings and quantified photo-orientation will trigger additional studies to reveal the symmetry of molecular polarizability tensors of photochromic isomers, and elucidate the true nature of the related photochemical transitions.

For future research, photo-orientation induced by two-photon absorption will have great potentialities for the applications of optical data storage. Recently, optical memory using two-photon absorption was extensively studied for high density recording [85,86]. Using two-photon orientation, the recording density can be further increased because multiplex recording by polarization will be possible. In the two-photon orientation, the experimental and theoretical method of quantification introduced in this thesis will be applicable with slight modifications.

## Acknowledgments

I wish to express my deepest appreciation to Professor Satoshi Kawata (Department of Applied Physics, Osaka University) for supervising my studies in his laboratory for six years. He gave me many opportunities of meeting and discussion with researchers.

I would like to express my sincere gratitude to Associate Professor Zouheir Sekkat (Department of Applied Physics, Osaka University) for a lot of support and advice. His comments on my studies always showed me a right direction. He showed me how a researcher should be.

Recommendations and comments for this thesis from Professor Kazuyoshi Itoh, Professor Hiroaki Ishii, Associate Professor Tsuyoshi Asahi, and Lecturer Yoshitaka Yamamoto (all from Department of Applied Physics, Osaka University) are deeply acknowledged.

I would like to show my thankfulness to Professor Masahiro Irie (Department of Chemistry and Biochemistry, Kyushu University) for valuable comments and discussion on photochromic reactions.

I would like to thank Associate Professor Osamu Nakamura and Assistant Professor Yasushi Inouye (both from Department of Applied Physics, Osaka University) and Associate Professor Tadao Sugiura (Department of Information Processing, Nara Institute of Science and Technology) for their precious comments for my research and creating adequate situation for it.

I also would like to thank Associate Professor Yoshimasa Kawata (Department of Mechanical Engineering, Shizuoka University) for supervising studies on optical memory with two-photon absorption in my undergraduate days.

Many thanks to members of Prof. Kawata's laboratory for helping my studies in various situation.

## Appendix

### 1. Photokinetic Factor

Knowledge about the amount of absorbed light is the prerequisite of all quantitative examinations in photokinetics. It can be obtained form Lambert-Beer's law. In **Figure Appendix-1** the given exponential dependence between the incident and transmitted intensity is plotted schematically for liquids. The derivations is based on the assumptions, that the light incident to the sample (i) is parallel and (ii) falls homogeneously onto the total front area of the sample.

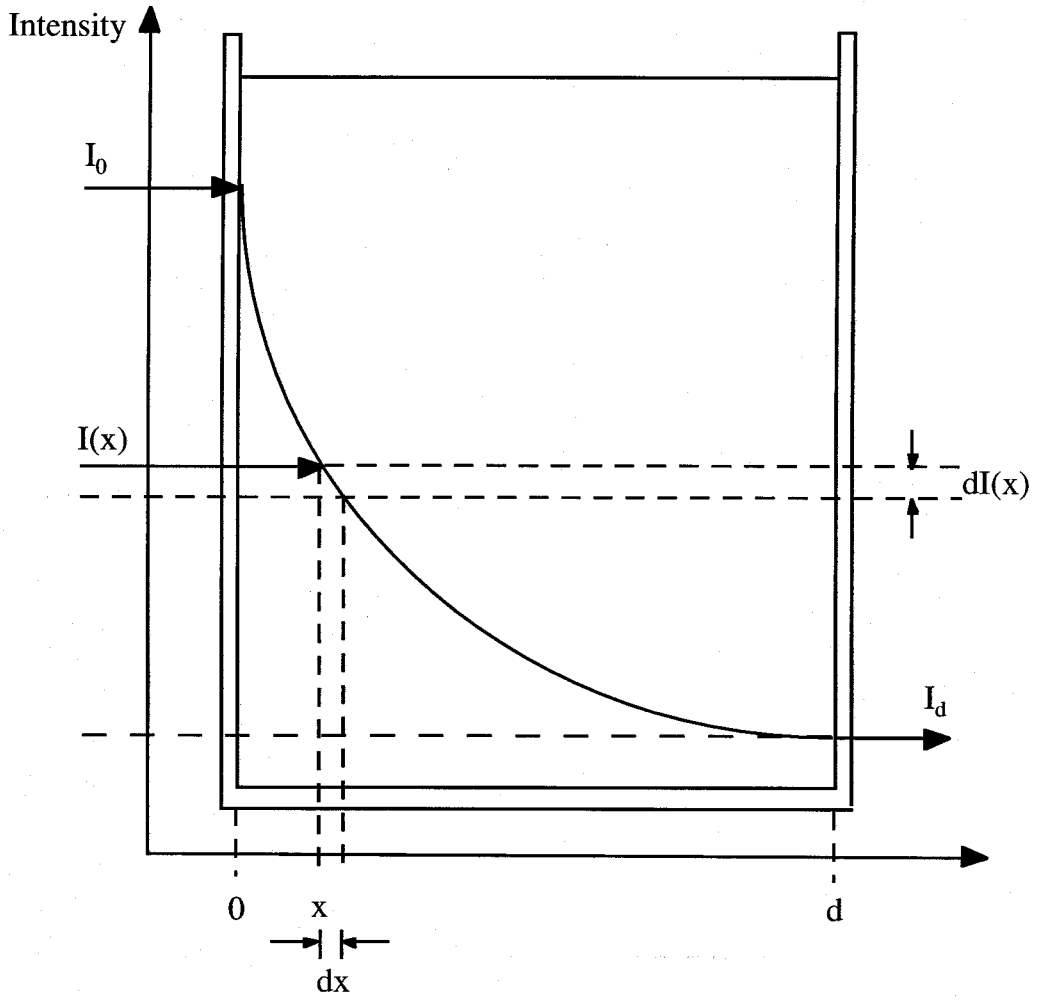


**Figure Appendix-1.** Exponential decay of light intensity in absorbing matter

Selecting a small volume element in the sample A with concentration $a$ and with the pathlength $dx$ as the position $x$, the intensity decreases in this volume element according to

$$-dI_x = I_x \cdot a \cdot \kappa \cdot dx.$$

This equation gives the intensity of light $I_x$ incident on the front area of this volume element. $\kappa$ is the natural absorptivity (a proportionality factor) and $a$ the concentration of the absorbing particles. By integration of this differential equation within the limits of the pathlengths 0 and $d$ either

$$I_d = I_0 \cdot e^{-\kappa a d} \qquad \text{with natural absorptivity } \kappa$$

or

$$I_d = I_0 \cdot e^{-\varepsilon a d} \qquad \text{with decadic absorptivity } \varepsilon$$

are obtained. This derivation applies to one component absorbing in the solution. Since the proportionality coefficient is a value which depends on the wavelength, the Lambert-Beer law is only valid for monochromatic radiation. Besides, this law is limited to diluted solutions(normally up to $10^{-3}$ mol $l^{-1}$).

The decrease in intensity is caused by all component absorbing in the solution. For this reason the amount of absorbed light in the solution by all particles is given by

$$I'_{abs} = I_0 - I_d = I_0 \cdot (1 - 10^{-E'})$$

in the units mol photons $cm^{-2}$ $s^{-1}$, where $E'$ defines the absorbance as a sum of all component's absorbances (n different absorbing samples, including the solvent). This absorbance at the wavelength of irradiation $\lambda'$ is given by

$$E' = d \cdot \sum_{i=1}^{i=n} \varepsilon'_i \cdot a_i$$

Normally only one component is photophysically excited and starts the photochemical process. Therefore its absorbance ($d \cdot \varepsilon'_A \cdot a$) has to be taken relative to the total absorbance ($E'$). One finds the following relationship for the amount of absorbed light by component $A$, which starts the photoreaction, to be:

$$I'_{absA} = \frac{I_0 \cdot (1 - 10^{-E'}) \cdot d \cdot \varepsilon'_A \cdot a}{d \cdot \sum_{i=1}^{i=n} \varepsilon'_i \cdot a_i}.$$

In this equation the intensity of irradiation is used in the units mol photon per area and second. The unit "mol of photons" is sometimes called Einstein. Assuming a homogeneously stirred solution the exponential decay of irradiation intensity can be averaged for each volume element of the solution by an additional factor $1/d$. Thus $I_{absA}$ is expressed by units mol $cm^{-3}$ $s^{-1}$ as

$$I_{absA} = I_0 \cdot (1 - 10^{-E'}) \cdot \varepsilon_A' \cdot a / E',$$

taking into account that the amount of light is absorbed per volume. Since usually the concentration $a_i$ are taken in units in of mol $l^{-1}$ and the irradiation intensity in mol $cm^{-2}$ $s^{-1}$ a factor of 1000 $cm^3$ $l^{-1}$ has to be used to combine these two units. Therefore the "corrected intensity"

$$I = 1000 \cdot I_0 \qquad \text{mol photons} \cdot \text{cm} \cdot \text{s}^{-1} \cdot \text{l}^{-1}$$

is obtained, which effects all photochemical reactions. In the equation derived above, the expression

$$F' = 1000 \cdot I_0 \frac{1 - 10^{-E'}}{E'}$$

is called the "photokinetic factor". It takes into account that only some part of the totally absorbed amount of light induces photoreaction. Using lasers as light sources or working in polymers the derived amount of light absorbed can depend on the volume element (varies with penetration depth $x$ in the sample). This fact has to be taken into account in the calculation of quantum yields.

**2. Fischer's Method (The Calculation of Photostationary States in Systems A $\leftrightarrow$ B When Only A is known).**

In studying photoisomerization it often happedns that the product of the phototransformation A $\rightarrow$ B is not known in the pure state and connot be isolated for technical reasons, such as lack of thermal stability or lack of stability toward oxdation by exygen.

It will be shown that the extent of the above phototransformation, and thus the absorption spectrum of B, can be estimated by measuring the absorption spectra obtaiend after a photostationary state has been reached by irradiation "to completion" with light at two different wavelengths. The essential experimental requirement for the application of the suggested method is thermally and

photochemically (=absence of side reactions) to make possible the establishment of true photostationary states.

In a solution of the photoreversible system A ↔ B in a noabsorbing solvent, a photostationary state will be established by irradiation at any wavelength absorbed by both A and B. Henceforth we shall deal only with such states and all concentrations will be those in the photostationary state attained with light at the wavelength indicated by the subscript.

Denoting concentrations by A and B, quantum yields A → B by $\phi_A$ and B → A by $\phi_B$, and extinction coefficients by $\varepsilon$, we have for the photostationary state at any wavelength $\lambda$

$$\left(\frac{A}{B}\right)_\lambda = \left(\frac{\phi_B}{\phi_A}\right)_\lambda \left(\frac{\varepsilon_B}{\varepsilon_A}\right)_\lambda = \left(\frac{\phi_B}{\phi_A}\right)_\lambda \left(\frac{D_B}{D_A}\right)_\lambda \quad \text{(A1)}$$

where $D_A$ and $D_B$ denote the optical densities, at this wavelength, of similar solutions containing only A or only B, respectively, (*i.e.*, the equilibrium A ↔ B is shifted completely toward either A or B).

When comparing the results of irradiation at any two wavelengths, we have two equations of type (A1), one of each wavlength. *If we assume that the ratio* $\phi_A/\phi_B$ *does not differ at the two wavelengths*, then by taking the ratio between these two equations, $\phi_A/\phi_B$ will cancel out and we end up with (A2).

$$\left(\frac{A}{B}\right)_1 \Big/ \left(\frac{A}{B}\right)_2 = \left(\frac{D_B}{D_A}\right)_1 \Big/ \left(\frac{D_B}{D_A}\right)_2 \quad \text{(A2)}$$

If we denote the extent of conversion A → B at any particular $\lambda$ of irradiation by $\alpha$, we get

$$\left(\frac{A}{B}\right)_\lambda = \left(\frac{1-\alpha}{\alpha}\right)_\lambda$$

Insertion in the left side of (A2) leads to

$$\frac{1-\alpha_1}{\alpha_1} \Big/ \frac{1-\alpha_2}{\alpha_2} = \left(\frac{D_B}{D_A}\right)_1 \Big/ \left(\frac{D_B}{D_A}\right)_2 \quad \text{(A3)}$$

It remains of express $D_B$, which is unknown, in terms of experimetal data and the $\alpha$'s. The optical density at any particular wavelength $\lambda$ of a mixture of A and B, where the over-all concentration [A] + [B] is constant, will be given by

$$D = D_A(1-\alpha) + D_B\alpha$$

If we denotes by $\Delta$ the observed change in optical density when starting A only, $\Delta = D_{obsd} - D_A$, we get after rearrangement

$$D_B = D_A - \Delta / \alpha \quad \text{(A4)}$$

at wavelength $\lambda$. Introducing (4) into (3) we have

$$\frac{1-\alpha_1}{\alpha_1} \Big/ \frac{1-\alpha_2}{\alpha_2} = \left(\frac{D_B}{D_A}\right)_1 \Big/ \left(\frac{D_B}{D_A}\right)_2 = \left(\frac{D_{A_1} + \Delta_1 / \alpha_1}{D_{A_1}}\right) \Big/ \left(\frac{D_{A_2} + \Delta_2 / \alpha_2}{D_{A_2}}\right) = \left(1 + \frac{\Delta_1 / D_1}{\alpha_1}\right) \Big/ \left(1 + \frac{\Delta_2 / D_2}{\alpha_2}\right) \quad \text{(A5)}$$

For the sake of simplicity $D_A$ has been replaced by $D$ in the final equation, where $\Delta / D$ denotes the relative change of absorbance observed at a wavelength $\lambda$ when a solution of A is photoequilibrated with at this wavelength.

Futhermore, the ratio of the the $\alpha$'s for two different photostationary states, resulting from irradiation by two different wavelengths, is equal to the corresponding ratio of $\Delta$'s measured at a wavelength chosen so as to maximize the $\Delta$'s. Denoting this ratio by $n$, $\alpha_1 = n\alpha_2$, and inserting it into (A5) we get

$$\frac{1-n\alpha_2}{n(1-\alpha_2)} = \left(1 + \frac{\Delta_1 / D_1}{n\alpha_2}\right) \Big/ \left(1 + \frac{\Delta_2 / D_2}{\alpha_2}\right)$$

where $\Delta / D$ is the relative change in absorbance at that particular wavelegth, $\lambda_1$ or $\lambda_2$, when passing from pure A to the photostationary state attained by irradiation at the same wavelength.

Multiplying the right-hand side of the expression by $\alpha_2$ we get

$$\frac{1-n\alpha_2}{n(1-\alpha_2)} = \left[\alpha_2 + (\Delta_1 / nD_1)\right] / \left[\alpha_2 + (\Delta_2 / D_2\right] \quad \text{(A6)}$$

Developing this expression, we finally arrive at

$$\alpha_2 = \left(\frac{\Delta_1}{D_1} - \frac{\Delta_2}{D_2}\right) \Big/ 1 + \frac{\Delta_1}{D_1} - n\left(1 + \frac{\Delta_2}{D_2}\right) \quad \text{(A7)}$$

The numerical value of $\alpha_2$ determined by this equation may then be used to calculate the spectrum of pure B by means of (A4).

## References


1. F. Weigert, Verh. Phys. Ges., **21**, 485(1919).
2. B. S. Neoport, O. V. Stolbova, Opt. Spectrosc., **10**, 146(1961).
3. T. Todorov, L. Nocolova, T. Tomova, Appl. Opt., **23**, 4309(1984).
4. T. Todorov, L. Nocolova, T. Tomova, Appl. Opt., **23**, 4588(1984).
5. M. Dumont, D. Morichère, Z. Sekkat, Y. Levy, SPIE Proc. **1559**, 127(1991).
6. Z. Sekkat, M. Dumont, Appl. Phys. B, **53**, 121(1991).
7. Z. Sekkat, M. Dumont, Appl. Phys. B, **54**, 486(1992).
8. M. Dumont, Z. Sekkat, R. Loucif-Saibi, K. Nakatani, J. A. Delaire, Mol. Cryst. Liq. Cryst. Sci. Technol. B, **5**, 395(1993).
9. Z. Sekkat, M. Dumont, Synth. Metals, **54**, 373(1993).
10. R. Loucif-Saibi, K. Nakatani, J. A. Delaire, M. Dumont, Z. Sekkat, Chem. Mater., **5**, 229(1993).
11. Z. Sekkat, M. Büchel, H. Orendi, H. Menzel, W. Knoll, Chem. Phys. Lett., **220**, 497(1994).
12. Z. Sekkat, J. Wood, W. Knoll, J. Chem. Phys., **99**, 17226(1995).
13. Z. Sekkat, J. Wood, Y. Geerts, W. Knoll, Langmuir, **11**, 2856(1995).
14. Z. Sekkat, W. Knoll, J. Opt. Soc. Am. B, **12**, 1855(1995).
15. Z. Sekkat, J. Wood, E. F. Aust, W. Knoll, W. Volksen, R. D. Miller, J. Opt. Soc. Am. B., **13**, 1713(1996).
16. Z. Sekkat, J. Wood, W. Knoll, W. Volksen, R. D. Miller, A. Knoesen, J. Opt. Soc. Am. B, **14**, 829(1997).
17. Z. Sekkat, P. Prêtre, A. Knoesen, W. Volksen, V. Y. Lee, R. D. Miller, J. Wood, W. Knoll, J. Opt. Soc. Am. B, **15**, 401(1998).
18. G. Kleideiter, Z. Sekkat, M. Kreiter, M. D. Lechner, W. Knoll, J. Mol. Struc., **521**, 167(2000).
19. G. Zimmerman, L. Y. Chow, U. Y. Paik, J. Am. Chem. Soc., **80**, 3528(1958).
20. E. Fisher, J. Phys. Chem., **71**, 3704(1967).
21. H. Rau, G. Greiner, G. Gauglitz, H. Meier, J. Phys. Chem., **94**, 6523(1990).
22. E. W. Thulstrup, J. Michil, J. Am. Chem. Soc., **104**, 5594(1982)
23. S. Hosotte, M. Dumont, SPIE Proc. **53**, 2852(1996).
24. A. El Osman, M. Dumont, Polym. Prepr, **39**, 1036(1998).
25. M. Dumont, A. El Osman, Chem. Phys. **245**, 437(1999).
26. F. Lagugné Labarthet, C. Sourisseau, New J. Chem., **21**, 879(1997).
27. M. S. Ho, A. Natansohn, P. Rochon, Macromolecules, **28**, 6124(1995).
28. X. Meng, A. Natanohn, P. Rochon, Polymer, **38**, 2677(1997).
29. O. K. Song, C. H. Wang, M. A. Pauley, Macromolecules, **30**, 6913(1997).

30. A. Natansohn, P. Rochon, J. Gosselin, S. Xie, Macromolecules, **25**, 2268(1992).
31. A. Natansohn, P. Rochon, Macromolecules, **31**, 7960(1998).
32. P. Rochon, D. Bissonnette, A. Natansohn, S. Xie, Appl Opt., **32**, 7277(1993).
33. D. Here, A. Natansohn, P. Rochon, Can. J. Chem., **76**, 1648(1998).
34. H. S. Blair, C. B. McArdle, Polymer, **25**, 100(1984); **25**, 1347(1984).
35. S. Yokoyama, M. Kakimoto, Y. Imai, Mol. Cryst. Liq. Cryst. **227**, 295(1993).
36. M. Eich, J. H. Wendorff, B. Reck, H. Ringsdorf, Makromol. Chem., Rapid Commun., **8**, 59(1987).
37. T. Bieringer, R. Wuttke, D. Haarer, Macromol. Chem. Phys. **196**, 1375(1995).
38. J. A. Delaire, K. Nakatani, Chem. Rev., **5**, 1817(2000).
39. R. A. Hill, S. Dreher, A. Knoesen, D. R. Yanakelevitch, Appl. Phys. Lett., **66**, 2156(1995).
40. G. R. Meredith, V. Krongauz, D. J. Williams, Chem. Phys. Lett., **87**, 289(1982).
41. Y. Atassi, J. A. Delaire, K. Nakatani, J. Phys. Chem., **99**, 16320(1995).
42. J. M. Nunzi, C. Fiorini, A. C. Etilé, F. Kajzar, Pure Appl. Opt. **7**, 141(1998).
43. F. Charra, F. Devaux, J. M. Nunzi, P. Raimond, Phys. Rev. Lett., **68**, 2440(1992).
44. F. Charra, F. Kajzar, J. M. Nunzi, P. Raimond, E. Idiart, Opt. Lett., **18**, 941(1993).
45. W. Chaulupczak, C. Fiorini, F. Charra, J. M. Nunzi, P. Raimond, Opt. Commun., **126**, 103(1996).
46. C. Fiorini, F. Charra, J. M. Nunzi, P. Raimond, J. Opt. Soc. Am. B, **14**, 1984(1997).
47. C. Fiorini, J. M. Nunzi, Chem. Phys. Lett., **286**, 415(1998).
48. A. C. Etilé, C. Fiorini, F. Charra, J. M. Nunzi, Phys. Rev. A, **56**, 3888(1997).
49. J. Si, G. Xu, X. Liu, Q. Yang, P, Ye, H. Li, H. La, Y. Shen, Opt. Commun., **142**, 71(1997).
50. J. Si, T. Mitsuyu, P. Ye, Y. Shen, K. Hirao, Appl. Phys. Lett., **72**, 762(1998).
51. G. Xu, Q. G. Yang, J. Si, X. Liu, P. Ye, Z. Li, Y. Shen, Opt. Commun., **159**, 88(1999).
52. C. Fiorini, J. M. Nunzi, F. Charra, F. Kajzar, M. Lequan, R. M. Lequan, K. Channe-Ching, Chem. Phys. Lett., **271**, 335(1997).
53. C. Fiorini, F. Charra, P. Raimond, A. Lorin, J. M. Nunzi, J. Opt. lett., **22**, 1846(1997).
54. J. M. Nunzi, F. Charra, C. Fiorini, J. Zyss, Chem. Phys. lett., **219**, 349(1994).
55. C. Fiorini, F. Charra, J. M. Nunzi, I. F. W. Samuel, J. Zyss, Opt. lett., **20**, 2469(1995).
56. P. Rochon, J. Mao, A. Natansohn, E. Batalla, Polym. Prepr. **35**, 154(1994).
57. P. Rochon, E. Batalla, A. Natansohn, Appl. Phys. Lett., **66**, 136(1995).

58. D. Y. Kim, S. K. Tripathy, L. Li, J. Kumar, Appl. Phys. Lett., **66**, 1166(1995).
59. D. Y. Kim, L. Li, X. Jiang, V. Shivshankar, J. Kumar, S. K. Tripathy, Macromolecules, **28**, 8835(1995).
60. S. K. Tripathy, D. Y. Kim, X. L. Jiang, L. Li, T. Lee, X. Wang, J. Kumar, Mol, Cryst. Liq. Cryst. Sci. Technol., A, **314**, 245(1998).
61. C. J. Barrett, A. L. Natansohn, P. L. Rochon, J. Phys. Chem., **100**, 8836(1996).
62. F. Lagugné Labarthet, T. Buffeteau, C. Sourisseau, J. Phys. Chem. B, **102**, 2654(1998).
63. X. L. jiang, L. Li, J. Kumar, D. Y. Kim, S. K. Tripathy, Appl. Phys. Lett., **72**, 2502(1998).
64. X. L. Jiang, L. Li, J. Kumar, D. Y. Kim, V. Shivshankar, S. K. Tripathy, Appl. Phys. Lett., **68**, 2618(1996).
65. N. C. R. Holme, L. Nikolova, P. S. Ramanjam, S. Hvilsted, Appl. Phys. Lett., **70**, 1518(1997).
66. P. S. Ramanjam, N. C. R. Holme, S. Hvilsted, Appl. Phys. Lett., **68**, 1329(1996).
67. F. Lagugné Labarthet, T. Buffeteau, C. Sourisseau, J. Phys. Chem. B, **102**, 5754(1998).
68. C. J. Barrett, P. L. Rochon, A. Natansohn, J. Chem. Phys., **109**, 1505(1998).
69. F. Lagugné Labarthet, P. Rochon, A. Natansohn, Appl. Phys. Lett., **75**, 1377(1998).
70. P. S. Ramanjam, M. Pedersen, S. Hvilsted, Appl. Phys. Lett., **74**, 3277(1999).
71. J. Paterson, A. Natansohn, P. Rochon, C. L. Caleender, L. Robitaille, Appl. Phys. Lett., **69**, 3318(1996).
72. X. L. Xiang, L. Li, D. Y. Kim, V. Shivshankar, J. Kumar, S. K. Tripathy, SPIE Proc., **2998**, 195(1997).
73. P. Rochon, A. Natansohn, C. L. Calender, L. Robitaille, Appl. Phys. Lett., **71**, 1008(1997).
74. N. K. Viswanathan, S. Balasubramanian, L. Li, J. Kumar, S. K. Tripathy, J. Phys. Chem. B, **102**, 6064(1998).
75. M. Irie, M. Mohri, J. Org. Chem., **53**, 803(1988).
76. V. D. Arsenov, S. D. Mal'tsev, V. S. Marevtsev, M. I. Cherkashin, Y. S. Freidson, V. P. Shibayev, N. A. Plate, Vysokomol. Soedin., **A 16**, 390(1974) and **A 24**, 2298(1982). In these papers, the rate constants in PMMA of the thermal back reaction of the SP molecule are $k_1 = 0.0012\ s^{-1}$ and $k_2 = 0.0001\ s^{-1}$ versus $k_1 = 0.00125\ s^{-1}$ and $k_2 = 0.00009\ s^{-1}$ in this thesis.
77. M. Irie, O. Miyatake, K. Uchida, J. Am. Chem. Soc., **114**, 8715(1992).
78. G. Gauglitz, in Photochromism Molecules and Systems; H. Dürr, H. Bouas-Laurent, eds.; Elsevier, Amsterdam, **Chap. 2**, 15(1990).
79. Z. Sekkat, W. Knoll, Phys. Chem., **98**, 1231(1994).

80. Y. Atassi,J. A. Delaire, K. Nakatani, J. Phys. Chem., **99**, 16320(1995).
81. V. D. Arsenove, S. D. Mal'tsev, V. S. Marevtsev, M. I. Cherkashin, Y. S. Freidson, V. P. Shibayev, N. A. Plate, Vysokoml. Soedin. A, **16**, 390(1974).
82. V. D. Arsenove, S. D. Mal'tsev, V. S. Marevtsev, M. I. Cherkashin, Y. S. Freidson, V. P. Shibayev, N. A. Plate, Vysokoml. Soedin. A, **24**, 2298(1982).
83. T. Tsujioka, M. Kume, M. Irie, J. Photochem. Photobio. A: Chem., **104**, 203(1997).
84. H. A. Kurtz, J. J. P. Stewart, K. M. J. Dieter, Comput. Chem., **11**, 82 (1990).
85. D. A. Parthenopoulos, P. M. Rentzepis, Science, **245**, 843(1989).
86. A. Toriumi, S. Kawata, Opt. Lett., **23**, 1924(1998).

## List of Publications

### Original Papers

[1] H. Ishitobi, Z. Sekkat, M. Irie and S. Kawata,
"The Photoorientation Movement of a Diarylethene-Type Chromophore,"
J. Am. Chem. Soc., **122**, 12802-12805(2000).

[2] H. Ishitobi, Z. Sekkat, and S. Kawata,
"Dynamical Studies of Optically Induced Orientation Processes in Photochromic Isomers : Experiment and Theory,"
Mol. Cryst. Liq. Cryst., **344**, 107-112(2000).

[3] H. Ishitobi, Z. Sekkat, and S. Kawata,
"Quantifying Theory of Optical Orientation Processes in Spectrally Distinguishable Photoisomers : application to a spiropyran-type chromophore," Chemical Physics Letters, **316**, 578-584(2000).

[4] M. Hisaka, H. Ishitobi, and S. Kawata,
"Optical Recording of Reversed Domains in Ce-doped SBN:75 Crystal for Bit-oriented Three-dimensional Optical Memory,"
J. Opt. Soc. Am. B, **17**, 422-426 (2000).

[5] Z. Sekkat, H. Ishitobi, and S. Kawata,
"Optical Orientation of Individualized Photoisomers,"
Nonlinear Optics, **22**, 501-504(1999).

[6] H. Ishitobi, Z. Sekkat, and S. Kawata,
"Individualized optically induced orientation of photochemical isomers," Chemical Physics Letters, **300**, 421-428(1999).

[7] Y. Kawata, H. Ishitobi, and S. Kawata,
"Use of two-photon absorption in a photorefractive crystal for three-dimensional optical memory ,"
Opt. Lett., **23**, 756-758(1998).

**International conferences/proceedings**

[1] Z. Sekkat, H. Ishitobi, and S. Kawata,
"Optical Orientation of Individual Isomers,"
6th International Conference on Organic Nonlinear Optics (ICONO'6), INV 18(Tucson, Dec. 16-20, 2001).

[2] H. Ishitobi, Z. Sekkat, and S. Kawata,
"Quantification of Optically Induced Orientation Processes in Spectrally Distinguishable Photo isomers,"
Fourth Japan-Finland Joint Symposium on OPTICS IN ENGINEERING (OIE'01), 79-80(Osaka, Oct. 25-27, 2001).

[3] H. Ishitobi, D. Yasumatsu, Z. Sekkat, and S. Kawata,
"Optically induced orientation processes in photochromic isomers,"
Technical Digest of CLEO/Pacific Rim 2001(Volume 2), 370-371(Chiba, July. 15-19, 2001).

[4] H. Ishitobi, Z. Sekkat, and S. Kawata,
"Optically induced orientation processes in photochromic isomers,"
The First Student's International Symposium on Advanced Engineering, 38(Osaka, Dec. 7-10, 2000).

[5] Z. Sekkat, H. Ishitobi, D. Yasumatsu, and S. Kawata,
"Quantified Photo-Orientation of Photoisomerizable Chromophores," Proceedings of the American Chemical Society : Division of polymeric materials : Science and Engineering(American Chemical Society 220th National Meeting), 194-195(Washington D.C., Aug. 20-24, 2000).

[6] Z. Sekkat, H. Ishitobi, D. Yasumatsu, and S. Kawata,
"Photo-orientation movement of photoisomerizable chromophores: quantifying analytical theory and application to spectrally overlapping and distinguishable isomers,"
Proceedings of SPIE(SPIE'45th Annual Meeting), **4106**, 133-145(San Diego, Jul. 30-Aug. 4, 2000).

[7] H. Ishitobi, Z. Sekkat, and S. Kawata,
"Dynamical studies of optically induced orientation processes in photochromic isomers : Experiment and theory,"

The 3rd International Symposium on Organic Photochromism(ISOP99), 49(Fukuoka, Nov. 14-18, 1999).

[8] H. Ishitobi, Z. Sekkat, and S. Kawata,
"Optically oriented isomers of diarylethene and spiropyran in polymeric thin films,"
International Conference on Optical Engineering for Sensing and Nanotechnology(ICOSN'99), 545-548(Yokohama, June 16-18, 1999).

[9] M. Hisaka, H. Ishitobi, and S. Kawata,
"Three-dimensional optical recording with the ferroelectric domain reversal in a Ce-doped SBN:75 crystal : experiment and calculation,"
International Conference on Optical Engineering for Sensing and Nanotechnology(ICOSN'99), 537-540(Yokohama, June 16-18, 1999).

[10] Z. Sekkat, H. Ishitobi, and S. Kawata,
"Individualization of optically oriented isomers in polymeric thin films," Extended abstracts of 4th international conference on organic nonlinear optics(ICONO'4), 308(Chitose, October 12-15, 1998).

[11] H. Ishitobi and S. Kawata,
"Two-photon recording in three-dimensional photorefractive data storage,"
Technical Digest of CLEO'98, 49-50(San Francisco, America, May 3-8, 1998).

[12] H. Ishitobi and S. Kawata,
"Two-photon absorption for three-dimensional optical memory with a photorefractive crystal,"
Technical Digest of International Conference on Optical MEMS and Their Applications(MOEMS97), 33-35(Nara, November 18-21,1997).

[13] Y. Kawata, H. Ishitobi, and S. Kawata,
"Two-photon absorption for three-dimensional optical memory with a photorefractive crystal,"
Program of OSA Annual Meeting, 77(California, October 12-17, 1997).

[14] Y. Kawata, H. Ishitobi, and S. Kawata,
"Two-photon absorption for three-dimensional optical memory with a photorefractive crystal,"
Proceedings of 1997 Topical Meeting on Photorefractive Materials, Effects and Devices (PR'97), 238-241(Chiba, June 9-10, 1997).

**Domestic meetings**

[1] H. Ishitobi, Z. Sekkat, and S. Kawata,
"The photo-orientation of diarylethenes,"
Extended Abstracts of 47th Spring Meeting(The Japan Society of Applied Physics), 1262(30a-Y-8)(Tokyo, March 28-31, 2000).

[2] H. Ishitobi, Z. Sekkat, and S. Kawata,
"Dynamics of optically induced orientation processes in photochromic isomers,"
Extended Abstracts of Optics Japan '99, 323-324(Osaka, Nov. 23-25, 1999).

[3] H. Ishitobi, Z. Sekkat, and S. Kawata,
"Dynamical studies of light-induced orientation processes in photochromic isomers : Experiment and theory,"
Extended Abstracts of 46th Spring Meeting(The Japan Society of Applied Physics), 1311(30a-W-10)(Chiba, March 28-31, 1999).

[4] H. Ishitobi, Z. Sekkat, and S. Kawata,
"Individualization of photoisomers during light-induced orientation of photochromic chromophores in polymeric thin films,"
Extended Abstracts of 59th Autumn Meeting(The Japan Society of Applied Physics), 1121(16a-ZP-8)(Hiroshima, September 15-18, 1998).

[5] H. Ishitobi, and S. Kawata,
"Two-photon absorption for three-dimension optical memory with a photorefractive crystal,"
Proceedings of LSM-21(21st Meeting Japan Society for Laser Microscopy), 30-37(Osaka, May 29, 1998).

[6] M. Hisaka, H. Ishitobi, and S. Kawata,
"Three-dimensional bit-oriented optical memory with the domain reversal technique : recording and readout of bit-data,"
Extended Abstracts of 45th Spring Meeting(The Japan Society of Applied Physics), 1021(30a-PA-4)(Tokyo, March 28-31, 1998).

[7] H. Ishitobi and S. Kawata,
"Longitudinal imaging of the three-dimension photorefractive memory recorded with two-photon process,"

Extended Abstracts of 58th Autumn Meeting(The Japan Society of Applied Physics), 1144(5a-ZE-3)(Akita, October 2-5, 1997).

[8] Y. Kawata, H. Ishitobi, and S. Kawata,
"Two-photon absorption for three-dimension optical memory with a photorefractive crystal,"
Extended Abstracts of 44th Spring Meeting(The Japan Society of Applied Physics), 919(30a-ZH-10)(Tokyo, March 28-31, 1997).